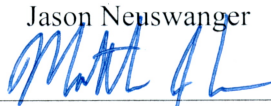


NEW 3-D VIDEO METHODS REVEAL NOVEL TERRITORIAL DRIFT-FEEDING  
BEHAVIORS THAT HELP EXPLAIN ENVIRONMENTAL CORRELATES OF  
CHENA RIVER CHINOOK SALMON PRODUCTIVITY

By

Jason Neuswanger

RECOMMENDED:



Mr. Matthew J. Evenson  
Advisory Committee Member



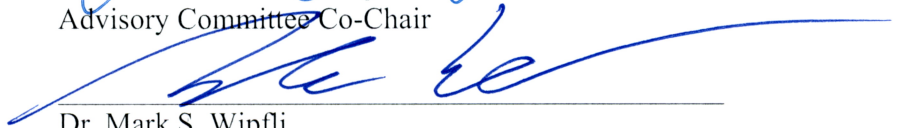
Dr. Milo D. Adkison  
Advisory Committee Member



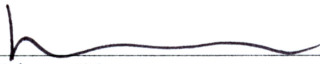
Dr. Michael J. Bradford  
Advisory Committee Member



Dr. Amanda E. Rosenberger  
Advisory Committee Co-Chair

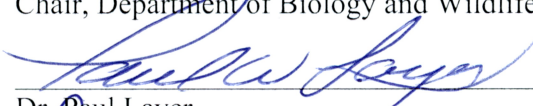


Dr. Mark S. Wipfli  
Advisory Committee Co-Chair

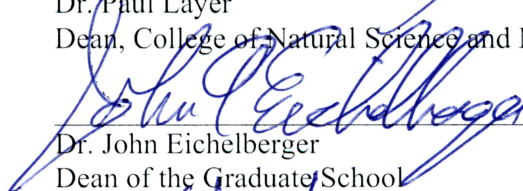


Dr. Diane Wagner  
Chair, Department of Biology and Wildlife

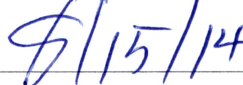
APPROVED:



Dr. Paul Layer  
Dean, College of Natural Science and Mathematics



Dr. John Eichelberger  
Dean of the Graduate School



Date



NEW 3-D VIDEO METHODS REVEAL NOVEL TERRITORIAL DRIFT-FEEDING  
BEHAVIORS THAT HELP EXPLAIN ENVIRONMENTAL CORRELATES OF  
CHENA RIVER CHINOOK SALMON PRODUCTIVITY

A  
DISSERTATION

Presented to the Faculty  
of the University of Alaska Fairbanks

in Partial Fulfillment of the Requirements  
for the Degree of

DOCTOR OF PHILOSOPHY

By

Jason Neuswanger, B.A.

Fairbanks, Alaska

August 2014

UMI Number: 3640327

All rights reserved

INFORMATION TO ALL USERS

The quality of this reproduction is dependent upon the quality of the copy submitted.

In the unlikely event that the author did not send a complete manuscript and there are missing pages, these will be noted. Also, if material had to be removed, a note will indicate the deletion.



UMI 3640327

Published by ProQuest LLC (2014). Copyright in the Dissertation held by the Author.

Microform Edition © ProQuest LLC.

All rights reserved. This work is protected against unauthorized copying under Title 17, United States Code



ProQuest LLC.  
789 East Eisenhower Parkway  
P.O. Box 1346  
Ann Arbor, MI 48106 - 1346

## Abstract

Chinook salmon (*Oncorhynchus tshawytscha*) are critical to subsistence and commerce in the Yukon River basin, but several recent years of low abundance have forced devastating fishery closures and raised urgent questions about causes of the decline. The Chena River subpopulation in interior Alaska has experienced a decline similar to that of the broader population. To evaluate possible factors affecting Chena River Chinook salmon productivity, I analyzed both population data and the behavior of individual fish during the summer they spend as fry drift feeding in the river. Using a stereo pair of high definition video cameras, I recorded the fine-scale behavior of schools of juvenile Chinook salmon associated with woody debris along the margins of the Chena River. I developed a software program called VidSync that recorded 3-D measurements with sub-millimeter accuracy and provided a streamlined workflow for the measurement of several thousand 3-D points of behavioral data (Chapter 1). Juvenile Chinook salmon spent 91% of their foraging attempts investigating and rejecting debris rather than capturing prey, which affects their energy intake rate and makes foraging attempt rate an unreliable indicator of foraging success (Chapter 2). Even though Chinook salmon were schooling, some were highly territorial within their 3-D school configurations, and many others maintained exclusive space-use behaviors consistent with the population regulatory effects of territoriality observed in other salmonids (Chapter 3). Finally, a twenty-year population time series from the Chena River and neighboring Salcha River contained evidence for negative density dependence and a strong negative effect of sustained high summer stream discharge on productivity (Chapter 4). The observed territoriality may explain the population's density dependence, and the effect of debris on foraging efficiency represents one of many potential mechanisms behind the negative effect of high stream discharge. In combination, these findings contribute to a statistically and mechanistically plausible explanation for the recent decline in Chena River Chinook salmon. If they are, in fact, major causes of the decline (other causes cannot be ruled out), then we can be tentatively hopeful that the population may be experiencing a natural lull in abundance from which a recovery is possible.



## Table of Contents

	Page
Signature Page .....	i
Title Page .....	iii
Abstract .....	v
Table of Contents .....	vii
List of Figures .....	xiii
List of Tables .....	xv
Acknowledgments .....	xvii
General Introduction .....	1
References .....	4
 CHAPTER 1: Measuring fish and their habitats: Versatile 2-D and 3-D video techniques with user-friendly software .....	7
1.1 Abstract .....	7
1.1 Introduction .....	8
1.2 Mathematics of 3-D measurement .....	10
1.2.1 Correcting non-linear optical distortion .....	11
1.2.2 From 2-D screen coordinates to 3-D lines of sight .....	13
1.2.3 Calculating 3-D measurements, camera positions, and error indices .....	14
1.3 The VidSync videogrammetry software .....	17
1.3.1 Video loading and navigation .....	18
1.3.2 How the user corrects distortion .....	19
1.3.3 How the user calculates a calibration .....	19
1.3.4 Measurement and categorization .....	20
1.3.5 Exporting data for analysis .....	21
1.4 Camera and calibration hardware .....	22
1.4.1 Cameras and camera mounts, and video storage and pre-processing .....	22
1.4.2 Calibration frame .....	25
1.4.3 Distortion correction chessboard .....	26
1.5 Protocol and best practices for recording video for measurement .....	27

	Page
1.6 Results.....	28
1.6.1 Precision and accuracy of length measurements .....	29
1.6.2 Distortion correction effectiveness .....	30
1.6.3 Diagnostic “error” measures.....	31
1.7 Discussion.....	31
1.7.1 Comparison to other visual measurement methods.....	32
1.7.2 Measurement error.....	34
1.7.3 Applications.....	36
1.8 Conclusions.....	37
1.9 Acknowledgments .....	37
1.10 References.....	38
1.11 Tables.....	43
1.12 Figures .....	47
Appendix 1.A.....	57
 CHAPTER 2: Mechanisms of drift-feeding behavior in juvenile Chinook salmon and the role of inedible debris in a clear-water Alaskan Stream .....	 61
2.1 Abstract.....	61
2.2 Introduction.....	62
2.3 Materials and methods.....	65
2.3.1 Study system .....	65
2.3.2 Video recording and processing .....	66
2.3.3 Classifying foraging attempt outcomes .....	68
2.3.3.1 Inspections .....	68
2.3.3.2 Expulsions.....	69
2.3.3.3 Ingestions .....	69
2.3.4 Spatiotemporal measurements of foraging attempts.....	70
2.3.5 Statistical analysis.....	71
2.4 Results.....	72
2.5 Discussion.....	74
2.5.1 Foraging attempt rate as a predictor of ingestion rate .....	74



	Page
2.5.2 Energy intake rate .....	76
2.5.3 Generality of debris effects.....	77
2.5.4 Limited attention and signal detection in drift feeding.....	79
2.5.4.1 Visual attention and the control of reaction volumes .....	79
2.5.4.2 Drift-feeding fish as signal detectors .....	81
2.5.5 Implications for foraging experiments.....	82
2.6 Conclusions.....	83
2.7 Acknowledgments .....	83
2.8 References.....	83
2.9 Figures .....	91
2.10 Tables.....	95
 CHAPTER 3: Territoriality within schools: dynamic competition of drift-feeding juvenile Chinook salmon in 3-dimensional space .....	 97
3.1 Summary.....	97
3.2 Introduction.....	99
3.3 Materials and methods.....	101
3.3.1 Study system .....	101
3.3.2 Collection and 3-D measurement of video footage .....	101
3.3.3 Behaviors recorded .....	102
3.3.4 The instantaneous region of influence (IROI) of a fish .....	104
3.3.5 Indices of proximity between competitors .....	105
3.3.6 Statistical analysis.....	108
3.4 Results.....	108
3.4.1 Site fidelity and characteristics of the IROI .....	108
3.4.2 Exclusive use of space .....	110
3.4.3 Aggression .....	111
3.4.4 Foraging attempt rate in relation to space use .....	112
3.5 Discussion.....	113
3.5.1 Territoriality while schooling .....	114
3.5.2 Competition in 3 spatial dimensions.....	115

	Page
3.5.3 Population-level implications of the observed behaviors .....	116
3.6 Acknowledgements .....	117
3.7 References .....	117
3.8 Tables .....	122
3.9 Figures .....	126

## CHAPTER 4: Low productivity of Chinook salmon strongly correlates with high summer stream discharge in two Alaskan rivers in the Yukon drainage .....133

4.1 Abstract .....	133
4.2 Introduction .....	134
4.3 Methods .....	136
4.3.1 Study rivers .....	136
4.3.2 Salmon run reconstructions .....	137
4.3.3 Stream discharge and temperature data sources .....	139
4.3.4 Stock-recruitment models and environmental predictors .....	140
4.3.5 Model fitting and assumptions .....	142
4.3.6 Model selection and evaluation .....	143
4.3.7 Explanation of the population decline .....	143
4.3.8 Sensitivity analysis .....	144
4.4 Results .....	144
4.4.1 Basic model and its residuals .....	144
4.4.2 Discharge model and its residuals .....	145
4.4.3 Exploratory analysis of other environmental variables to select the full model....	146
4.4.4 Explaining the decline in productivity .....	148
4.5 Discussion .....	148
4.5.1 Strength of evidence for the detected effects .....	149
4.5.2 Possible mechanisms by which discharge might affect productivity .....	151
4.5.3 Implications for broader Yukon River and Alaska Chinook salmon populations..	156
4.6 Acknowledgments .....	158
4.7 References .....	158
4.8 Tables .....	166

	Page
4.9 Figures .....	170
General Conclusions .....	179
References .....	181



## List of Figures

	Page
Fig. 1.1. Correcting non-linear distortion .....	47
Fig. 1.2. The VidSync measurement interface.....	48
Fig. 1.3. General-purpose calibration frame for two side-by-side cameras.....	49
Fig. 1.4. Screen and calibration frame coordinate systems.....	50
Fig. 1.5. Obtaining 3-D world coordinates to measure fish length.....	51
Fig. 1.6. Deployed stereo camera system. ....	53
Fig. 1.7. Length errors (VidSync-measured length minus true length) in measuring a 50.8mm object.....	54
Fig. 1.8. Relation between absolute error and (a) the maximum angle between the target and either of the cameras, and (b) the maximum distance of one of the measurement's endpoints from the principal point.....	55
Fig. 1.9. Error metrics .....	56
Fig. 2.1. Videotaping fish amidst debris in clear water .....	91
Fig. 2.2. Histograms of foraging summary statistics .....	92
Fig. 2.3. Foraging effort categorized according to whether the item was inspected and rejected, captured and expelled, or captured and ingested.....	93
Fig. 2.4. Foraging attempt rate underestimates ingestion rate .....	94
Fig. 3.1. Single camera view of sites from (a) Aug 14, 2009, (b) Jul 9, 2010, and (c) Jun 11, 2009.....	126
Fig. 3.2. Example 2-D (left) and 3-D (right) IROI representations of (a) a highly stationary fish (Aug14_38) and (b) a moderately stationary fish (Aug14_44).....	127
Fig. 3.3. 3-D plots of foraging attempts (spheres) and IROI centers (lines) for the three pairs of fish in closest proximity to each other .....	128
Fig. 3.4. 2-D and 3-D plots that illustrate examples of two different pairs of fish .....	129
Fig. 3.5. Spatial plots of aggression displayed by Chinook salmon .....	130

	Page
Fig. 3.6. Relationships between aggression rate in the Aug 14 video and the aggressor's (a) fork length, (b) IROI movement speed, an indicator of long-term motion of the space the fish is using, and (c) total foraging proximity index .....	131
Fig. 4.1. Basic Ricker model fit for the (a) Chena River (1986-2005) and (b) Salcha River (1987-2005).....	170
Fig. 4.2. Relationship between discharge during the summer growing season and Chinook salmon log-productivity relative to the predictions of the basic Ricker model .....	171
Fig. 4.3. Annual (a) Chena River and (b) Salcha River discharge summaries shaded by residuals from the basic Ricker model.....	172
Fig. 4.4. Predictions of the discharge and full models.....	174
Fig. 4.5. AICc values for the discharge model for the Chena River using different start and end dates for calculating median discharge. ....	175
Fig. 4.6. Residuals from the discharge model plotted against the top four other environmental correlates .....	176
Fig. 4.7. Trends over time in log productivity .....	177

## List of Tables

	Page
Table 1.1. Example protocol for filming fish behavior <i>in situ</i> for analysis in VidSync...	43
Table 1.2. Summary of 1,010 measurements of objects of 4 known lengths at various distances.....	45
Table 1.3. Some usability features of VidSync's measurement process. ....	46
Table 2.1 Environmental conditions at five sites observed on separate dates .....	95
Table 2.2 Fish attributes and foraging behavior for five groups of fish observed on separate dates. ....	96
Table 3.1 Foraging and territorial behavior of Chinook salmon fry.....	122
Table 4.1. Chinook salmon run reconstructions for the Chena River (1986-2005) and Salcha River (1987-2005). ....	166
Table 4.2. Variables evaluated in generalized Ricker models for Chena and Salcha River Chinook salmon. ....	167
Table 4.3. Model performance compared for all models in the confirmatory analysis ..	168
Table 4.4. Top ten models (ranked by $\Delta$ AICc relative to the best model).....	169





## **Acknowledgments**

I am grateful to my co-advisors Dr. Mark Wipfli and Dr. Amanda Rosenberger and the rest of my committee for their advice, patience, and encouragement throughout this long project, and for having the flexibility to let me pursue time-consuming methods development and interesting discoveries outside the originally planned scope of my work. I thank my wife, Dr. Elena Vayndorf, for patience and flexibility of a different sort—moving with me from New York to Alaska for years longer than advertised. All the major contributions of this dissertation resulted from these people giving me an exceptional amount of time and freedom to pursue interesting ideas in depth.

I am especially indebted to my late co-advisor Dr. Nicholas Hughes, who shaped my way of thinking about ecology during many treasured conversations over dinner or tea, or while sitting on a logjam in the river on a bright June midnight, observing fish behavior many hours after we were supposed to go home, because it there was seemingly no place he would rather be than helping a student discover something new about fish. My chapters on 3-D video methods and stock-recruitment analysis are both elaborations upon Nick’s unpublished exploratory work. Lon Kelly helpfully collaborated with Nick and me on the video methods. Also not listed on my signature page, but deserving of equal credit, is my father David Neuswanger, a fellow fishery biologist and a skillful editor who was my first line of defense against poor wording.

Except for the general introduction and conclusion, all chapters have multiple coauthors who supported this work intellectually, financially, and logistically. The stock-recruitment analysis would also not have been possible without the hard work of the Alaska Department of Fish and Game to compile a decades-long run reconstruction, and my coauthor Matthew Evenson of ADF&G, who spearheaded that sampling program and drafted the methods subsection about the run reconstruction in Chapter 4. I am also grateful for help and feedback in the lab and field from my fellow “Chena Project” graduate students (Megan Perry, Laura Gutierrez, Emily Benson, Elizabeth Green) and technicians (TJ Fayton, Ruth Rawcliffe, Jason McFarland, Stephanie Fischer, Katie Skogen, Melody Durrett).

The Arctic-Yukon-Kuskokwim Sustainable Salmon Initiative and the Alaska Department of Fish and Game funded the first several years of this project. Later support, ranging from annual funding to travel and equipment purchases, came from from the Institute of Arctic Biology, UAF Department of Biology and Wildlife, Alaska Cooperative Fish and Wildlife Research Unit, UAF College of Natural Sciences and Mathematics, Alaska EPSCoR, and US Fish and Wildlife Service.

## General Introduction

A broad goal of ecology is to understand the mechanisms by which population-scale patterns emerge from the myriad of complex interactions among individual animals and their environment (Grimm and Railsback 2005). Mechanistic understanding is especially important when biologists are tasked with explaining a decline in an economically and culturally important population such as Chinook salmon (*Oncorhynchus tshawytscha*) in the Yukon River drainage. Prior to 1998, the Yukon River Chinook salmon run averaged approximately 300,000 fish per year, of which 143,000 were harvested by the commercial or subsistence fisheries (ADF&G 2013; Schindler et al. 2013). Since 1998, a roughly 45% decline in run abundance has forced frequent closures of both the commercial and subsistence fisheries, creating hardship for thousands of rural villagers and other stakeholders in these fisheries, and prompting state or federal disaster declarations in nine years from 1997 to 2012 (Milkowski 2009; Schindler et al. 2013). Although the causes of this decline are unknown, a preliminary analysis in the proposal through which my work was funded (Wipfli et al. 2006) identified some important potential correlates of Chinook salmon productivity in the Chena and Salcha rivers, the only individual spawning streams in the Yukon River drainage for which we have both long-term run reconstructions and environmental data. The preliminary analysis linked Chinook salmon productivity to two factors, density dependence and stream discharge, that affect juvenile salmon during the summer they spend feeding in freshwater before smolting the following spring.

These possible effects are broadly consistent with the literature on population regulation in other salmonids. Productivity of salmonid populations (the number of progeny per spawner that eventually return to spawn or be captured in the fishery) often depends on population density and the competitive behaviors of individuals, such as territoriality (Elliott 1990; Grant and Kramer 1990). Productivity also depends on abiotic environmental variation, although the plethora of environmental factors exposes researchers to substantial risk of detecting spurious correlations (Myers 1998). Determining which effects are real is difficult if based on analysis of population data

alone, because we cannot perform controlled experiments on entire wild populations to establish cause-and-effect. Exacerbating this problem, observational population data sets grow at the tedious rate of one data point per year, meaning a hypothesis generated from one data set cannot be tested with sufficient new data collected under similar conditions until many years later, if ever. To move beyond the realm of interesting possibility, trends identified by correlational analysis of population data must be matched with knowledge of the mechanisms by which such relationships arise. This requires a detailed understanding of how individuals in the population are affected by each other and their environment.

The original goal of this research project was to synthesize previous knowledge of behavioral mechanisms relevant to salmonid population regulation into a single, process-based, conceptual and mathematical model of primary relationships between Chena River Chinook salmon and their environment. My ambition was to develop a model with the population-level simulation capacity of InSTREAM (Railsback and Harvey 2001) combined with the realism of certain habitat selection models. These models use computational fluid dynamics to map distribution of water velocity (Guensch et al. 2001), or water velocity and drift density (Hayes et al. 2007), integrated with a model of drift-feeding behavior (Hughes et al. 2003) to estimate the potential rate of energy intake for drift-feeding fish throughout a pool.

An accurate model of the mechanisms by which factors affecting individual Chinook salmon lead to population-level trends might help to diagnose their troubling decline and perhaps offer some habitat-related amelioration strategies. However, a significant flaw in this original project goal was my discovery that Chinook salmon in the Chena River exhibited behavioral strategies dramatically different from those in other populations where models linking individual-level processes to population dynamics are well established. Instead of prematurely constructing an integrated model based on non-applicable components, I shifted to developing a stronger foundation for future integrative modeling efforts by investigating some of the previously undocumented behaviors of my study animals and their possible relationship to population-level effects.

I chose to document and analyze the novel foraging behavior of juvenile Chena River Chinook salmon using videography. Video has been used in the past to study salmonid foraging behavior in three dimensions, but previous analytical methods were cumbersome and limited any detailed analysis to a very small number of individuals (Hughes et al. 2003). As described in Chapter 1, I developed new, open source software called VidSync (<http://www.vidsync.org>) that improves upon the video analysis methods of Hughes and Kelly (1996) in accuracy, general applicability, and—above all—the ease and speed with which the methods can be used. These improvements made it possible to capture and organize several thousand accurate 3-D measurements of juvenile Chinook salmon position and relational movement in schools.

I applied this technology to study two novel behaviors of juvenile Chinook salmon that may have fitness implications worth investigating. Chapter 2 describes the propensity of drift-feeding Chinook salmon fry to pursue inedible debris. It explores the foraging efficiency consequences of these pursuits and discusses how the observed effects are consistent with a radically revised view of the mechanisms underlying all drift-feeding behavior.

Chapter 3 investigates the consequences of Chinook salmon fry feeding in tightly spaced schools in a 3-D configuration along the deep margins of a large river, in contrast with the 2-D mosaic of broadly spaced territories associated with population regulation in other salmonids (Elliott 1990; Grant and Kramer 1990). It explores whether juvenile Chinook salmon exhibit any of the population-regulatory aspects of territoriality, such as exclusive space use.

Chapter 4 revisits the original rationale for this study—the detection of possible effects of density and stream discharge on Chinook salmon productivity—with twenty years of population data (double the original ten). It evaluates the realism of the detected effects and weighs the evidence for various causal mechanisms. The behavioral patterns described in Chapters 2 and 3 describe likely mechanisms for the main population effects detected in Chapter 4. The advances in video analysis technology in Chapter 1 were crucial to uncovering these relationships.

## References

- ADF&G Chinook Salmon Research Team. 2013. Chinook salmon stock assessment and research plan, 2013. Alaska Department of Fish and Game, Special Publication No. 13-01, Anchorage.
- Elliott, J. M. 1990. Mechanisms responsible for population regulation in young migratory trout, *Salmo trutta*. III. The role of territorial behavior. *J Anim Ecol* 59(3): 803-818.
- Grant, J. W. A. and Kramer, D. L. 1990. Territory size as a predictor of the upper limit to population density of juvenile salmonids in streams. *Can. J. Fish. Aquat. Sci.* 47: 1724-1737.
- Grimm, V. and Railsback, S. F. 2005. Individual-based modeling and ecology. Princeton University Press, Princeton, NJ.
- Guensch, G. R., Hardy, T. B., and Addley, R. C. 2001. Examining feeding strategies and position choice of drift-feeding salmonids using an individual-based, mechanistic foraging model. *Can. J. Fish. Aquat. Sci.* 58: 446-457.
- Hayes, J. W., Hughes, N. F., and Kelly, L. H. 2007. Process-based modelling of invertebrate drift transport, net energy intake and reach carrying capacity for drift-feeding salmonids. *Ecol Model* 207: 171-188.
- Hughes, N. F., Hayes, J. W., Shearer, K. A., and Young, R. G. 2003. Testing a model of drift-feeding using three-dimensional videography of wild brown trout, *Salmo trutta*, in a New Zealand river. *Can. J. Fish. Aquat. Sci.* 60(12): 1462-1476.

Hughes, N. F. and Kelly, L. H. 1996. New techniques for 3-D video tracking of fish swimming movements in still or flowing water. *Can. J. Fish. Aquat. Sci.* 53(11): 2473-2483.

Milkowski, S. 2009. Scarcity of king salmon hurt Alaskan fishermen. *The New York Times Business*: B1.

Myers, R. A. 1998. When do environment-recruitment correlations work? *Rev. Fish. Biol. Fisher.* 8(3): 285-305.

Railsback, S. F. and Harvey, B. C. 2001. Individual-based model formulation for cutthroat trout, Little Jones Creek, California. USDA Forest Service General Technical Report PSW-GTR-182:

Schindler, D., C. Krueger, P. Bisson, M. Bradford, B. Clark, J. Conitz, K. Howard, M. Jones, J. Murphy, K. Myers, M. Scheuerell, E. Volk, and J. Winton. 2013. Arctic-Yukon-Kuskokwim Chinook salmon research action plan: Evidence of decline of Chinook salmon populations and recommendations for future research. Prepared for the AYK Sustainable Salmon Initiative (Anchorage, AK). v + 70 pp.

Wipfli, M. S., Evenson, M., and Hughes, N. F. 2006. AYK SSI proposal: ecology and demographics of Chinook salmon.





## CHAPTER 1:

### **Measuring fish and their habitats: Versatile 2-D and 3-D video techniques with user-friendly software<sup>1</sup>**

#### **1.1 Abstract**

Applications of video in fisheries research vary in complexity, from simple biodiversity surveys to 3-dimensional (3-D) measurement of swimming, schooling, feeding, and territorial behavior. However, researchers lack a transparent, easy-to-use, general-purpose tool for 3-D video measurement. Thus, we developed a new measurement system, with freely available, user-friendly software, easily obtained hardware, and flexible underlying mathematical methods capable of high precision and accuracy. The software, called VidSync, allows users to quickly and easily measure, organize, and navigate complex 3-D data on fish and their habitats. Its customizable playback control and data organization features are equally useful for 2-D applications. We tested it using hardware optimized for studying juvenile Chinook salmon at close range ( $< 2$  m) in a clear water Alaskan river. Tests showed sub-millimeter accuracy in length measurements of 50.8-mm targets at close range, with increasing errors (mostly  $< 1$  %) at longer range and for longer targets. This system makes 3-D video measurement a practical addition to a researcher's toolkit for studying animal biology with freshwater, saltwater, or terrestrial applications in the laboratory or field.

---

<sup>1</sup> Measuring fish and their habitats: Versatile 2-D and 3-D video techniques with user-friendly software. Neuswanger, J., Wipfli, M.S., Rosenberger, A.E., and Hughes, N.F. Prepared for submission in Canadian Journal of Fisheries and Aquatic Sciences.

## 1.2 Introduction

Methods to remotely measure animal length and position have diverse applications in fish research (Shortis et al. 2009), especially for species sensitive to handling or difficult to capture (Ellender et al. 2012). Three-dimensional (3-D) position measurements can provide unique insights into the fine-scale spatial nature of locomotion (Hughes and Kelly 1996a; Butail and Paley 2012), habitat use (Laurel and Brown 2006; Fischer et al. 2007), and social and predatory behaviors (Potel and Wassersug 1981; Hughes et al. 2003; Mussi et al. 2005; Piccolo et al. 2007; Uglem et al. 2009). Such measurements are often estimated by direct visual observation, but they can be calculated with more precision and less bias from calibrated video footage (Harvey et al. 2001), a process we refer to as videogrammetry. That video preserves observations for repeated viewing has many benefits for analyzing behavior: ambiguous events can be interpreted by multiple observers, recordings can be re-analyzed from a new perspective as new questions arise, observers can measure the simultaneous actions of many interacting subjects instead of a single focal animal, and fleeting events can be interpreted in slow motion or frame-by-frame. Each video of fish behavior theoretically contains a great quantity of information, but its utility is limited by our finite capacity to extract biological data from images on a screen. Ideally, it would be feasible to analyze a video and obtain well-organized, annotated spatiotemporal coordinates of every physical, individual, and group phenomenon of interest within the field of view. Although many studies have simpler requirements such as length measurements, video analysis methods should enable such high-capacity processing of complex information, so that research questions, not technological limitations, dictate the type and quantity of information analyzed.

We submit that videogrammetric methods and software to date do not fully exploit the potential of this technology to produce a fast, easy-to-use, general-purpose measurement tool. Previous methods have been published as mathematical descriptions without accompanying software programs, or as processes requiring passing of data or still images among multiple programs (e.g., Hughes and Kelly 1996b; Harvey and Shortis 1996). Video methods are typically described with an emphasis on their mathematical

machinery and performance, with little emphasis on practical concerns about how to get started using them. The resulting learning curve and the cumbersome process of measurement may be major reasons why videogrammetry is often overlooked in favor of simpler but less powerful methods. These problems suggest a need for a broadly applicable measurement method to be implemented in a single, user-friendly software program that performs all steps of calibration, playback, measurement, and data organization. A practical description of the method is as important to these goals as the method itself, as it must equip unfamiliar readers to apply the method in novel situations without a costly process of trial and error.

We wanted to develop improved videogrammetric techniques and software to study the fine-scale *in situ* drift-feeding behavior and territoriality of juvenile (30-85 mm) Chinook salmon (*Oncorhynchus tshawytscha*) in the Chena River, Alaska, which is a clear, mid-sized (median summer flow 25 m<sup>3</sup>/s) river in the Yukon drainage. We observed that these salmon feed in tight shoals, presumably to evade predation, yet they possess the common salmonid propensity to defend territories as they feed. Studying this intriguing juxtaposition of opposing behaviors meant measuring and organizing an interrelated hierarchy of thousands of 3-D data points relevant to territorial structure, such as the positions and frequency of foraging attempts and conflicts between competitors. Our example illustrates a general challenge in behavioral studies, which is to observe and analyze the behavior of groups of animals, including the simultaneous actions of multiple individuals, over a range of conditions in wild settings. To meet this challenge, we developed a free, open-source Mac OS application called VidSync (<http://www.vidsync.org>). It is intended to improve upon existing techniques' accuracy, breadth of applications, and, most importantly, usability: the speed and simplicity with which measurements can be made, retrieved, modified, organized, and shared. Speed enhancements enable larger sample sizes relevant to new types of questions, and improved simplicity makes videogrammetry easier to learn for simple tasks like remote length measurement. Although VidSync was developed for 3-D measurement with two or

more cameras, many of its playback and data organization functions are equally useful for single-camera work such as biodiversity surveys.

In this paper, we 1) describe a novel synthesis of mathematical methods for videogrammetry, compatible with versatile camera configurations suitable for laboratory or field and terrestrial or aquatic settings; 2) describe a free, open-source software program for Mac OS called VidSync, which we designed to simplify and accelerate 2-D and 3-D video analysis; 3) describe the design and configuration of hardware appropriate to the methods; and 4) provide a field protocol to help users avoid the costly, non-intuitive pitfalls of filming underwater for measurement. We then 5) test the system's accuracy and precision, emphasizing how those measures relate to user choices about hardware design and use. Based on our results, we discuss our approach in terms of its relative usability, transparency, and potential applications in both 2- and 3-dimensional systems. We then provide suggested best practices to minimize error and avoid methodological pitfalls. We conclude with suggestions for future methodological advancements and research.

### **1.3 Mathematics of 3-D measurement**

The VidSync software incorporates a novel combination of mathematical techniques based on the simple principle that one can triangulate a 3-D position from two or more known lines of sight. To establish the validity of these specific methods, this section describes how lines of sight from separate camera views are calculated in a common coordinate system, and how their intersection is triangulated. VidSync performs all the calculations for these measurements automatically, and one can use it proficiently without understanding the details. However, basic familiarity with the mathematics helps to understand the reasoning behind our hardware and software guidelines, and to better interpret program output.

Each 3-D position is calculated from points on two or more video screens, which the user digitizes by clicking on the same object (e.g., a fish's snout) in each view. The 2-D screen coordinates (measured in pixels) from these clicks are then converted into 3-D

lines of sight. This takes two steps. The first adjusts the input point to compensate for non-linear (radial and decentering) distortion caused by optical imperfections in the lens and housing system. This enables use of a linear method to project the 2-D coordinates of each point into a line of sight in 3-D space. When at least two lines of sight are obtained from different camera views, their approximate intersection can be triangulated to find the final 3-D coordinates of the measured point. Each step of this process is detailed in the following sections.

### 1.3.1 Correcting non-linear optical distortion

Optical imperfections in camera lenses and underwater housings distort the image they project onto the film or digital sensor. Even the slight distortion in high-quality optics causes errors in 3-D reconstruction, which are minimized in VidSync by modeling and correcting for the largest distortion effects (Fig. 1.1). This correction allows further calculations to assume a distortion-free camera model in which points in 3-D object space are related to points on the 2-D image plane by linear transformations, which means that straight lines in the real world are represented by straight lines in the corrected image. Wide-angle images common in underwater work often have radially symmetric “barrel” distortion, in which the image appears to bulge outward relative to a point near the image center, the principal point. The principal point may be offset from the image center by slight misalignments among the many lens and housing elements, causing asymmetric radial and tangential distortion effects known as decentering distortion.

To correct for both radial and decentering distortion, VidSync uses the Brown-Conrady model (Brown 1966) with 8 parameters: the principal point or center of distortion ( $u_0, v_0$ ), and three coefficients each for radial ( $k_1, k_2$ , and  $k_3$ ) and decentering ( $p_1, p_2$ , and  $p_3$ ) distortion. Let  $(u_d, v_d)$  represent the measured (distorted) pixel coordinates of an image point, as measured from the bottom left corner of the image. Define new coordinates, centered about the principal point, as  $\bar{u} = u_d - u_0$  and  $\bar{v} = v_d - v_0$ . Letting  $r = \sqrt{\bar{u}^2 + \bar{v}^2}$ , the model calculates undistorted coordinates  $(u_u, v_u)$  as:

$$(1.1) \quad \begin{aligned} u_u &= u_d + \bar{u}(1 + k_1 r^2 + k_2 r^3 + k_3 r^3) + [p_1(r^2 + 2\bar{u}^2) + 2p_2\bar{u}\bar{v}][1 + p_3 r^2] \\ v_u &= v_d + \bar{v}(1 + k_1 r^2 + k_2 r^3 + k_3 r^3) + [2p_1\bar{u}\bar{v} + p_2(r^2 + 2\bar{v}^2)][1 + p_3 r^2] \end{aligned}$$

Distortion is modeled separately for each camera, which makes the corrections available for single-camera or 2-D applications as well as 3-D. This also enables the use of a correction method that finds the best parameters to remove distortion for the entire screen, not just a small, calibrated volume. Parameters are estimated from footage of a calibration object that contains several straight lines, or plumblines. The user digitizes several points along the distorted image of each plumblines, a process VidSync can automate when a chessboard pattern is used as the calibration object. To obtain the distortion parameters that best straighten those plumblines in the corrected image, VidSync uses non-linear minimization of a cost function that represents the total deviation from straightness of all the plumblines. This cost function is defined as the sum, over all plumblines, of the squared residuals from an orthogonal regression through each plumblines, divided by the total length of all plumblines. (Without this division, the cost function is minimized by shrinking all points to the origin instead of straightening the lines.) To specify this cost function, consider a set of  $m$  plumblines that have been undistorted with a candidate parameter set, of which the  $i$ th plumblines is defined by  $n_i$  points. Let  $\epsilon_{ij}$  represent the distance from the  $j$ th point on the  $i$ th plumblines to an orthogonal regression fit to that plumblines, and let  $\ell_i$  represent the distance between the endpoints of that plumblines. The cost function is

$$(1.2) \quad C(\text{parameters}, \text{plumblines}) = \frac{\sum_i^m \sum_j^{n_i} \epsilon_{ij}^2}{\sum_i^m \ell_i}$$

VidSync minimizes this function using the downhill simplex method (Nelder and Mead 1965) as implemented in the GNU Scientific Library (<http://www.gnu.org/software/gsl/>), using scale factors so all the parameters are of the same order of magnitude during the minimization.

The distortion corrections are applied to each measurement in the background, without altering the image the user sees on the screen. Therefore, when overlaying some results of 3-D calculations on the screen (e.g., hint lines, Fig. 1.2), it is necessary to re-

distort their coordinates to overlay the distorted image, using the inverse of the distortion model. No closed-form inverse is known for the Brown-Conrady distortion model (Mallon and Whelan 2004), so it is instead found numerically using Newton’s Method as implemented in the “gnewton” solver of the GNU Scientific Library (<http://www.gnu.org/software/gsl/>).

### **1.3.2 From 2-D screen coordinates to 3-D lines of sight**

VidSync adopts the main concept of Hughes and Kelly (1996b) to convert 2-D screen coordinates into 3-D lines of sight, although it differs in detail. A measurement’s 2-D screen coordinates are projected onto each of two planes in world coordinates, and the third coordinate (the known position of each plane in the third dimension) is inserted into both points to make a pair of 3-D points, which define a line of sight from the camera to the object being measured. Noteworthy differences between this method and others, and between its implementation in VidSync and that of Hughes and Kelly (1996b), are described in the discussion.

The first step of the process is to establish the mapping between each screen’s pixel coordinates and the pair of known planes in a 3-D coordinate system shared among all cameras. This requires filming a calibration frame (Fig. 1.3), which consists of known points called nodes arranged in grids in two parallel planes. The cameras may view different points, or even different planes perpendicular to those from other cameras (i.e., a “top view” camera may view different planes than a “side view” camera), provided all points are known in the same 3-D coordinate system. The position of the calibration frame during the calibration defines the 3-D coordinate system that is used throughout the video. The orientation, origin, and scaling of those coordinates can be adjusted arbitrarily; however, this explanation adopts the convention that the front and back frame faces both lie in the x-z plane in 3-D, and the bottom left point on the front surface grid is the origin (0, 0, 0). The front and back calibration frame faces are located in the planes  $y=0$  and  $y=d$ , where  $d$  is the separation between the faces.

To perform a calibration, the user inputs the real-world  $(x, z)$  coordinates for the dots on each face of the calibration frame, and clicks on each dot on the screen to establish corresponding screen coordinates in pixels  $(u_d, v_d)$ . VidSync corrects these points for non-linear distortion to obtain undistorted screen coordinates  $(u_u, v_u)$ . Having established correspondences between  $(x, z)$  and  $(u_u, v_u)$  coordinates for each node on one face of the calibration frame, VidSync estimates a homography (or projective transformation), represented by a 3x3 matrix  $H$ , that converts *any* undistorted screen coordinates  $(u_u, v_u)$  into  $(x, z)$  coordinates in that plane (Fig. 1.4). The homographies operate on homogeneous coordinates, so screen coordinates are represented as  $(u_u, v_u, 1)$ . Calibration frame coordinates  $(x, z)$  are recovered from the product  $H \cdot (u_u, v_u, 1)$  by factoring out a scalar  $w$  such that the third element of that product is 1:

$$(1.3) \quad w \begin{pmatrix} x \\ z \\ 1 \end{pmatrix} = H \begin{pmatrix} u_u \\ v_u \\ 1 \end{pmatrix}$$

$H$  is estimated using the normalized Direct Linear Transformation (DLT) algorithm as described by Hartley and Zisserman (2004 Algorithm 4.2). The calculation requires at least four point correspondences, preferably more, in which case the points define an over-determined linear system to which the DLT algorithm provides a least squares solution. The transformation's inverse  $H^{-1}$  is also calculated for the purpose of converting world coordinates back into screen coordinates when overlaying on-screen feedback, and for estimating reprojection errors, which are described later.

For each camera, homographies are calculated for front ( $H_f$ ) and back ( $H_b$ ) faces of the calibration frame. To obtain a 3-D line of sight, the projective transformations for the front ( $H_f$ ) and back ( $H_b$ ) surfaces convert each point in screen coordinates  $(u_u, v_u)$  into two 3-D points—one on each face of the frame:  $(x_f, 0, z_f)$  and  $(x_b, d, z_b)$ . These two points define a line of sight from the camera through the measured object.

### 1.3.3 Calculating 3-D measurements, camera positions, and error indices

VidSync calculates 3-D positions by estimating the intersections of lines of sight defined by screen clicks (Fig. 1.5). Noise in this input (even if infinitesimal) prevents



these lines from intersecting exactly, so we can only estimate their closest point of approach (CPA). To this end, VidSync uses either a geometrically intuitive linear method or an iterative method that is usually more accurate. The linear method is used to calculate the camera positions, which then are used by the iterative method to calculate more accurate 3-D measurements. However, the iterative method assumes that light travels in a straight line from the subject to the cameras, so the linear method is more appropriate for footage filmed through a tank wall or the surface of the water. The situation-dependent method can be selected in the VidSync user interface.

The linear method's position estimate is the CPA of the lines of sight. For two lines from two cameras, the CPA is the midpoint of the shortest possible line segment that connects the other two. For any number of lines, let  $p_i$  represent the first point on line  $i$ , let  $I_{3 \times 3}$  represent the 3-by-3 identity matrix, and let  $v_i$  be the unit vector along line  $i$ . The CPA  $(x, y, z)$  of any number of lines is

$$(1.4) \quad CPA = \left( \sum_i (I_{3 \times 3} - v_i v_i^T) \right)^{-1} \left( \sum_i (I_{3 \times 3} - v_i v_i^T) p_i \right)$$

From the CPA a useful index of error is calculated, the mean distance from the CPA to the lines from which it was calculated, which we term the point-line distance or PLD error:

$$(1.5) \quad PLD \text{ error} = \sum_i \|(CPA - p_i) \times (CPA - p_i - v_i)\|_2$$

Importantly, this is not a true error in the sense of a quantity that could be used to calculate confidence intervals or p-values. Instead, it provides a rough sense of how true errors scale with distance from the cameras, and it can help diagnose data entry mistakes, such as clicking different fish in different camera views when trying to measure just one of them.

Hartley and Zisserman (2004) show that linear triangulation methods such as the CPA are not optimal estimates of 3-D intersections in projective geometry. They provide an optimization procedure that assumes the 3-D point satisfies the epipolar constraint (exact intersection of the lines), and finds “new” screen points that satisfy the constraint

at a minimized distance from the input screen points. They show this to be a maximum likelihood estimate of the 3-D position, assuming normally distributed errors. The iterative triangulation method used by VidSync is analogous to theirs. It minimizes the same cost function in screen coordinates, but the components of that cost function are calculated in a different way, consistent with our two-plane geometric method.

VidSync's method also requires the 3-D positions of the cameras, which are estimated as the CPA of several lines of sight from each camera. The choice of these lines is somewhat arbitrary, but VidSync used lines calculated from the screen positions of the back frame nodes during calibration, so that small errors from extrapolating laterally outside the frame do not influence the camera position estimate. These screen points are projected onto the front and back frame surfaces, and the mutual CPA of all these lines is the estimated camera position.

Given known camera positions, any 3-D point can be reprojected onto the screen. The point is found at which a line from the 3-D point to the camera intersects the front frame plane. That intersection point is converted to homogeneous coordinates in that plane, which the homography  $H_f^{-1}$  then projects into undistorted screen coordinates. The difference between the originally input screen point and the reprojected screen coordinates of the calculated 3-D point is the reprojection error. VidSync's iterative triangulation method finds the 3-D position that minimizes the total reprojection error across all cameras. Let  $s_i$  be the undistorted screen coordinates of an input point in camera  $i$ , and let  $s'_i$  be the reprojected screen coordinates of the 3-D point  $(x, y, z)$  in that camera. Using the CPA as a starting point to speed convergence, VidSync uses the downhill simplex method (Nelder and Mead 1965) to estimate the 3-D position that minimizes a cost function defined as the sum of squared reprojection errors in all cameras,  $C(x, y, z)$ :

$$(1.6) \quad C(x, y, z) = \sum_i (\|s_i - s'_i(x, y, z)\|_2)^2$$

The square root of  $C(x, y, z)$  is reported in VidSync as the reprojection error. This is useful as an indicator of mismatched screen points and potential errors in 3-D

reconstruction, although it does not scale with distance like the PLD error. When the iterative triangulation method is used, the PLD error is calculated using linear triangulation of the reprojected points  $s'_i$ .

Reprojection is also useful for placing visual feedback on the screen. VidSync can overlay reprojection errors from all measurements onto the screen together, which helps visualize any systematic errors such as those arising from poor calibration. Reprojection also provides for a useful visual cue for finding corresponding objects in different cameras. When an object has been clicked in one camera, the line of sight defined by that click (the epipolar line) appears on the other screen, facilitating matching objects that would otherwise be difficult to pinpoint in different perspective views, such as individual fish in a school. Reprojection errors and epipolar lines have their coordinates re-distorted for display overlaying the distorted image; these curved images of the epipolar lines are termed “hint lines” in VidSync.

#### **1.4 The VidSync videogrammetry software**

This section describes VidSync, a Mac application we developed to provide fine control over video playback and to collect and organize 2-D and 3-D measurements using the methods described above. VidSync is freely available (<http://www.vidsync.org>) under the GNU Public License (<http://www.gnu.org/software/gsl/>), and its source code is open and version-controlled, so ambitious users may scrutinize or customize the program to fit their needs. VidSync is written in the Objective-C language for Mac OS 10.9 Mavericks and later. VidSync itself has modest system requirements, so performance is limited by the computer’s ability to play multiple videos simultaneously, which depends on its speed and on how the video clips are encoded. VidSync’s design largely limits its demand for human input to decisions requiring human judgment, minimizes the number of steps in repetitive tasks, and makes human input as intuitive, accurate, correctable, and customizable as possible.

A typical VidSync analysis consists of 1) loading and synchronizing videos, 2) detecting plumb lines and calculating distortion parameters, 3) digitizing the calibration

frame nodes and calculating the calibration, 4) defining measurement types or loading predefined ones, and 5) making and exporting measurements. Here each step is described in enough detail to help prospective users evaluate the suitability of VidSync for their applications.

#### **1.4.1 Video loading and navigation**

Upon creating a new VidSync document, the user loads each video clip into the document and names it (e.g., “Left Camera”). The video clips appear in separate windows from the main document window (Fig. 1.2). The first video is by default designated the “master clip,” and all measurements and annotations are recorded with the master clip’s timecode. The user navigates each video independently to find a synchronization point, such as a flash from an LED light, and checks a box to lock the synchronization of the non-master clips based on that point. Thereafter, the synchronized clips are navigated together. After synchronization, it is recommended to save this work, creating a VidSync document (.vsd) file that contains all the information about each video set’s calibration, measurements, annotations, and metadata.

In addition to standard playback buttons (play/pause, play backward, fast forward/rewind, step one frame forward/back), there are customizable playback controls. These include buttons to step forward or backward by a specified number of frames, buttons to play forward or backward at a customizable speed, and two pairs of customizable-speed “play while pressed” buttons. By default, one pair is set for fast playback, and the other for slow motion. The “play while pressed” buttons are particularly useful, because they facilitate sudden pausing and easy, repeated review when an event of interest is observed. Other controls instruct VidSync to play the video for a fixed or random duration and then pause, facilitating systematic or random sampling schemes. Navigation is further enhanced by allowing users to select any previous measurement and press a “go to” button to view the video at the frame where that measurement was taken. The program separately allows unmeasured text annotations with the same “go to” functionality, serving as bookmarks for video frames of interest.

### **1.4.2 How the user corrects distortion**

To find the 8 distortion parameters for one video in VidSync, the user locates a clear, full-screen view of the chessboard pattern and presses a button to automatically detect the corners and arrange them into plumblines. Detected plumblines are overlaid on the video, where the user can click on any erroneous points to edit them. After that, the program calculates the distortion parameters. If no chessboard image was filmed, the user can manually digitize plumblines by clicking other straight objects in the image (such as the edge of the calibration frame), but this time-consuming approach is less accurate than the automatic, chessboard method. Users can import distortion parameters from other VidSync documents that used the same camera system; however, any optical adjustment (such as removing a camera from its underwater housing to change a battery) may affect the parameters and warrant re-calculation.

### **1.4.3 How the user calculates a calibration**

Before calibrating a video clip, the user enters the distance between the calibration frame faces and a list of physical 2-D coordinates of the nodes on each face of the calibration frame. The length units in which these node coordinates are provided become the measurement and output units for VidSync. The user can optionally customize the coordinate axes ( $x$ ,  $y$ , and  $z$ ) corresponding to each face of the frame, for example, to tell the program if a top-view camera and a side-view camera are looking through different, perpendicular faces of the frame. These frame descriptions can be saved as a separate file and reloaded for any other video filmed with the same calibration frame.

The user begins calibration by finding a synchronized timecode at which all cameras have a clear view of the calibration frame, and the frame and cameras are both as motionless as possible. A button click loads the frame node coordinates into a table matching them with (so far, blank) screen coordinates. Screen coordinates are recorded by clicking on the center of each node. If a node center is unclear due to poor visibility, it can and should be deleted from the list, because visual guesswork increases error.

Throughout this process, each point's matched 3-D coordinates are overlaid on the video, so mistaken correspondences are easy to detect. Once the user completes this process for the front and back faces of the frame in one camera, VidSync calculates the projection matrices, and the calibration of that camera is complete. Each camera is calibrated separately in the same manner. Using two cameras and a 5-by-4 node calibration frame, a typical calibration takes 5 to 10 minutes. Completed calibrations can be saved as separate files and reused for other videos shot with the cameras in the same relative orientation.

#### **1.4.4 Measurement and categorization**

Measurements in VidSync are defined within a reusable hierarchy consisting of two main categories: 1) objects, such as fish, and 2) events, such as prey captures and length measurements. Specific objects and events are defined by the user through a simple interface with built-in examples. Objects are often associated with multiple events, and events can be associated with multiple objects (e.g., a territorial dispute event between two fish objects). Objects and events in this system need not always correspond to physical objects and events. For example, when making single length measurements of many different fish, it is easiest to define one object (e.g., "All Fish") and measure each fish as a separate event for the same object, rather than creating a new object for every new fish measured.

Each measured point is shown on the screen with a marker, the color of which depends on the specific object being measured (e.g., different colors for different individual fish). The measurement's event type determines the marker's shape, size, duration of visibility, and whether or not lines are drawn and measured to connect consecutive points for that event. Event types may also be defined with a maximum number of points, which speeds automatic creation of new events. As an example, when a single-point event like a prey capture is selected and its point has already been measured, the next click on the video screen creates a new event of the same type. In this flexible system, length measurements are defined as two-point events (one for the head, one for the tail) with a length-labeled connecting line, and the length shows up immediately on

the screen once both points have been measured. The next click on the screen begins a new measurement automatically.

VidSync contains efficient systems for selecting and precisely editing existing measurements. Any input can be selected through tables in the main document window at any time. When a measurement's marker is visible on the video overlay, the user can select it by right-clicking near the marker. Newly measured points are automatically selected. A selected point's position can be "nudged," by a configurable distance with sub-pixel precision (e.g., 0.2 pixel) by using the keyboard arrows. The exact position of the measurement on the video is reflected in a "magnified preview" box in the document window, which shows a marker in the exact position of the point against a magnified version of the local region of the video. The magnification of the preview is configurable, as are its brightness, contrast, sharpening, and the size and type of the point marker (a small dot or a concentric arc reticle). This system enables arbitrarily precise placement with no ambiguity about which exact point under the cursor is recorded when clicked.

The usual process for measuring a point is to click near it on the video and, if high precision is required, nudge it into exact position using the arrow keys and the magnified preview. A hint line is automatically projected across other video clips, making it easy to locate the same fish or object in those clips and place the desired measurement similarly. This requires only a few seconds to perform.

### **1.4.5 Exporting data for analysis**

VidSync can export measurement data in two forms: as an XML (eXtensible Markup Language) file or a CSV (Comma-Separated Value) spreadsheet file. Though spreadsheets are adequate for processing simple length and position data, the XML format better reflects detailed measurement hierarchies. VidSync's mathematical role ends with calculating and organizing 3-D point and length measurements. Further analyses diverge for different users who prefer different programs for analysis and visualization, and VidSync's XML files can be imported into several general-purpose mathematics programs, including Mathematica®, R, and MatLab®. VidSync can also

export still images and video clips, with or without overlaid measurements and annotations.

## **1.5 Camera and calibration hardware**

The utility of these methods depends on the quality of video footage—a function of hardware capability and the manner of its use (protocol discussed in Appendix B). Recognizing that camera technology becomes outdated quickly, we describe our current system sparingly and focus instead on practical field considerations and general camera characteristics we expect to remain relevant as technology advances.

### **1.5.1 Cameras and camera mounts, and video storage and pre-processing**

We used a pair of Sony ® HDR-SR12 digital video cameras inside Ikelite ® #6038.94 underwater housings with Zen Underwater ® WAVP-80 wide-angle dome ports (Fig. 1.6). Desiccant packets within the housings prevented condensation. The handle assemblies of the housings were bolted exactly 33 cm apart on a 55-cm length of 2-inch (5.08-cm) aluminum angle beam with its top surface covered in waterproof nonslip tape. The bolts were secured from the bottom with wing nuts over pressure washers, making it easy to loosen the cameras and adjust their orientation as each field site might demand. To create a handle for lowering the system into the river, we bolted a 1.8-m length of 1-inch (2.54-cm) square aluminum tubing to the center of the perpendicular side of the angle bracket. A U-bolt mounted low on the handle tube provided a carrying handle. Miscellaneous other U-bolts and eyebolts and a crossbar served as attachment points for ratchet straps and clamps to secure the system to nearby logs for lengthy observations in a fixed reference frame. In the absence of logs, steel reinforcing bars were driven into the substrate and used to stabilize the cameras. We were satisfied with the durability and performance of this self-contained system while filming in and around logjams in a mid-sized river. However, the cameras and housings we purchased in 2007 are now obsolete, so we offer general guidelines for selecting those.



One of the main factors in camera selection is resolution. Cameras with full high-definition resolution (1920 x 1080 pixels) currently provide the most accurate measurements (Harvey et al. 2001), but they also require more disk space and processing power to play the videos, a particular concern for playing multiple videos simultaneously. A video camera's vertical resolution (e.g., 1080 lines) is written in combination with its scan mode, (e.g., 1080p for progressive scan, and 1080i for interlaced scan). Our cameras used 1080i, but 1080p cameras have since become common, and they are preferred for measurement work because interlaced video makes exact positions ambiguous in paused frames, and transcoding it to progressive scan reduces its quality (we used Final Cut Compressor to convert our 1080i videos to 1080p). A high resolution increases visible detail, while a faster frame rate allows for synchronizing multiple videos more precisely (potentially improving measurement precision for moving targets) and recording details of fleeting events with greater temporal resolution. One should obtain, at the start of a project, enough storage capacity for video of the appropriate resolution in the camera itself, at remote field sites, and in the lab. If the project's requirements for detail are minimal, (e.g., length measurements with some tolerance for inaccuracy), then low-resolution video is sufficient and simpler to manage. It is also not necessary to use full-sized video cameras and underwater housings for all applications. Recently, compact and inexpensive high-definition cameras have become popular for action sports enthusiasts, and those made by GoPro® have been used with VidSync with good results (Aurélian Vivancos, Department of Zoology, Otago University, Dunedin, NZ, personal communication).

The configuration of the cameras on their mount can significantly affect the accuracy of measurements. The framing should be strong enough to hold the cameras fixed against it without flexing. Separation and angles of the cameras affect accuracy and precision, which depend on the angle of convergence of the lines of sight from the different cameras. When the subject is far from the cameras compared to their separation, the lines converge at a narrow angle, and small errors in line positions create relatively large errors in 3-D positions. Precision is maximized at the opposite extreme, when the

cameras are separated so far (or the subject is so close) that the lines intersect at a right angle. This setup is ideal for many lab experiments. For the common “stereo pair” setup of two side-by-side cameras, Harvey and Shortis (1996) found (using calculation methods different from ours) that cameras should be separated by  $1/3$  to  $1/5$  of the camera-to-subject range for acceptable precision. We found suitable precision at a greater distance. In general, camera separation should be maximized subject to the constraints of subject distance, field of view, and field handling convenience for the cameras and the calibration frame (which must be larger as camera separation increases). Underwater work usually benefits from the use of wide-angle optics to increase the field of view, particularly because refraction at the water-glass-air interface “zooms in” the view by a factor of about 1.3. We found that a high-quality, wide-angle dome port minimized picture distortion with fewer lighting artifacts than a flat lens port; however, the opposite may be true for some systems (notably, GoPro® cameras require a flat underwater housing port for optimal image quality).

Cameras best suited for videogrammetry allow manual focusing at repeatable distances. Less expensive, fixed-focus cameras suffice if the non-adjustable focus is set at a distance that maximizes depth-of-field. Autofocus systems should be disabled, because changing the focus alters the optical geometry of the system and invalidates the camera’s calibration. Users of adjustable manual-focus cameras should experiment with their systems to determine the best focal distance, because the optics of housing ports and the air-water interface affect focus in difficult-to-predict ways, and the camera’s stated focal distance may be far from the distance at which it is actually focused through the housing and water. This empirical determination of ideal focus settings should be done in the same optical environment as actual measurements (e.g., underwater), and only needs to be done once per system.

System design is also influenced by whether or not the operator requires a live view of the objects being filmed. A live view can help with verifying suitable lighting, focus, and aim. Self-contained camcorders in underwater housings do not offer such live views unless manually operated by a diver. An alternative is to use a closed-circuit video

system, with cameras tethered to external recorders or computers. It is an advantage that these systems are not limited by the size of the battery and recording medium that fit inside a housing, but they may be more fragile and less portable than the self-contained system we described.

### **1.5.2 Calibration frame**

The calibration frame is critical to the system's accuracy. Its design should vary based on the intended working distance. It must consist of at least one pair of precisely parallel planes, separated by a distance that must be meticulously measured, because it is VidSync's only source of information on the scaling of that dimension. Each plane is marked at four or more points, called nodes, at known 3-D coordinates. In practice, the nodes are located on a regular grid. Variations on this theme are suited for different settings, including cage-like grids of rods (Hughes and Kelly 1996b) or dots painted on the sides of an aquarium. A calibration frame may have points on only two surfaces if both cameras are to look through it from one side, as in a typical stereo camera system. Alternatively, it may have dots on four surfaces, such as in a laboratory with a side-view camera and a top-view camera. In general, the cameras need not be aimed at the same nodes, as long as all node positions are known in the same 3-D coordinate system and each camera has a clear view of two parallel surfaces. Different cameras are often calibrated with a slightly different selection of nodes because debris or lighting obscures some of them; this is not a problem as long as enough other nodes remain visible that the calibration result is not overly sensitive to errors digitizing any single node.

The optimal calibration frame design for any given project depends on expected subject distance, camera focal length, and the relative positions and orientation of the cameras. Ideally, the frame should be large enough to span most of the screen in each camera when it is located at the same distance from the cameras as the expected measurement subjects. For distances of several meters this is impractical, and there is a tradeoff between screen coverage and matching the expected subject distance. Our results show that extrapolating outside a small frame close to the cameras is possible with minor errors, but filming a

frame too far away to fill most of the screen creates larger errors, so this tradeoff should be resolved in favor of screen coverage.

The calibration frame used for this study (visible in Fig. 1.4) was a durable, mobile design for fieldwork with two side-by-side cameras, but it had some minor flaws that are corrected in the improved design described in Fig. 1.3. We constructed a clear box by bonding 3/8-inch (0.9525-cm) Lexan ® sheeting with IPS Weld-On ® #3 polycarbonate adhesive. To place the nodes, we created a point grid with 10-cm spacing using a computer graphics program, then printed it on transparency sheets and taped the transparencies together to produce a larger, precise 5-by-4 grid. We taped this grid to the Lexan ® and punched pilot holes through the grid points. We expanded each hole to 3/8-inch (0.9525-cm) diameter using a Forstner bit in a drill press, then backed each hole with masking tape and filled it with black CRL 33S silicone sealant. This method produced uniform, bold dots on both surfaces. However, the dots were actually thin 3-D cylinders with sides visible when viewed at oblique angles, complicating pinpointing the precise center of the circular front of the dot.

For future calibration frame construction, we recommend having a professional sign maker print the nodes directly on rigid materials with a computer printer. The surface closest to the camera must be printed on a clear material, such as Lexan, but the far surface may be opaque white, for improved contrast (Fig. 1.3). One problem with using a front grid printed on a clear material is that the material refracts the images of the dots on the back surface, altering their apparent positions very slightly. This can significantly affect measurements, particularly at long distances. VidSync includes a correction for this effect, based on the material thickness and published refractive index (Appendix A).

### **1.5.3 Distortion correction chessboard**

The chessboard pattern should be a stiff, flat material printed with black and white squares with precisely aligned corners, large enough to fill the screen when positioned far enough from the cameras to be in focus when the focus is set for filming fish. The

squares should be large enough to be distinct from one another at that distance, and small enough that each plumbline comprises a large number of points. Use of a professional sign printer is recommended to obtain a precise, waterproof grid.

## **1.6 Protocol and best practices for recording video for measurement**

In the field, it is easy to overlook small problems and ruin hours of data collection, e.g., by not noticing that an accidental bump changed the camera's zoom setting. Experiencing such errors during our pilot work prompted our development of a checklist-like protocol (Table 1.1) to prevent such problems. Here we discuss some other issues that are not part of the step-by-step list, but are still important to obtaining useful footage.

The relative orientation of the cameras (including their underwater housings and positions within those housings) must remain fixed from the time of calibration until all measurements using that calibration are completed. Even if waterproof housings are fixed firmly in place, cameras may shift slightly within them. Care should be taken to secure all potentially movable parts and to re-calibrate after each change to the system such as removing cameras from their housings to change batteries. With very stable hardware, it may not be necessary to perform a new calibration for each recording. Regardless of configuration, the calibration frame and chessboard should be filmed under similar conditions to the intended measurements, because the refractive index of water and the shape of the housings/ports may vary with large changes in temperature, depth, and salinity (Shortis et al. 2007a).

Lighting is extremely important for recording fine detail. Dim lighting forces the camera to use either a slower shutter speed, which increases motion blur, or a higher light sensitivity (ISO), which increases image noise. The presence of very bright and very dim areas in the same scene forces the camera to expose for one or the other, thereby either overexposing highlights or underexposing shadows. Pointing the cameras toward the sun, even if not directly, may scatter so much light off small suspended particles that distant objects are obscured. Direct sunlight refracting through waves may cause a constant

shifting pattern of highlights and shadows on all objects in the image. Uniform, bright sunlight from behind the cameras is usually acceptable, but the clearest footage comes from the diffuse light of a brightly overcast day. Analogously, diffuse light sources may provide ideal footage in a lab setting. Users setting stationary cameras outdoors should consider the position of the sun not only when they set their cameras, but throughout the duration of the video.

The quality of video measurements depends not only on how the video was filmed, but also on how it is saved and encoded digitally. This process will vary among users, but we describe our own steps here as an example. Our Sony ® HDR-SR12 cameras recorded 1080i video on internal hard drives in AVCHD format, and we used the “Log and Transfer” function of Apple Final Cut Pro ® 6 to import videos as QuickTime .mov files encoded using the Apple Intermediate Codec. Files using this low-compression codec took too much space (~120 gb per camera for 2 hours) and the files from our cameras were interlaced, so we used Apple Final Cut Compressor 3 to create the final deinterlaced .mov files in the H.264 codec with a 4 mb/s bitrate (about 30gb per camera for 2 hours of footage). Bitrate controls the tradeoff between image quality and file size; we chose 4 mb/s after determining by trial-and-error that it was the smallest value that preserved the very fine detail we required. We preserved the original AVCHD files as disk images (.dmg files) of the camera hard drive contents, and we recommend such preservation of the raw data to all users, so footage can be re-imported later using different settings (e.g., a higher bitrate for more detail) if needed.

## **1.7 Results**

We tested our hardware system and VidSync with 1,010 measurements of objects of known length in the University of Alaska Fairbanks swimming pool (Table 1.2). We examined the effects of various factors on precision and accuracy at the intended working distance of our hardware ( $< 1.5$  m) and at greater distances. We calculated all measurements with each of two calibrations to learn how calibration distance affects accuracy. In Calibration A, the calibration frame was centered 0.6 m from the cameras,

and the front face grid minus the top row filled the screen view. Calibration B was centered 0.9 m from the cameras, with the entire calibration frame visible but occupying a much smaller portion of the screen. Calibration A was closer to the intended working distance of our system, so we used it for all analyses shown here, except that a row of results from Calibration B is included to show how accuracy at longer distances may be improved by calibrating at longer distances.

### 1.7.1 Precision and accuracy of length measurements

For the pool test, we used sections of the distortion correction chessboard in 4 different lengths as measurement targets, held still or nearly still in front of our stationary camera system. The grid's precise design and sharp corners provided unambiguous endpoints and dimensions. Measurements were grouped by their estimated distance  $d$  from the midpoint between the cameras, with four distance categories determined by the position of the calibration frame during Calibration A: 1) measurements closer to the cameras than the front face of the frame,  $0.142 \text{ m} \leq d < 0.389 \text{ m}$ ; 2) within the “calibrated range” between the front and back of the frame,  $0.389 \text{ m} \leq d < 0.828 \text{ m}$ ; 3) close behind the frame,  $0.828 \text{ m} \leq d < 2.000 \text{ m}$ ; and 4) far behind the frame,  $2.000 \text{ m} \leq d \leq 7.058 \text{ m}$ .

Our hardware was configured to measure small objects close to the cameras, via our choice of camera separation, calibration frame dimensions, and the position of Calibration A. In our most relevant test of this application, 618 measurements of 50.8 mm targets within 2 m of the cameras had mean absolute errors  $< 0.5 \text{ mm}$ —less than one percent of the target length. For all target lengths, accuracy (small absolute errors) and precision (small standard deviations) decreased as distance from the cameras increased (Fig. 1.7). At all distances, measurements of longer objects were less accurate and precise in absolute length units, but most remained within 1% of the true target length. When we recalculated all measurements using Calibration B, precision and accuracy were improved at long distance but reduced slightly in the region closest to the cameras. We found no negative effect of measuring lengths at oblique angles of up to 50 degrees from the cameras (Fig. 1.8a).

Length measurements of real fish were less precise than measurements of our chessboard, because they included more sources of uncertainty, such as the flexing of a fish's body. In a test of 10 repeated measurements of three juvenile Chinook salmon 0.5 m from the cameras, we measured lengths (mean  $\pm$  sd) of  $54.5 \pm 1.6$  mm,  $57.3 \pm 1.5$  mm, and  $54.8 \pm 0.8$  mm. These contrast with a standard deviation of only 0.23 mm for an artificial target of similar length, measured at similar distances, in our pool test (Table 1.2).

### 1.7.2 Distortion correction effectiveness

Distortion corrections applied to measurements from the pool test video reduced the value of the distortion cost function (Equation (1.2) by 97.7% for the left camera and 99.2% for the right camera. The cost function is based on the residuals from a straight line regressed through each set of plumbline corners, so it reflects both distortion and random variation in the detected chessboard corner coordinates. These results indicate a near-complete elimination of the systematic distortion, which is visually evident by comparing the barrel distortion in Fig. 1.1*b* to the corrected grid in Fig. 1.1*d*. Parameter estimates, and the point corrections calculated from them, were similar across several images of the chessboard at different distances, provided the board was close enough to fill the screen. Parameter estimates were less consistent when the board did not fill the screen (data not shown), suggesting that complete screen coverage is important for obtaining the best parameters (see Fig. 1.1*a* for an ideal image of the chessboard).

To diagnose any uncorrected effects of radial distortion on length measurements, Fig. 1.8*b* plots absolute error against the maximum distance of each measurement's endpoints from the principal point, or center of distortion, in either camera. During our early investigation of simpler distortion models, this type of plot revealed a clear increase in absolute error for measurements near the edge of the screen (data not shown). The absence of that trend from this figure suggests that the current model adequately mitigates distortion.



### 1.7.3 Diagnostic “error” measures

By design, the two “error” measures provided for each 3-D point by VidSync do not estimate the actual error in the 3-D measurement, and they are not visibly related to the small, random errors in good measurements (Fig. 1.9). Instead, they help diagnose large errors arising from data entry mistakes or calibration problems. In our pool test, examining points with the highest reprojection errors revealed several points for which the target (a chessboard corner) had been poorly located. The reprojection error also indicated groups of measurements taken while the target was moving slightly, creating a minor but detectable motion parallax error. Although they are useful, these diagnostic measures must not be interpreted as literally quantifying measurement error – they are no substitute for comparing measurements against a test target of known length.

## 1.8 Discussion

VidSync made 3-D measurements with high precision and accuracy—generally within 1% of the true length of the measured object (Table 1.2). Its advances in usability, softening the learning curve and speeding up repetitive tasks, are evident in our description of its features. We also demonstrated its capacity to process large quantities of data, such as the 1,010 length measurements used for our accuracy test. Our test results provided insight into the hardware and procedural design tradeoffs that affect VidSync’s accuracy and precision. There is no single best design for all projects, so we described the system in a manner that allows researchers to optimize the method for their particular circumstances.

We learned that our own design left room for improvement, and our tests did not quite reach the maximum limit of accuracy possible with VidSync. Foremost, our calibration frame (Fig. 1.4) could have benefitted from the improvements shown in the recommended design (Fig. 1.3). Also, we would have filmed progressive-scan instead of interlaced video if it were possible with our cameras. Finally, we would have placed our cameras farther apart for higher accuracy, if not for our project-specific need to fit the system into unusually tight spaces with fish very close to the cameras.

### **1.8.1 Comparison to other visual measurement methods**

Videogrammetry has many advantages over traditional measurement methods. Other visual methods may rely on the variable estimation skills of observers, and even skilled observers were shown to be much less accurate than an early videogrammetry system (Harvey et al. 2001). Video also has qualitative benefits for both 3-D measurement and general observation. It is ideal for studying sensitive species with minimal disturbance. The ability to watch events repeatedly, and in slow motion, reveals important details that cannot be perceived in real time. Visual studies of animal behavior by human observers are often limited to one focal animal at a time (Dawkins 2007), but video allows detailed analysis for all on-camera animals simultaneously, providing a complete account of the interactions among all visible animals. Finally, video preserves a permanent record of animal behavior and our initial interpretations for later review and analysis.

There are many other videogrammetric and related photogrammetric methods (see Harvey et al. (2010) for a review), but VidSync differs from them in terms of precision and accuracy, limiting assumptions, and software implementation. In contrast to the intent of VidSync as a general-purpose videogrammetric tool, many other methods were designed for specific tasks, with restrictive assumptions that limit their general applicability. They may require cameras with parallel optical axes (Boisclair 1992; Petrell et al. 1997), or subjects with visible shadows against a flat surface (Laurel et al. 2005) or a dorsal view presented to the cameras (Dunbrack 2006). Each method is suited to its intended purpose, but few qualify as flexible, general-purpose videogrammetric systems. Hughes and Kelly (1996b) developed one such system, which was our starting point for developing VidSync. We used its original concept of projecting screen coordinates onto two planes in world space and intersecting the lines of sight defined by points in the front and back planes. Other methods implicitly assume light travels in a straight line from the subject to the camera housings. The two-plane method does not make this assumption, so it is suited to aquatic applications that involve measuring through air-water interfaces such as the side of a tank. However, the form of the method implemented by Hughes and

Kelly (1996b) allowed measurement only within the volume occupied by the calibration frame at the time of calibration, a consequence of using polynomial fitting to convert screen coordinates to calibration frame face coordinates. Our method overcomes that major limitation by using linear transformations to convert those coordinates. Hughes and Kelly (1996b) reported mean errors in locating 3-D points of 4.7 mm with a standard deviation of 2.7 mm, more than the system we describe here. Their method has been used in other behavioral studies (e.g., Uglem et al. 2009; Piccolo et al. 2007), but its adoption has been limited by the lack of easy-to-use software and the restricted measurement volume.

We know of only one general-purpose system for videogrammetry with standalone software comparable to VidSync—a commercial software suite by SeaGIS ® (<http://www.seagis.com.au>) that includes their CAL calibration program and EventMeasure Stereo™ and PhotoMeasure™ measurement programs, which are mathematically based on a bundle adjustment method (Granshaw 1980). In a recent test (Harvey et al. 2010), this system's accuracy and precision were very close to those of VidSync. The mean absolute error was 0.5 mm for measurements of a 50.5 mm-long target within 1 to 3 m from the cameras, close to our mean absolute error of 0.37 mm for a 50.8 mm-long target within 0.828 to 2 m from the cameras. Although their other tests were not directly comparable to ours, they summarized their results as being accurate to approximately 1% of the true length of the object being measured, similar to our results.

Since both systems are very accurate, their main differences are in their features and the limiting assumptions of their calibration methods. The SeaGIS ® programs are commercial Windows applications, while VidSync is a free, open-source Mac OS X application, so its methods are transparent and modifiable. VidSync's two-plane calibration method is uniquely compatible with systems of 3+ cameras and is preferable for filming through air-water interfaces. We also argue that VidSync's usability (Table 1.3) make it simpler, faster, more precise, and better organized than other tools, thereby expanding the application of videogrammetry to studies that require larger sample sizes and more complex analyses.

One feature notably absent from VidSync and other comparable tools is automated object tracking. It was not included, in part because underwater tracking of fish in visually complex environments poses many problems that are difficult to solve in a general-purpose way (see Trucco and Plakas (2006) for a review of underwater tracking technology), and also because most work we envision requires elements of human judgment for the foreseeable future. However, VidSync is primed for future implementation of tracking features because it already incorporates the OpenCV computer vision library, which contains tracking functions. As an open source project, VidSync could be adapted to use these functions by anyone with the requisite expertise. Currently, other programs such as DLTv3 (Hedrick 2008) or custom implementations of task-specific tracking algorithms (Delcourt et al. 2009; Butail and Paley 2012) may be better suited for very high-volume 3-D motion-capture measurements of certain conspicuous targets.

### **1.8.2 Measurement error**

Absolute errors in measurement increased as the distance from the cameras increased, and as the length of the target increased (Table 1.2). The increase with distance is intuitive, but it is less obvious why error increases with target length. Harvey et al. (2010) noted that, “It has not been unequivocally demonstrated whether error is absolute (i.e. constant irrespective of the length of the object) or relative to the length of the object being measured.” We think different sources of error scale in different ways, some of which depend on the length of the object being measured. Some errors result from random factors specific to each point measurement, especially when the target is visually ambiguous (e.g., the fork of a translucent fish tail). Similar uncertainty can arise from motion blur, camouflage, a high-contrast background, turbidity, poor lighting, image noise, poor image resolution, video interlacing, or occlusion by closer objects. These random errors should not logically scale with the length of the object.

Each system is also subject to systematic errors. Inevitable imperfections in the calibration frame, including both the design and the digitization in VidSync, result in a

reconstructed 3-D space that is slightly warped compared to the real space it is meant to represent. Uncorrected components of non-linear distortion may have a similar effect. Other systematic errors are more situational; for example, misalignment of the cameras in between calibration and measurement can warp the reconstructed space. Another potentially systematic error arises if the cameras or target objects are moving. When video clips are synchronized to the nearest frame, they are still out of sync by up to one-half the duration of a frame, averaging one-quarter frame. In video shot at 30 frames per second, the average position error in one camera is equivalent to the distance the object moved in one-quarter frame, or  $1/120$  s. This motion-dependent error is termed motion parallax (Harvey and Shortis 1996) or synchronization error (Hughes and Kelly 1996b). These systematic errors, particularly those related to the calibration, explain why absolute length errors increase with target length. Consider measuring a 100 mm fish and a 200 mm fish at the same location in an imperfectly reconstructed 3-D space, which is slightly stretched compared to real space such that the 100 mm fish is measured as 101 mm. The front and back halves of the 200 mm fish would likewise measure as 101 mm, giving a total length of 202 mm – twice the absolute error as for the shorter fish, but a similar percentage error. Although the errors in our test system were small, they were clearly target-length-dependent (Table 1.2), suggesting that they were caused more by systematic errors than random errors. This understanding emphasizes the importance of constructing the calibration frame with precision and digitizing it carefully.

Both random and systematic errors increase with distance. Random errors in screen coordinates cause uncertainty in the angle of the 3-D line of sight, which corresponds to a small spatial uncertainty close to the cameras, and a much larger one far away. Also, the lines of sight from multiple cameras converge at a narrower angle for more distant targets, so small angular uncertainty in each line of sight leads to a larger uncertainty in their intersection than it does for nearby targets. Finally, systematic errors associated with imperfections in the calibration frame should also scale with distance outside the frame, because small imperfections will be extrapolated outward into larger ones.

### 1.8.3 Applications

Various 3-D videogrammetric methods have been used in ecological research for remote length measurement (Petrell et al. 1997; Shieh and Petrell 1998), biomass estimation (Lines et al. 2001), habitat mapping (Shortis et al. 2007b), abundance surveys (Williams et al. 2010), mapping foraging behaviors (Hughes et al. 2003; Piccolo et al. 2007; Piccolo et al. 2008); and for studying the kinematics of swimming maneuvers (Hughes and Kelly 1996b; Butail and Paley 2012), octopus grasping (Yekutieli et al. 2007), and insect flight (Hedrick 2008; Ardekani et al. 2013). VidSync is compatible with any such application, provided that the water is not too dark or turbid to observe targets clearly on video, and that the number of desired measurements does not require automated object tracking. VidSync's applicability is best described in general terms: it is equally useful to freshwater, saltwater, laboratory, or terrestrial environments, and it can be used by mobile or stationary observers. It measures 3-D positions with precise timestamps, allowing users to derive not only spatial quantities such as length, area, and volume, but also spatiotemporal measurements such as rates, including velocity and acceleration. VidSync directly records only positions, timestamps, and lengths, but it structures and exports that information so that users can easily calculate derived quantities such as volume and acceleration in whatever analytical software they prefer.

We have emphasized 3-D applications of VidSync, but its customizable video playback and hierarchical measurement organization are equally useful for other video analyses. Without any calibration, it can be used as an event logger for single video clips or several synchronized ones, allowing users to save the screen positions and timecodes of observations for easy retrieval or export. Our method of correcting non-linear distortion using plumblines can be applied to single cameras for 2-D analyses, from which the corrected screen coordinates can be exported for 2-D spatial analysis in other programs. This makes VidSync a feature-rich video player and annotator for 2-D analyses of one or more videos—much more efficient than standard methods such as saving still frames of all observations to measure in an image analysis program.

## 1.9 Conclusions

Researchers have barely tapped the quantifiable visual information available on fish and their interactions with their environment, in part because it is difficult to measure and organize these data efficiently and accurately in large quantities. Past advances in videogrammetry have alleviated these problems to some extent, but such work has typically emphasized precision and accuracy more than practical considerations about procedural ease, speed, and cost of use. We think these issues of usability are key reasons videogrammetric methods are underused in fishery research despite the knowledge, for many years, that they are more accurate than human-estimation alternatives. Furthermore, improvements to usability not only encourage the adoption of these more accurate methods, but also expand the quantity and complexity of data that can be collected and questions that can be asked. We have strongly emphasized this quality in both the design of VidSync and the focus of this paper on questions of practical value, such as field protocol and optimal design and use of calibration frames. Usability has not come at the expense of accuracy and precision; VidSync matches or surpasses contemporary alternatives in both respects. The idea of spatial measurement from video is not new, but we have addressed the main weakness of earlier methods by designing an accurate system that emphasizes usability and opens the door to new, data-hungry research questions.

## 1.10 Acknowledgments

This work was supported by the Arctic-Yukon-Kuskokwim Sustainable Salmon Initiative, the Institute of Arctic Biology, Alaska EPSCoR NSF award #OIA-1208927 and the state of Alaska, and the Department of Biology and College of Natural Sciences and Mathematics at the University of Alaska Fairbanks. Lon Kelly contributed to the early development of the mathematical methods underlying VidSync. Megan Perry, Aurélian Vivancos, Darren Whitehead, and Erik Schoen tested prototypes of VidSync and contributed ideas about software and calibration frame design. David Neuswanger

and Milo Adkison helpfully critiqued the manuscript. This work was conducted under IACUC protocols #134754-1 and #175627-1. Any use of trade, product, or firm names in this publication is for descriptive purposes only and does not imply endorsement by the U.S. Government.

### **1.11 References**

Ardekani, R., Biyani, A., Dalton, J., Saltz, J., Arbeitman, M., Tower, J., Nuzhdin, S., and Tavaré, S. 2013. Three-dimensional tracking and behaviour monitoring of multiple fruit flies. *J. Roy. Soc., Interface* 10(78): 20120547.

Boisclair, D. 1992. An evaluation of the stereocinematographic method to estimate fish swimming speed. *Can. J. Fish. Aquat. Sci.* 49(3): 523-531.

Brown, D. 1966. Decentering distortion of lenses. *Photogramm. Eng.* 32(3): 444-462.

Butail, S., and Paley, D. 2012. Three-dimensional reconstruction of the fast-start swimming kinematics of densely schooling fish. *J. Roy. Soc., Interface* 9(66): 77-88.

Dawkins, M. S. 2007. *Observing animal behaviour: design and analysis of quantitative data*. Oxford University Press, Oxford.

Delcourt, J., Becco, C., Vandewalle, N., and Poncin, P. 2009. A video multitracking system for quantification of individual behavior in a large fish shoal: Advantages and limits. *Behav. Res. Meth.* 41(1): 228-235.

Dunbrack, R. 2006. In situ measurement of fish body length using perspective-based remote stereo-video. *Fish Res* 82(1-3): 327-331.



Ellender, B., Becker, A., Weyl, O., and Swartz, E. 2012. Underwater video analysis as a non-destructive alternative to electrofishing for sampling imperilled headwater stream fishes. *Aquat. Conserv.* 22(1): 58-65.

Fischer, P., Weber, A., Heine, G., and Weber, H. 2007. Habitat structure and fish: assessing the role of habitat complexity for fish using a small, semiportable, 3-D underwater observatory. *Limnol. Oceanogr.: Methods* 5: 250-262.

Granshaw, S. 1980. Bundle adjustment methods in engineering photogrammetry. *Photogramm. Rec.* 10(56): 181-207.

Hartley, R., and Zisserman, A. 2004. Multiple view geometry in computer vision. Cambridge University Press, Cambridge.

Harvey, E., Fletcher, D., and Shortis, M. 2001. A comparison of the precision and accuracy of estimates of reef-fish lengths determined visually by divers with estimates produced by a stereo-video system. *Fish. Bull.* 99(1): 63-71.

Harvey, E., and Shortis, M. 1996. A system for stereo-video measurement of sub-tidal organisms. *Mar. Technol. Soc. J.* 29(4): 10-22.

Harvey, E., Goetze, J., McLaren, B., Langlois, T., and Shortis, M. 2010. Influence of range, angle of view, image resolution and image compression on underwater stereo-video measurements: high-definition and broadcast-resolution video cameras compared. *Mar. Technol. Soc. J.* 44(1): 75-85.

Hedrick, T. 2008. Software techniques for two- and three-dimensional kinematic measurements of biological and biomimetic systems. *Bioinspiration Biomimetics* 3(3): 034001.

Hughes, N. F., Hayes, J. W., Shearer, K. A., and Young, R. G. 2003. Testing a model of drift-feeding using three-dimensional videography of wild brown trout, *Salmo trutta*, in a New Zealand river. Can. J. Fish. Aquat. Sci. 60(12): 1462-1476.

Hughes, N. F., and Kelly, L. H. 1996a. A hydrodynamic model for estimating the energetic cost of swimming maneuvers from a description of their geometry and dynamics. Can. J. Fish. Aquat. Sci. 53(11): 2484-2493.

Hughes, N. F., and Kelly, L. H. 1996b. New techniques for 3-D video tracking of fish swimming movements in still or flowing water. Can. J. Fish. Aquat. Sci. 53(11): 2473-2483.

Laurel, B., and Brown, J. 2006. Influence of cruising and ambush predators on 3-dimensional habitat use in age 0 juvenile Atlantic cod *Gadus morhua*. J. Exp. Mar. Biol. Ecol. 329(1): 34-46.

Laurel, B., Laurel, C., Brown, J., and Gregory, R. 2005. A new technique to gather 3-D spatial information using a single camera. J. Fish. Biol. 66(2): 429-441.

Lines, J., Tillett, R., Ross, L., Chan, D., Hockaday, S., and Mcfarlane, N. 2001. An automatic image-based system for estimating the mass of free-swimming fish. Comput. Electron. Agr. 31(2): 151-168.

Mallon, J., and Whelan, P. F. 2004. Precise radial un-distortion of images. Pattern Recognition, 2004. ICPR 2004. Proceedings of the 17th International Conference on 1: 18-21 Vol. 1.

- Mussi, M., Mcfarland, W., and Domenici, P. 2005. Visual cues eliciting the feeding reaction of a planktivorous fish swimming in a current. *J. Exp. Biol.* 208(Pt 5): 831-842. doi:10.1242/jeb.01406.
- Nelder, J., and Mead, R. 1965. A simplex method for function minimization. *Comput. J.* 7: 308-313.
- Petrell, R., Shi, X., Ward, R., Naiberg, A., and Savage, C. 1997. Determining fish size and swimming speed in cages and tanks using simple video techniques. *Aquacult Eng* 16(1-2): 63-84.
- Piccolo, J. J., Hughes, N. F., and Bryant, M. D. 2008. Water velocity influences prey detection and capture by drift-feeding juvenile coho salmon (*Oncorhynchus kisutch*) and steelhead (*Oncorhynchus mykiss irideus*). *Can. J. Fish. Aquat. Sci.* 65(2): 266-275.
- Piccolo, J. J., Hughes, N. F., and Bryant, M. D. 2007. The effects of water depth on prey detection and capture by juvenile coho salmon and steelhead. *Ecol Freshw Fish* 16(3): 432-441.
- Potel, M. J., and Wassersug, R. J. 1981. Computer tools for the analysis of schooling. *Environ. Biol. Fish.* 6(1): 15-19.
- Shieh, A., and Petrell, R. 1998. Measurement of fish size in Atlantic salmon (*Salmo salar* L.) cages using stereographic video techniques. *Aquacult Eng* 17(1): 29-43.
- Shortis, M., Harvey, E., and Abdo, D. 2009. A review of underwater stereo-image measurement for marine biology and ecology applications. *Oceanogr. Mar. Biol.* 47: 257-292.

Shortis, M., Harvey, E., and Seager, J. 2007a. A review of the status and trends in underwater videometric measurement. SPIE Conference 6491 Videometrics IX: 26.

Shortis, M., Seager, J., Williams, A., Barker, B., and Sherlock, M. 2007b. A towed body stereo-video system for deep water benthic habitat surveys. Eighth Conf. Optical 150-157.

Trucco, E., and Plakas, K. 2006. Video tracking: A concise survey. IEEE J Ocean Eng 31(2): 520-529.

Uglem, I., Kjorsvik, E., Gruven, K., and Lamberg, A. 2009. Behavioural variation in cultivated juvenile Atlantic cod (*Gadus morhua* L.) in relation to stocking density and size disparity. Appl. Anim. Behav. Sci. 117(3-4): 201-209.

Williams, K., Rooper, C., and Towler, R. 2010. Use of stereo camera systems for assessment of rockfish abundance in untrawlable areas and for recording pollock behavior during midwater trawls. Fish. Bull. 108(3): 352-362.

Yekutieli, Y., Mitelman, R., Hochner, B., and Flash, T. 2007. Analyzing octopus movements using three-dimensional reconstruction. J. Neurophysiol. 98(3): 1775-1790.

## 1.12 Tables

Table 1.1. Example protocol for filming fish behavior *in situ* for analysis in VidSync

Description of step	
1 <b>Evaluate site suitability.</b> Individual protocols should list study-specific biological criteria as well as video quality criteria (e.g., lighting, field of view, background, contrast, obstructions between cameras and fish).	
2 <b>Verify lenses are clean</b> of debris or residue.	
3 <b>Clean and re-grease the waterproof housing O-rings.</b>	
4 <b>Turn the cameras on.</b>	
5 <b>Write down the current time and remaining battery life</b> if the cameras are to be deployed until batteries die.	
6 <b>Manually focus</b> both cameras for the intended subject distance. A camera's displayed focus distances aren't correct for shooting through a housing into water; develop custom focus distances by testing beforehand.	
7 <b>Place cameras in housings</b> and double-check fasteners.	
8 <b>Place a desiccant packet</b> in the housings to prevent condensation-caused fogging in cold water.	
9 <b>Verify the zoom setting</b> on both cameras (usually, widest angle). Keep zoom and focus fixed hereafter.	
10 <b>Start recording. Write down the time</b> , so video timecodes can be linked to real times and noteworthy observations (e.g., a loud boat passing by).	
11 <b>Videotape a whiteboard with site name &amp; date.</b> This prevents confusion when naming or reorganizing video files. Site name may correspond to a GPS waypoint name.	

Table 1.1 continued...

- 
- 12 **Blink an LED light** once, in view of all cameras, for synchronizing video clips in VidSync.
  - 13 **Videotape the checkerboard in each camera separately** with both board and cameras submerged. It should face each camera as flatly as possible, and be far enough away to be in focus, but close enough to fill the screen. Avoid the uneven lighting of bright sunlight under a wavy surface, and seek to film in bright shade.
  - 14 **Videotape the calibration frame** with similar lighting, with both frame and cameras as still as possible, making sure both faces are close enough to the cameras to take up a reasonably large portion of the screen. Only one ideal shot is needed, but try many poses to assure a good view. Allow time for settling of any disturbed detritus that might block the view of the frame nodes.
  - 15 **Verify that the cameras are still set properly**, double-checking recording status, zoom, and focus.
  - 16 **Deploy the cameras** to observe fish, securing the system as needed.
- ... Individual protocols should describe additional measurements (e.g., drift net samples, temperature measurements, above-water site photographs) to be taken during filming at each video site.
- 

**Note:** This protocol was designed for using a side-by-side stereo camera system in a river, but it is easily modified for other filming situations.

Table 1.2. Summary of 1,010 measurements of objects of 4 known lengths at various distances

True length (mm)	Distance $d$ from cameras (m)	n	Calibration A			Calibration B	
			Mean error (mm)	Mean abs error (mm)	Std dev (mm)	Mean abs % error	Mean abs % error
50.8	$0.142 \leq d < 0.389$	119	-0.02	0.16	0.19	0.30%	0.40%
	$0.389 \leq d < 0.828$	371	0.13	0.22	0.23	0.40%	0.50%
	$0.828 \leq d < 2.000$	128	0.37	0.43	0.44	0.90%	0.70%
	$2.000 \leq d < 7.058$	70	0.95	1.01	1.07	2.00%	1.40%
152.4	$0.142 \leq d < 0.389$	30	-0.07	0.45	0.49	0.30%	0.40%
	$0.389 \leq d < 0.828$	31	0.26	0.59	0.62	0.40%	0.40%
	$0.828 \leq d < 2.000$	31	0.98	0.99	0.68	0.70%	0.60%
	$2.000 \leq d < 7.058$	30	1.53	1.69	1.44	1.10%	0.60%
381	$0.389 \leq d < 0.828$	33	1.69	1.69	0.39	0.40%	0.60%
	$0.828 \leq d < 2.000$	44	1.88	2.46	1.95	0.70%	0.70%
	$2.000 \leq d < 7.058$	30	5.95	5.95	2.63	1.60%	0.60%
	$0.389 \leq d < 0.828$	31	1.02	1.06	0.87	0.20%	0.10%
596.9	$0.828 \leq d < 2.000$	31	3.28	3.28	2.43	0.60%	0.20%
	$2.000 \leq d < 7.058$	31	5.91	6.06	3.71	1.00%	0.40%

**Note:** Measurements were binned into four ranges of estimated distance  $d$  from the midpoint between the cameras. No measurements are shown for the largest 2 targets at the smallest distance range because they did not fit within the field of view at that distance. Metrics of accuracy and precision included the mean error (measured length - true length), mean absolute error (absolute value of error), standard deviation of the measured length, and mean absolute error as a percentage of the true length. All metrics are shown for Calibration A. To show the effect of calibration distance on errors, the exact same measurements were recalculated for comparison using Calibration B, which was obtained with the calibration frame 0.3 m farther from the cameras than in Calibration A.

Table 1.3. Some usability features of VidSync’s measurement process.

<b>Task simplified</b>	<b>VidSync usability features</b>
Locating things to measure	<ul style="list-style-type: none"> <li>– Fine-scale controls with keyboard shortcuts allow custom playback at any speed, and random or interval sampling.</li> <li>– Mouse wheel steps through the video frame-by-frame.</li> <li>– Non-measurement text annotations mark items of interest.</li> <li>– “Hint lines” find matching objects in other views.</li> </ul>
Editing past measurements	<ul style="list-style-type: none"> <li>– Measurements are organized in an intuitive hierarchy of objects (e.g. fish) and events (e.g. conflicts).</li> <li>– Retrieve measurements through tables or clicking markers on video.</li> </ul>
Inputting precise spatial coordinates	<ul style="list-style-type: none"> <li>– Arrow keys relocate input with sub-pixel precision.</li> <li>– Magnified preview shows precise measurement location clearly.</li> </ul>
Initiating new measurements	<ul style="list-style-type: none"> <li>– New events are auto-created by clicking on video, if input for the previous event is complete.</li> </ul>
Interpreting past measurements	<ul style="list-style-type: none"> <li>– Measurement marker size, color, and shape code measurement type.</li> </ul>
Data organization and sharing	<ul style="list-style-type: none"> <li>– Full analysis is self-contained in one file.</li> <li>– Reusable information (e.g., calibrations and object/event types) can be exported separately for sharing across projects.</li> <li>– Full object and event hierarchy is exported in CSV or XML files.</li> </ul>



### 1.13 Figures

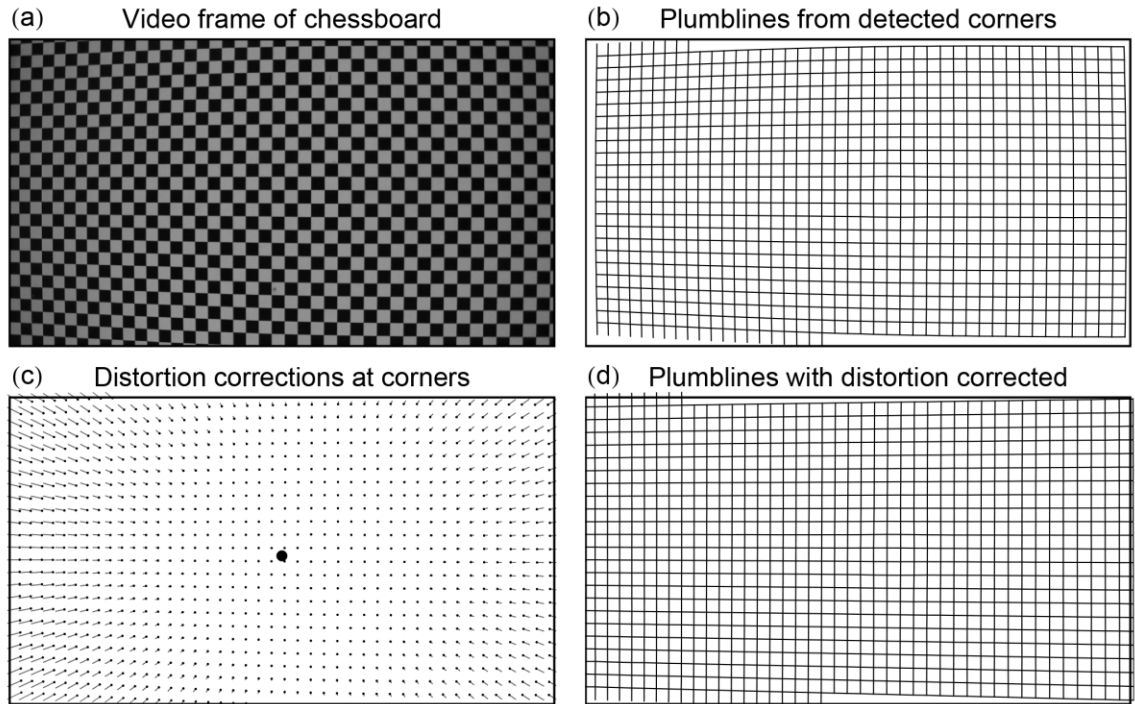


Fig. 1.1. Correcting non-linear distortion. (a) A sign printed with a chessboard pattern is filmed close enough to fill the screen. (b) VidSync detects corners of the chessboard and arranges them into plumblines for estimating the distortion model parameters. (c) Lines radiating from the principal point (large black dot) show the magnitude and direction of distortion correction from each detected chessboard corner. (d) Applying the correction to the original plumblines has straightened them. Some corrected coordinates lie outside the original boundary of the image.

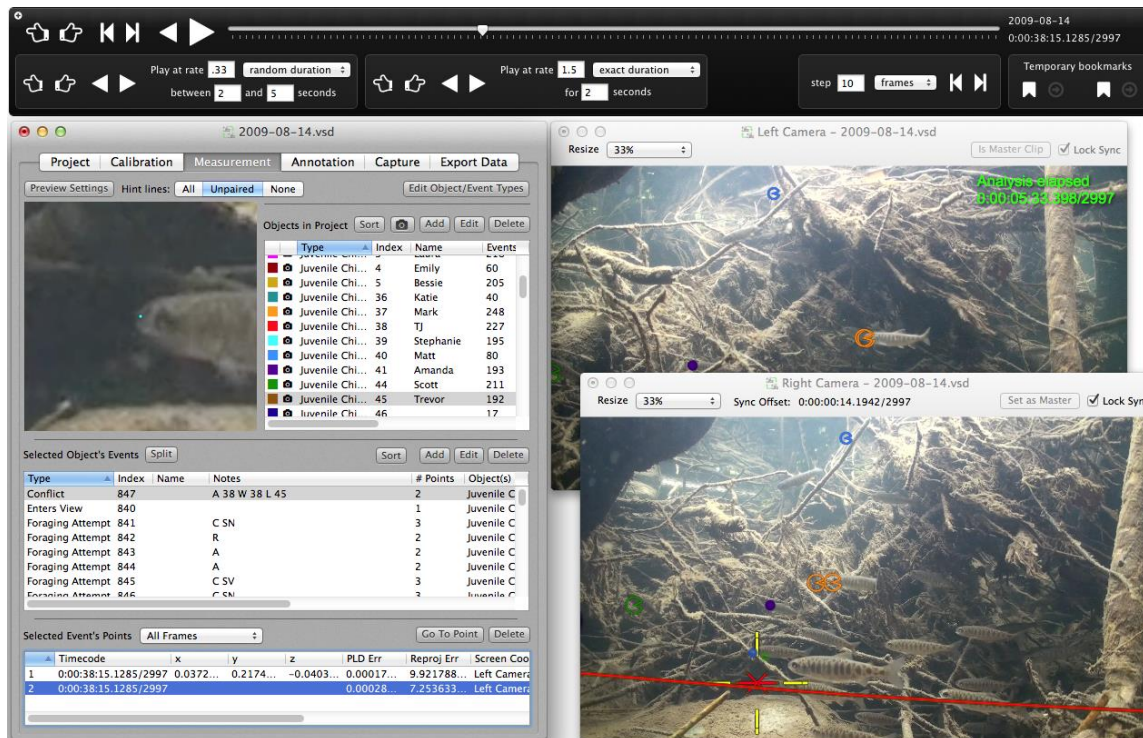


Fig. 1.2. The VidSync measurement interface. The tables in the main window list the objects in the project, the events for the selected object, and the measurements for each event. The video windows on the right are typically larger, but were sized down to fit on this page. Circular symbols mark foraging attempts recorded on recent frames, and the red asterisk in the top video framed by the yellow cross (i.e. selected) marks a new measurement of a conflict, which has not yet been input on the lower video. The yellow lines around it indicate that it is selected, and its position is reflected in the magnified preview in the main window. The red hint line in the lower video window shows potential positions of the conflict measurement in that camera, to help locate the same event from a different perspective view.

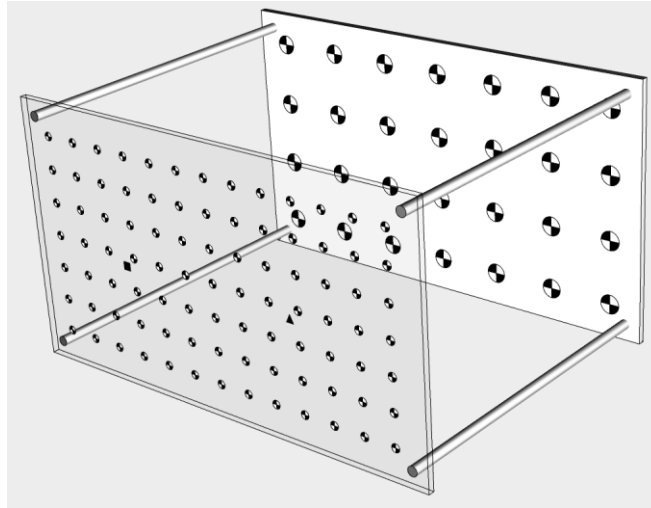


Fig. 1.3. General-purpose calibration frame for two side-by-side cameras. The cameras view it at a close enough distance that the opaque back face fills most of the screen in each camera. Not all of the nodes on the transparent front face are visible in each camera, so the density of nodes there is higher, and some irregular shapes are printed as reference points to indicate which nodes are visible. Nodes are marked at known coordinates on the outside of the front surface, and, with larger markers for greater visibility, on the inside of the back surface. Node markers are preferably checkered so their precise center is easily located, but solid circles are adequate. The dimensions of the calibration frame depends on its intended application, with larger frames preferred for long-distance measurement.

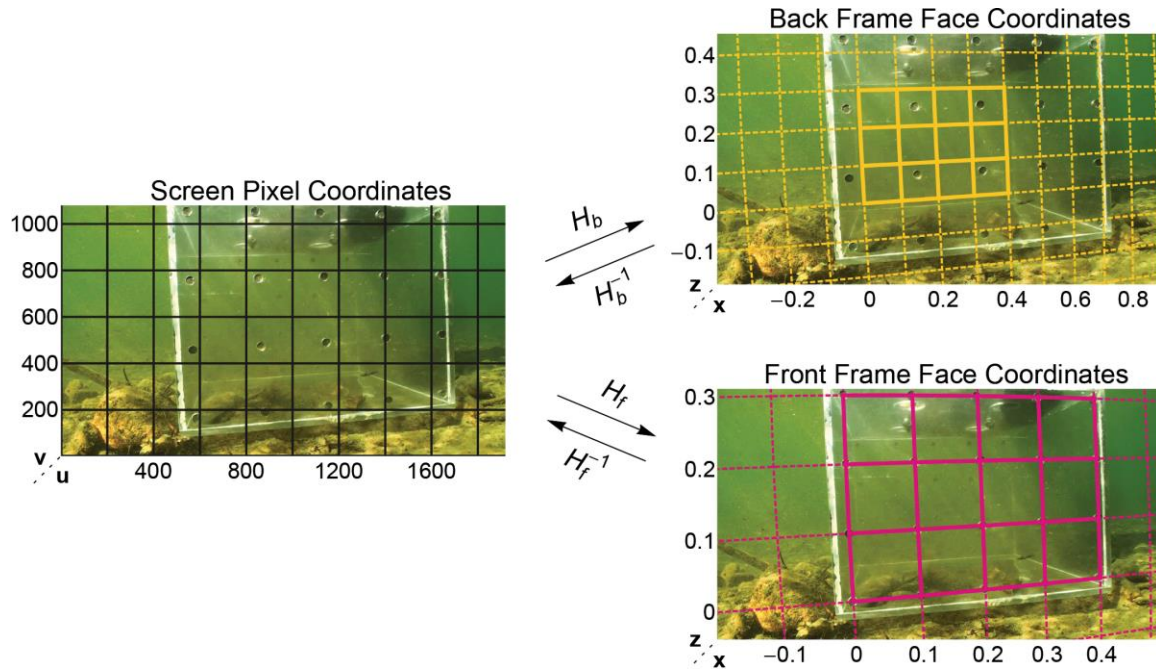


Fig. 1.4. Screen and calibration frame coordinate systems. A single image is overlaid with the  $(u, v)$  pixel coordinates in which input is received and the  $(x, z)$  world coordinates (in meters) in the 2-D planes of the front ( $y = 0$ ) and back ( $y = 0.439$ ) faces of the calibration frame. The homographies calculated during this calibration step convert between these coordinate systems as shown, and they remain valid for measurement throughout the video (note the identical grid overlays in Fig. 1.5). Some nodes on the back face were not clearly visible, a common problem that prompted our suggestion of an improved frame design in Fig. 1.3. However, an adequate calibration was completed with the visible nodes.

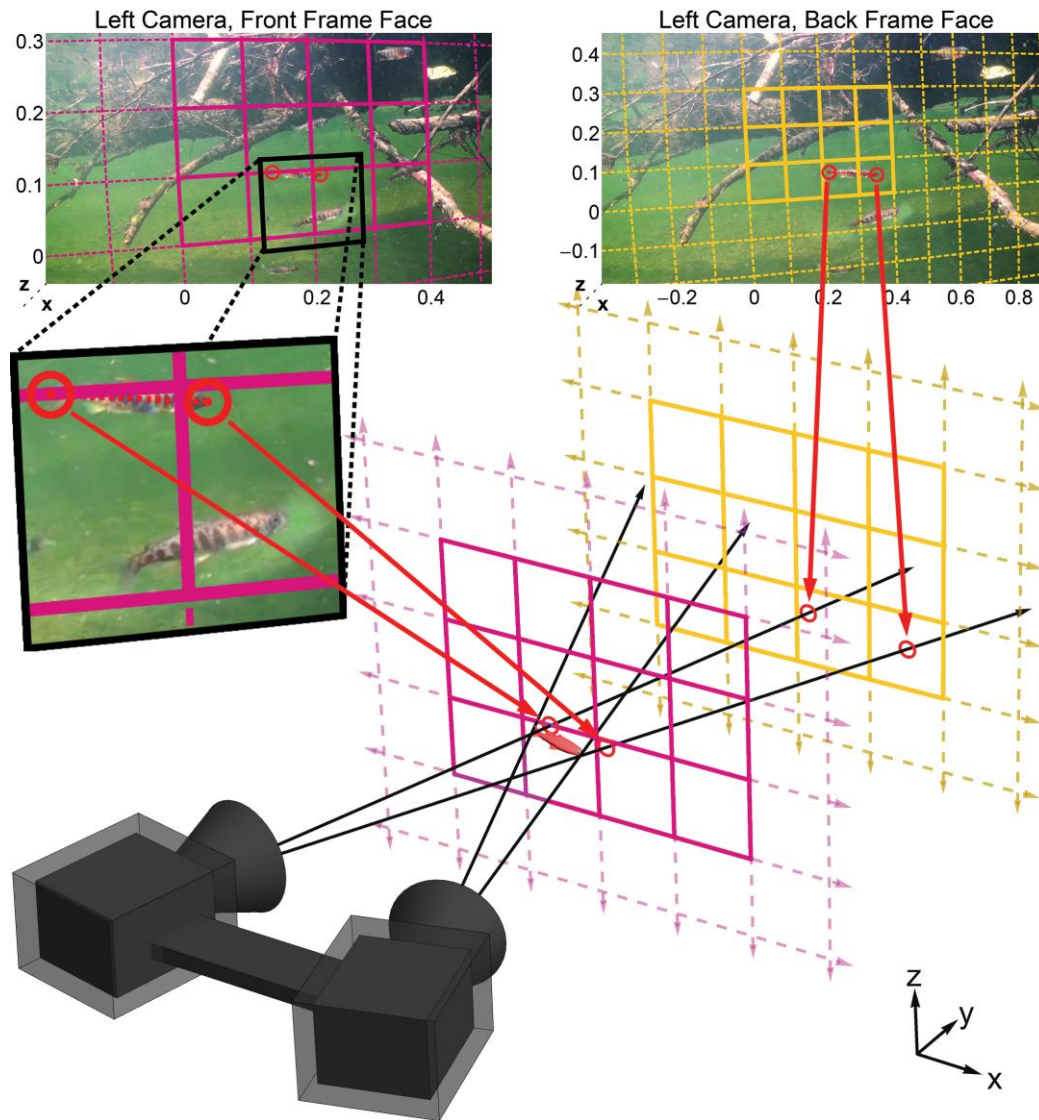


Fig. 1.5. Obtaining 3-D world coordinates to measure fish length. In the left camera, the user clicks on the fish's head and tail. Those clicks (red circles) are expressed in  $(x, z)$  coordinates in the planes of the front and back faces of the calibration frame, using the homographies described in Fig. 1.4. Each of the two 2-D points (head and tail) is converted into two 3-D points using the known  $y$  coordinates of the front and back frame faces. Mapped out in 3-D, these points define the line of sight from the camera through the fish's head and tail. The 3-D positions of the head and tail are measured as the

estimated intersection of each line with the corresponding line from the other camera.

The fish's length is the Euclidean distance between its head and tail points.





Fig. 1.6. Deployed stereo camera system. Also shown is each camera's view of a rootwad and associated juvenile Chinook salmon. In this slow-water set, the blue ratchet strap attached to a log behind the cameras was sufficient to hold them steady. Some extraneous attachments are visible, but are not described in our text because they are not all necessary and will vary with each study's needs.

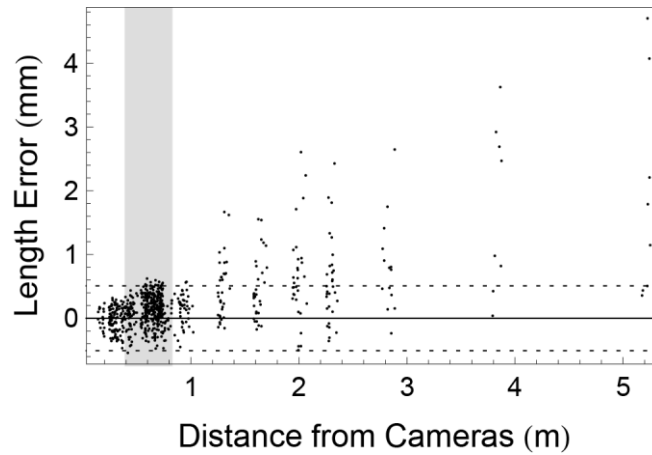


Fig. 1.7. Length errors (VidSync-measured length minus true length) in measuring a 50.8mm object. Camera distance is measured from the midpoint of the length measurement to the midpoint between the cameras. The calibrated distance range, shaded in gray, is defined by the front and back plane positions of the calibration frame at the time of calibration. The dotted lines mark a threshold of 1% error in the length measurement.



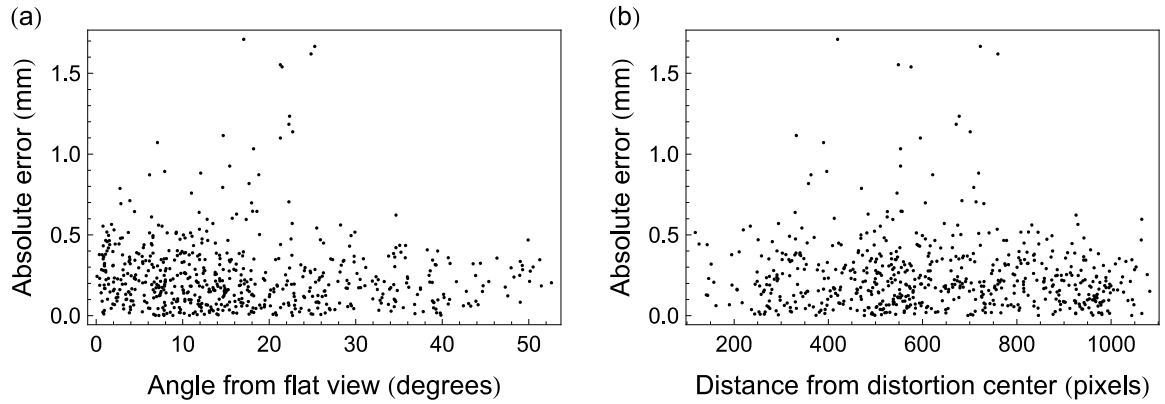


Fig. 1.8. Relation between absolute error and (a) the maximum angle between the target and either of the cameras, and (b) the maximum distance of one of the measurement's endpoints from the principal point, or center of distortion, in that camera. Both plots use only data from 50.8mm targets within 2 m of the cameras, to reduce confounding effects of larger sources of error, such as distance from the cameras.

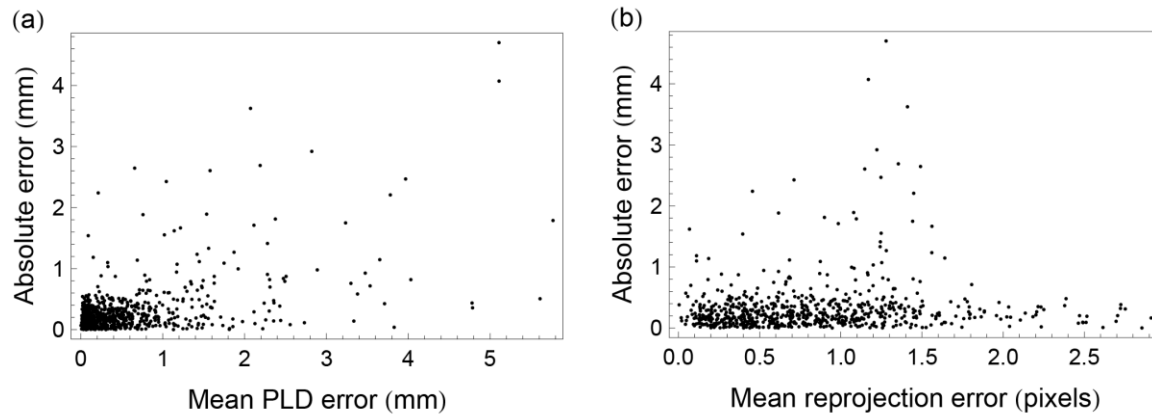


Fig. 1.9. Error metrics. The absolute error in length measurement of a 50.8mm object, at a variety of distances, is compared to VidSync's "error" measures, (a) the mean point-line distance (PLD) and (b) the mean reprojection error, each of which is averaged here over the two endpoints for each length measurement. These data show that the error metrics reported by VidSync are diagnostic tools, not measures of the actual measurement error.

## Appendix 1.A

### Correcting refraction of the back plane points in a transparent calibration frame

Calibration frames with a transparent front face are appealing because of their potential precision and durability, but they introduce a small error that warrants correction. During calibration, light from the back surface passes through the front surface en route to the cameras, and it is refracted twice—as it enters and leaves that material—altering the apparent position of the points on the back face. These errors were on the order of 0.1 to 1mm in our system, but importantly they are not random noise: their main effect is a slight apparent magnification of the entire back face, which substantially affects 3-D measurements. To eliminate this problem, consider a set of screen coordinates that were input by clicking on the refracted image of a back frame node during calibration. Because the frame is physically absent during later measurements, the calibration homographies should be calculated not with the real physical coordinates of the frame node's true position, but instead with its apparent position: the physical coordinates in the back frame face plane that would correspond to the same screen coordinates in the absence of the front face's refractive effect. For example, if a back frame node were physically located at  $(x, z) = (0.4, 0.3)$ , the correct homographies would map its screen coordinates not to  $(0.4, 0.3)$ , but instead to its apparent position such as  $(0.4008, 0.3004)$ .

This adjustment requires calculating the apparent position of a point  $B$  on the back frame plane, as viewed from a camera located at point  $C$ . A light ray traveling from  $B$  to  $C$  enters the front frame plane material at unknown point  $P_1$  on the  $B$  side and exits at unknown point  $P_2$  on the  $C$  side, so the full path of the light ray from  $B$  to  $C$  is  $\vec{v}_1 + \vec{v}_2 + \vec{v}_3$ , where  $\vec{v}_1$  is a vector from  $B$  to  $P_1$ ,  $\vec{v}_2$  is from  $P_1$  to  $P_2$ , and  $\vec{v}_3$  is from  $P_2$  to  $C$ . Let  $\eta_2$  be the refractive index of the medium through which  $\vec{v}_2$  passes (the transparent frame

material), while  $\vec{v}_1$  and  $\vec{v}_3$  pass through (usually the same) media such as water, with refractive indices  $\eta_1$  and  $\eta_3$ .

Although VidSync performs this calculation with any coordinate orientation, assume for this explanation that the frame surfaces are parallel to the  $x$ - $z$  plane, with known  $y$  coordinates. A unit vector normal to those planes is  $\hat{n} = (0, 1, 0)$ . Let subscripts  $x$ ,  $y$ , and  $z$  denote their respective elements of the subscripted points. Having measured the thickness of the front frame material,  $P_{1y}$  and  $P_{2y}$  are known, and the unknowns are  $P_{1x}$ ,  $P_{1z}$ ,  $P_{2x}$ , and  $P_{2z}$ . These are calculated using Snell's law of refraction, which governs the angles (relative to the surface normal vector) at which light enters and leaves a surface. Let the ray coming from  $B$  enter the first interface at angle  $\theta_1$  from the normal and exit at  $\theta_2$ . It enters the second interface at the same angle  $\theta_2$  (because the surfaces are parallel) and exits at  $\theta_3$ , pointing toward  $C$ . These angles may be expressed in terms of the defined vectors as:

$$(1.7) \quad \theta_i = \cos^{-1} \left( \frac{\vec{v}_i \cdot \hat{n}}{\|\vec{v}_i\|_2} \right)$$

These are used to write a system of four equations that depend on the four unknowns:

$$(1.8) \quad \begin{aligned} \eta_1 \sin \theta_1 &= \eta_2 \sin \theta_2 \\ \eta_2 \sin \theta_2 &= \eta_3 \sin \theta_3 \\ (\vec{v}_1 \times \hat{n}) \cdot \vec{v}_2 &= 0 \\ (\vec{v}_2 \times \hat{n}) \cdot \vec{v}_3 &= 0 \end{aligned}$$

The first two equations are the familiar form of Snell's law of refraction. The others specify that the light ray leaving each surface lies in the plane spanned by the normal vector and the ray that entered the surface (so the ray bends directly toward or away from the normal, rather than rotating around it).

VidSync solves this system for  $P_{1x}$ ,  $P_{1z}$ ,  $P_{2x}$ , and  $P_{2z}$  using a discretized version of the Hybrid algorithm for multidimensional root-finding, specifically the `gsl_multiroot_fsolver_hybrids` function of the GNU Scientific Library (<http://www.gnu.org/software/gsl/>). The points  $C$  and now-known  $P_2$  define the camera's

line of sight to the apparent position of the back frame point, which is recorded as the  $(x, z)$  coordinates at which that line passes through the  $y$  coordinate of the back frame plane. This apparent position is then used to calculate the calibration homography for the back frame surface.

VidSync users applying this correction need only specify the thickness of their front frame surface and refractive index of the medium (water or air) and frame material. Indices for several common materials are listed in the program. The correction can be disabled for users of wireframe-type calibration frames. Although the process described here is a type of refraction correction, it is specific to the described situation, and does not apply directly to the problem of correcting refraction through aquarium walls. However, analogous mathematics could be employed to extend VidSync for that purpose, and VidSync's two-plane calibration method is less sensitive to that problem than other common methods.



## CHAPTER 2:

### **Mechanisms of drift-feeding behavior in juvenile Chinook salmon and the role of inedible debris in a clear-water Alaskan Stream<sup>1</sup>**

#### **2.1 Abstract**

Drift-feeding fish are challenged to discriminate between prey and similar-sized particles of debris, which are ubiquitous even in clear-water streams. Spending time and energy pursuing debris mistaken as prey could affect fish growth and the fitness potential of different foraging strategies. Our goal was to determine the extent to which debris influences drift-feeding fish in clear water under low-flow conditions when the distracting effect of debris should be at a minimum. We used high-definition video to measure the reactions of drift-feeding juvenile Chinook salmon (*Oncorhynchus tshawytscha*) to natural debris and prey *in situ* in the Chena River, Alaska. Among all potential food items fish pursued, 52% were captured and quickly expelled from the mouth, 39% were visually inspected but not captured, and only 9% were ingested. Foraging attempt rate was only moderately correlated with ingestion rate (Kendall's  $\tau = 0.55$ ), raising concerns about the common use of foraging attempts as a presumed index of foraging success. The total time fish spent handling debris increased linearly with foraging attempt rate and ranged between 4% and 25% of total foraging time among observed groups. Our results help motivate a revised theoretical view of drift feeding that emphasizes prey detection and discrimination, incorporating ideas from signal detection theory and the study of visual attention in cognitive ecology. We discuss how these ideas

---

<sup>1</sup> Neuswanger, J., Wipfli, M. S., Rosenberger, A. E., and Hughes, N. F. 2014. Mechanisms of drift-feeding behavior in juvenile Chinook salmon and the role of inedible debris in a clear-water Alaskan stream. *Environ. Biol. Fish.* 97(5): 489-503. doi:10.1007/s10641-014-0227-x.

could lead to better explanations and predictions of the spatial behavior, prey selection, and energy intake of drift-feeding fish.

## 2.2 Introduction

Drift feeding is a foraging tactic used by many fishes in flowing water, in which they hold a steady upstream-facing position and visually search for drifting prey to intercept (Jenkins 1969). Visual searches in general are hindered by the presence of abundant non-target objects that resemble targets (Palmer 1995), so drift feeding by fish may be hindered by fine particles of leaf litter, insect exuviae, and other inedible debris that can resemble prey. Under certain light conditions, underwater video captures the remarkable visual prominence of debris, even in water that appears extremely clear (Fig. 2.1). It seems challenging for drift-feeding fish to locate viable prey amidst this dynamic field of distracting debris in the brief moment before it passes their position. However, the effects of debris have received little attention in the voluminous literature on prey detection and the energy budgets of drift-feeding fish.

Only one study to date has measured how debris affects drift-feeding behavior. In an artificial stream, adult Arctic grayling (*Thymallus arcticus*) reacted to prey at shorter distances and narrower angles in the presence of debris compared with prey-only controls (O'Brien and Showalter 1993). Just as fish may overlook distant prey in the presence of debris, they may also commit the opposite error—mistaking debris for prey and spending time and energy pursuing it. Many researchers have noted the occurrence of unsuccessful foraging attempts in which drift-feeding fish either captured and expelled inedible items or investigated items they did not attempt to capture (e.g. Irvine and Northcote 1982; Bachman 1984; McNicol et al. 1985; Kiflawi and Genin 1997). However, the frequency of unsuccessful foraging attempts has not been reported, so we do not yet understand their energetic costs or implications for drift-feeding theory.



Hypotheses about the effects of debris on drift-feeding fish may be informed by two studies of recently emerged age-0 brook trout (*Salvelinus fontinalis*) in still water. In a lake, age-0 brook trout ingested only 46% of items they captured (Biro et al. 1996). In still pools along the margins of streams, age-0 brook trout ingested 80% of items they captured, but they had captured only 54% of the items they attacked (McLaughlin et al. 2000). Foraging attempt rate (McLaughlin et al. 2000) and capture rate (Biro et al. 1996) were only moderate predictors of the rate at which real prey were ingested, casting doubt on the reliability of foraging attempt rate as a commonly used index of foraging success. Fish in flowing water might have to contend with much more mid-water debris than fish in still water, because particles in streams are easily re-suspended by turbulence and can travel hundreds of meters before settling (Webster et al. 1999). Because of this debris density, and the difficulty of discriminating among objects moving at high speed, we anticipate that drift-feeding fish pursue and reject far more mid-water debris than their still-water counterparts.

Visually or physically reacting to debris might affect the profitability of different foraging strategies, creating behavioral tradeoffs. An overly discriminating fish might fail to react to actual prey, while an overly aggressive one might waste too much time pursuing debris. All else being equal, a fish feeding in swift current encounters more prey than it would in slow current, but it has less time to distinguish prey from debris, creating a speed-accuracy tradeoff (Abbott and Sherratt 2013). Further tradeoffs might arise from the constraint that animals have limited visual attention—the cognitive mechanism that “turns looking into seeing” (Carrasco 2011). Selectively allocating attention among different prey types or different regions of the visual field might improve a fish’s ability to discriminate between debris and prey, but only for the selected prey types or visual angles. When discrimination is difficult, attention tradeoffs can lead to search image formation (Dukas and Kamil 2001), which might explain why drift-feeding salmonids often temporarily specialize on a single prey type, even when many others are available (Allen 1941; Bryan and Larkin 1972; Bisson 1978; Ringler 1979; Ringler 1985).

Mechanistic models that simulate drift-feeding processes (e.g., Hughes and Dill 1990; Dunbrack 1992; Kiflawi and Genin 1997; Guensch et al. 2001) might benefit from incorporating debris-related tradeoffs. Such models have diverse applications including predicting habitat quality (Nislow et al. 2000; Jenkins and Keeley 2010), microhabitat selection (Guensch et al. 2001; Grossman et al. 2002; Hayes et al. 2007), prey selection (Grant and Noakes 1986; Hughes et al. 2003), and growth (Fausch 1984; Hayes et al. 2000). Foraging models are frequently important components of broader, individual-based models that simulate the population-level consequences of mechanisms that act on individuals (Van Winkle et al. 1998; Gowan and Fausch 2002; Harvey and Railsback 2007). Drift-feeding model predictions can depend on the time and energy fish spend pursuing and manipulating prey, but current models do not include the analogous costs of handling debris.

Current mechanistic drift-feeding models also disregard the potential for debris to hinder prey detection by attention-limited fish. Incorporating this effect might resolve a long-recognized problem with one of the models' key functions: predicting the distance at which fish react to prey. Visual acuity alone does not fully determine reaction distance, because reaction distance decreases as current velocity increases under otherwise identical visual conditions (Hill and Grossman 1993; O'Brien and Showalter 1993; Piccolo et al. 2008a). Mechanistic drift-feeding models capture this dependence on water velocity by using rigid geometric assumptions (Hughes and Dill 1990) that consistently fail observational tests (Hughes et al. 2003). An alternative explanation for the velocity relationship is that fish with finite visual attention can only productively search and discriminate prey from debris within a limited volume of water per unit time, so fish in swifter current must focus on a smaller region to maintain their ability to detect prey (Dukas 2002). This idea represents a crucial shift in perspective, viewing not only physical but also cognitive constraints as key determinants of the behavior and success of drift-feeding fish. However, we lack quantitative data regarding whether wild, drift-

feeding fish react to debris to an extent that warrants such a fundamental change in our mechanistic understanding.

To measure the influence of debris on drift-feeding fish under low-flow conditions, we observed the reactions of juvenile Chinook salmon (*Oncorhynchus tshawytscha*) to natural prey and debris in the main channel of a mid-order clear-water stream. We sought to 1) measure how many foraging attempts were directed at debris versus prey, 2) measure the spatial and temporal characteristics of these attempts to assess their relevance to foraging models, 3) determine whether foraging attempt rate predicts ingestion rate, and 4) measure the variation in these responses within and among groups of fish under different conditions. The first and third objectives partly mirror Biro et al. (1996) and McLaughlin et al. (2000), but differ in our focus on a different species, exhibiting a different type of feeding behavior, in flowing instead of still water, and over a longer period of time. We discuss what our findings imply about the interpretation of drift-feeding behavior, and we outline some ways drift-feeding theory might be improved by incorporating the tradeoffs involved in detecting prey amidst debris under the constraint of limited visual attention.

## **2.3 Materials and methods**

### **2.3.1 Study system**

The Chena River is a clear-water, 5<sup>th</sup>-order tributary of the Tanana River in the Yukon River drainage in central Alaska. We observed fish in 2009 and 2010 in a reach from 100 to 160 km upstream from the confluence of the Chena with the Tanana. Median discharge in this reach from June through September was 25 m<sup>3</sup>/s (calculated using 1968 to 2011 data from USGS hydrograph #15493000 near Two Rivers, AK). Drift nets samples collected from this reach contained an amount of debris similar to that observed in many other clear-water streams throughout Alaska and the Pacific northwest (M. Wipfli, personal observation), suggesting that the Chena is representative of “typical”

debris conditions. Most prey-sized debris particles were fragments of plant matter in varied shapes and shades of brown. A much smaller but substantial portion consisted of insect exuviae, noteworthy for their resemblance to the insects that shed them.

The stream-type Chinook salmon in the Chena emerge from the gravel in late May and early June, feed all summer and overwinter in the river system, and then migrate downstream to the Bering Sea the following spring. In this river, their diverse diet of aquatic and terrestrial invertebrates is dominated by the aquatic families Chironomidae (Diptera), Chloroperlidae (Plecoptera), and Baetidae (Ephemeroptera) in the 1- to 5-mm length range, although many other taxa are locally important at times (Gutierrez 2011).

We chose specific observation sites within our study reach by locating schools of foraging juvenile Chinook salmon in positions amenable to capturing video footage with enough detail to discern foraging attempt outcomes. Visual criteria included the uniformity and brightness of lighting, proximity of fish to a possible camera mounting point, and field-of-view. We chose schools of fish associated with well-defined structures along the margins of the river, such as root wads or gaps inside logjams, because such schools reliably returned to their positions after we disturbed them by placing the cameras. The depths at all observations sites were much greater than the prey reaction distances of fish, so depth did not constrain prey captures. All recordings were made in low flow conditions (below median summer flow) when water was clear (Fig. 2.1*a*). Within these practical constraints, we chose sites and times to represent a broad range of water depths, current velocities, water temperatures, and dates (Table 2.1). Each sampling date represents observations of a single group of fish.

### **2.3.2 Video recording and processing**

We recorded schools of drift-feeding fish at close range (0.2 to 2 m) using a stationary stereo pair of Sony® HDR-SR12 high-definition digital video cameras inside Ikelite® #6038.94 underwater housings with Zen Underwater® WAVP-80 wide-angle dome ports. Videos were analyzed using VidSync software (<http://www.vidsync.org>),

which allows calculating 3-dimensional (3-D) positions from multiple camera views with sub-millimeter precision, organizing measurements according to object (e.g., individual fish) and measurement type (e.g., a foraging attempt or a fish fork length), coding of measurements (e.g., foraging attempt outcomes), and fine-scale playback control with a magnified preview of an area of interest (J. Neuswanger, Chapter 1, this dissertation). Despite cautious site selection and high quality cameras, many videos did not capture the fine detail necessary to discern the outcomes of most foraging attempts; therefore, we analyzed only the nearest several (five to twelve) fish to the cameras in each of the five best recordings, totaling 35 individual fish. These videos were representative of typical behavior observed qualitatively under a wider range of conditions.

In each video selected for analysis, a starting time was chosen at least ten minutes after the last visible disturbance associated with camera placement, by which time the fish had resumed pre-disturbance position and behavior for several minutes. A subject fish was chosen and its activity recorded until at least 25 foraging attempts were measured, or until it swam off-screen permanently. Some fish that swam off-screen returned later and were identified by their parr marks, in which case analysis continued and the missed time was noted. Each fish's length was measured as the distance between the tip of its upper jaw and the fork of its tail when its body was nearly straight. Rates (e.g., foraging attempts per minute) were calculated based on the amount of time each fish was observed on screen. In addition to fish data, we calculated a mean water velocity vector for the foraging area by averaging the trajectories of 10 natural debris particles.

To gauge the potential effects of competition on debris reactions, we calculated nearest-neighbor distances for all visible fish in each school we analyzed. These were the 3-D Euclidean distances from the tip of the snout of each fish to that of its nearest neighbor. Nearest-neighbor distances were calculated from video frames at five-minute intervals throughout an approximately 90-minute period. These calculations included, but were not limited to, the specific individuals and time ranges for which detailed foraging records were obtained.

### **2.3.3 Classifying foraging attempt outcomes**

We classified all foraging attempts with discernable outcomes into three mutually exclusive categories: 1) “inspections,” in which fish moved to investigate items but did not capture them; 2) “expulsions,” in which fish captured and then expelled items from their mouths (colloquially, “spit them out”); and 3) “ingestions,” in which fish captured items they did not appear to expel. Inspections and expulsions were both types of “rejections,” and expulsions and ingestions were both types of “captures.” Rejected items were assumed to be debris, although a few might be unpalatable prey. Any foraging maneuver culminating in the fish widely opening its mouth was assumed to be a capture, because we observed no evidence of misses or evasive prey. When a foraging attempt’s outcome could not be discerned, it was classified as “unclear,” and was used for spatiotemporal and rate analyses (e.g., foraging attempts per second) but not for analyses of outcomes. Observational ambiguity persisted in some of the attempts we deemed discernable, which motivated the development of detailed classification conventions designed to err (when unavoidable) toward conservatively estimating the fish’s time, energy, and attentive involvement with debris.

#### **2.3.3.1 Inspections**

Fish made a range of motions that did not culminate in opening their mouths to capture drifting items. Motions were classified as inspections of potential prey if they began and ended with sudden changes of body orientation or if the particles of interest were clearly visible. These stringent criteria were necessary to avoid counting both brief and extended motions made for other reasons. However, some confirmed captures would not have met these criteria, so it is likely that inspections were undercounted and our numbers represent only the most unambiguously observable portion of a continuum of

debris-related distractions ranging from quick visual fixations (with no body motion at all) to pursuits lasting several seconds.

### **2.3.3.2 Expulsions**

We directly observed many particles expelled from the mouths of fish after capture. However, despite our use of modern high-definition cameras, video quality still limited our ability to visually confirm expulsions. Many expulsions required repeated viewings in slow motion at 2.5x magnification, and in some cases, we could not see the expelled particle at all. However, the motion characteristic of confirmed expulsions was distinctive—opening and closing the mouth one time, approximately 1 s (range 0.5-3 s) after capture. For fish of which we had superb views (those very close to the cameras and well-illuminated against a dark, low-contrast background), this characteristic motion was almost always associated with a visibly expelled particle. We therefore considered observations of this motion to be indirect observations of expulsion. However, a few indirectly observed expulsions might have actually been swallowing manipulations; likewise, some subtle expulsions may have been missed and reported as ingestions. Both errors were probably rare and should partially offset each other.

### **2.3.3.3 Ingestions**

In straightforward observations of ingestions, particles were clearly captured without expulsion or further manipulation. In other cases, fish repeatedly and irregularly opened and closed their mouths after capture, as if manipulating an item to swallow. These manipulations very rarely culminated in visible particle expulsions, so we classified them as ingestions unless an expelled particle was visible. We assumed all ingested items were prey, in agreement with a concurrent diet study that found almost no debris in the stomachs of juvenile Chinook salmon from the same population (Gutierrez 2011).

### 2.3.4 Spatiotemporal measurements of foraging attempts

To measure the trajectories and elapsed times for different stages of each foraging attempt, we recorded timecodes (to the nearest frame, i.e. 1/30 s) and 3-D coordinates of fish position (measured at the tip of the upper jaw) at multiple points of interest. Foraging attempts that occurred off-screen in one camera but on-screen in another were used to calculate times but not distances. Making the assumption that fish reacted to items immediately upon detecting them, we recorded detection positions in the frame immediately preceding movement toward an item. We then recorded either capture position (in the first frame with maximum mouth gape during capture) or visual rejection position (in the frame preceding a turn away from the item). When particles were captured and either expelled or extensively manipulated for ingestion, we recorded the end of involvement (the first frame of maximum mouth gape during expulsion or the last of a series of manipulations for ingestion). These measurement conventions conservatively estimated total involvement time for both captures and inspections, effectively assuming that all time before the first motion and after the maximum mouth gape or shift of direction was available for searching for other items. Use of conservative estimates seemed justified based on occasional observations of back-to-back foraging attempts separated by less than 1/15 s.

For each foraging attempt measured as described above, we calculated pursuit time, pursuit distance, and pursuit speed based the difference between the reaction position and the capture or visual rejection position. We calculated the time to expel an item as the elapsed time between capture and expulsion. We calculated how far downstream the fish pursued the item as the shortest distance from the capture position to a plane passing through the detection position perpendicular to the mean current velocity vector. We estimated detection distance under the assumptions that the trajectory of the particle followed the mean current velocity vector through the foraging area, and that the particle was at the fish's position at the time of capture (a valid assumption) or the time at which point the fish turned away from it (only sometimes valid). From that position, the



particle's position was back-calculated along the mean velocity vector to the point in time at which the fish first reacted; this was taken to be the position of the particle at detection, and the distance between this point and the fish's position at detection was taken to be the detection distance.

### **2.3.5 Statistical analysis**

To describe the relative magnitude of variation in prey capture outcomes among individuals within a group, compared to variation across different groups (which were each filmed on different dates, in different sites), we used two logistic regressions with group and individual as nominal independent variables. One regression was performed on all discernable-outcome foraging attempts, with capture as the dependent variable. The other was performed on all captures, with ingestion as the dependent variable. We reported results from deviance tables for these regressions, roughly analogous to sums of squares in ANOVA models for continuous predictors.

To evaluate foraging attempt rate as a predictor of ingestion rate, we replicated the way Biro et al. (1996) and McLaughlin et al. (2000) used distribution-free regression and correlation analysis (Hollander and Wolfe 1999), because it is not strongly affected by the part-whole correlation between ingestions (the “part”) and total foraging attempts (the “whole” of which ingestions are a part) (Biro et al. 1996). We calculated Kendall's population correlation coefficient  $\tau$ , a rank comparison statistic with a value of 0 if foraging attempt rate and ingestion rate are independent. This coefficient determines the more easily interpreted distribution-free parameter  $Y=(1+\tau)/2$ , which represents the probability that an individual fish with a higher attempt rate than another individual also had a higher ingestion rate. A value of  $Y=0.5$  would indicate that attempt rate had no value as a predictor of ingestion rate. To calculate the slope and intercept of the relationship between foraging attempt rate and ingestion rate, we used distribution-free regression based on the Theil statistic  $C$ .

Additional statistics supported two minor points. We used the Kruskal-Wallis test (Kutner et al. 2005) to determine whether the pursuit time (the time between reacting to an item and capturing or visually rejecting it) differed between all captures and all visual rejections on each date, as might be expected if more convincingly prey-like items elicit a response from a greater distance. Also, we used standard, parametric linear regression to test the significance of a relationship between the daily means of foraging attempt rate and the time spent handling items.

## 2.4 Results

We observed 35 fish on five separate dates making a total of 930 foraging attempts, of which 837 had discernible outcomes and 867 had usable 3-D spatial coordinates (were not partially off-screen). Almost all foraging took place in mid-water. Only seven attempts were directed toward the surface, and three were aimed at benthic targets. Fish moved only  $4.4 \pm 3.1$  cm (mean  $\pm$  standard deviation) during foraging attempts (Fig. 2.2a), which terminated in capture or visual rejection at a distance of  $0.8 \pm 2.8$  cm downstream of the detection position (i.e., downstream of a plane passing through the detection position perpendicular to the current direction) (Fig. 2.2b). Items were pursued at a speed of  $6.3 \pm 3.6$  cm/s. Particles were detected from an estimated distance of  $6.3 \pm 3.7$  cm, and 99% of items were detected within 17.1 cm (Fig. 2.2c).

Overall, fish captured 61% of the items to which they visibly reacted, and they ingested 15% of the items they captured. Combined, 9.4% of all foraging attempts led to ingestion, 52.0% led to capture and expulsion, and 38.6% were inspections without capture. These results were qualitatively similar for all five groups of fish (Fig. 2.3a). The probability of an attempt culminating in capture varied to a similar degree within and among groups of fish (logistic regression,  $N=837$ , deviance within groups = 44.1, deviance among groups = 41.9, residual deviance = 1030.4). The probability of ingestion following capture varied more within groups than among groups (logistic regression,

$N=514$ , deviance within groups = 39.5, deviance among groups = 8.9, residual deviance = 392.6).

The proportion of total foraging time spent pursuing and manipulating items (percent handling time) ranged between 4.5% and 27.1% for different groups of fish (Table 2.2), and most of that time (3.5% to 24.9%) was spent handling debris items that were inspected without capture or captured and expelled (Fig. 2.3*b*). The mean handling time per item was 1.16 s. This mean was fairly consistent among groups (ranging from 0.94 to 1.29 s), which implies that the large variation in overall percent handling time resulted mostly from the large variation in foraging attempt rate, with which the percent handling time increased linearly (linear regression,  $R^2=0.86$ ;  $N=5$ ;  $P=0.02$ ).

Subdividing handling time by activity shows that foraging attempts with stages beyond the initial pursuit contributed disproportionately to total percent handling time. The overall time between reacting to an item and capturing or visually rejecting it was  $0.72 \pm 0.34$  s (mean  $\pm$  standard deviation, Fig. 2.2*d*) and did not differ significantly between captures and visual rejections (Kruskal-Wallis tests for each date individually,  $P > 0.25$  in all cases). Expelling a captured item took  $0.67 \pm 0.47$  s (Fig. 2.2*e*), and the relatively rare events in which an item was repeatedly manipulated prior to assumed ingestion took  $3.53 \pm 1.93$  s. Handling time did not appear to continue beyond the stages described above, as might be expected if fish waited to resume searching until they had returned to a focal position. Instead, fish often began a new pursuit immediately (within 1/15 s) following a rejection.

Foraging attempt rate was moderately related to ingestion rate across all fish combined ( $N = 35$ ). Kendall's  $\tau$  was 0.553 (95% C.I.: 0.358-0.748). The estimate of the probability  $Y$  that, in comparing two fish, the fish with the higher foraging attempt rate also had a higher ingestion rate was 0.78 (0.68-0.87). The distribution-free regression line for foraging attempt rate as a predictor of ingestion rate had a shallow slope of 0.108 (0.072-0.150) and an intercept of -0.019 (-0.249-0.060), indicating that foraging attempt rate greatly underestimated ingestion rate (Fig. 2.4).

## 2.5 Discussion

Under low-flow conditions in the clear-water Chena River, drift-feeding juvenile Chinook salmon pursued and captured far more debris than prey. Some observed groups spent enough time pursuing and processing debris to substantially reduce their energy intake rates. Analysis of deviance showed that the variation in debris pursuit behavior among groups of fish filmed on different dates (Fig. 2.3a) was smaller than the variation among individuals within groups (Fig. 2.3c), which suggests that water velocity, water temperature, and fish size and age did not greatly modulate the effect of debris within the range of conditions represented in our observations. Although this study was the first to measure a strong effect of debris on drift-feeding fish in the wild, it is consistent with still-water results (Biro et al. 1996; McLaughlin et al. 2000) and with qualitative observations of failed foraging attempts by drift-feeding fish (Irvine and Northcote 1982; Bachman 1984; Kiflawi and Genin 1997). Although debris effects likely vary among different streams, species, life stages, and environmental conditions, our demonstration of strong effects in a clear-water river under low-flow conditions suggests involvement with debris is often an unavoidable part of the drift-feeding process. The observed magnitude and likely generality of debris effects motivate consideration of the cognitive mechanisms underlying prey discrimination. In the section on attention and signal detection, we discuss how these cognitive concepts might form the foundation of new drift-feeding models that explain important empirical results current models either contradict or do not address.

### 2.5.1 Foraging attempt rate as a predictor of ingestion rate

We investigated two distinct aspects of the relationship between foraging attempts and ingestion. First, we found that foraging attempt rate (items/minute) was not a good direct estimate of ingestion rate (items/minute). The shallow slope (0.108) of the regression line in Fig. 2.4 indicated that attempt rate greatly overestimated ingestion rate,

a fact also reflected in the low frequency of ingestions (only 9%) among all foraging attempts.

The second distinct question was whether foraging attempt rate was sufficiently correlated with ingestion rate to be a useful predictor, despite its overestimation. In pairwise comparisons of all individual fish across all dates, the individual with the higher foraging attempt rate also had a higher ingestion rate with probability  $Y = 0.78$ , corresponding to a value of Kendall's population correlation coefficient  $\tau = 0.553$ . A similar result was reported for age-0 brook trout feeding in still-water streamside pools ( $Y = 0.76$ ; McLaughlin et al. [2000]), and for capture rate (not attempt rate) as a predictor of ingestion rate for age-0 brook trout in a lake ( $Y = 0.77$ ; Biro et al. [1996]). These results together suggest that foraging attempt rate and capture rate should be used cautiously, if at all, as predictors of ingestion rate (i.e. indices of fitness) in both still and flowing water.

Marked differences between our results and the above-cited still water studies are consistent with expected differences between the two habitats. Both still water studies reported that fish ingested more than 90% of items they captured mid-water, but overall ingestion frequencies were lower (46% in a lake, 80% in still pools) because fewer items captured from the surface were ingested (1% in a lake, about 60% in still pools). In our observations, which were almost all (830/837) mid-water, drift-feeding fish ingested far fewer—only 15%—of the items they captured. McLaughlin et al. (2000) also found that brook trout were less likely to ingest a captured item if they detected it while moving. This is consistent with our observation of a much lower mid-water ingestion frequency in drift-feeding fish, because flowing water guarantees motion between fish and prey. Further, drift-feeding fish have less time to inspect each item before losing the opportunity, and flowing water suspends more mid-water debris that would quickly settle out of still water.

### 2.5.2 Energy intake rate

The proportion of total foraging time fish spent handling debris (3.5% to 24.9%; Fig. 2.3*b*) corresponds to an equal reduction in search time and energy intake rate, assuming that search and handling are mutually exclusive activities. This assumption appeared valid in our videos; fish almost never changed course mid-pursuit to react to new items, nor did they react to new items prior to expelling captured items. The energy cost of maneuvering to intercept potential prey is higher than the cost of holding a steady position (Hughes and Kelly 1996), so spending almost 25% of all foraging time engaged in such maneuvers could decrease net energy intake beyond what would be expected from lost time alone. The time spent handling debris is important to foraging models that incorporate the logic of Holling's (1959) disc equation, which predicts that energy intake rate increases with prey encounter rate asymptotically, instead of linearly, because of handling time. However, we have shown that total handling time can depend more on debris encounters than prey encounters, so debris can greatly influence this functional response.

Spending a large percentage of time handling debris is not necessarily an ineffective feeding strategy. Instead, it can be a side effect of foraging in swifter current, which may increase prey encounter rate to a degree that compensates for the time lost handling debris. Two of the groups we studied (June 28 and September 15) exemplified this effect. They spent more time handling debris than the others because they were feeding in faster water (Table 2.1) and had higher overall foraging rates, which also led to higher ingestion rates (Table 2.2). In this case, debris did not eliminate the benefit of high overall encounter rate; it only reduced the potential benefit. This reduction should be incorporated into models of energy intake, which could overestimate energy intake by up to 33% if they ignore debris handling time. Bioenergetics models (e.g., Elliott and Hurley 1999) show that a difference of this magnitude in energy intake rate can make a large difference in growth rate.

### 2.5.3 Generality of debris effects

The effects of debris on drift feeding persisted under diverse conditions throughout the first summer of feeding for fish between 35 and 75 mm fork length (Table 2.2); debris likely affects most other drift-feeding fish, but to a highly variable degree. We detected no evidence that fish reacted to debris less often as they grew and gained experience (i.e., on later sampling dates; Fig. 2.3a), contrasting with the finding of McLaughlin et al. (2000) that larger brook trout within the 20- to 30-mm fork length range were more likely than smaller fish in that range to capture items they attacked and to ingest items they captured. Their finding may reflect larger fish learning to better discriminate prey without pursuit, developing improved eyesight, more effectively pursuing evasive prey, or any combination thereof. The absence of this size-based relationship in our data, despite our observing fish over a longer time period and size range, may reflect limited statistical power to detect this relationship in results dominated by larger sources of variation such as water velocity; or it may reflect the greater difficulty of discriminating prey while drift feeding compared to feeding in still water. Though encompassing a greater size range than prior studies, our observations were confined to young-of-the-year fish, and greater changes with size may be evident in other species that drift feed for more than one year.

In addition to visual and cognitive improvements with size and experience, we might expect the distracting effect of debris to diminish for larger fish that focus on larger prey, because larger debris is less abundant and larger fish might easily ignore debris smaller than their prey. However, larger fish often feed in faster water and have greater reaction distances, both of which may increase the debris encounter rate and make prey discrimination more difficult. Even for large trout feeding in water with extraordinarily scarce debris, the drifting exuviae of insect prey may trigger enough foraging attempts to substantially bias estimates of energy intake based on visual estimates of foraging attempt rate (John Hayes, Cawthron Institute, NZ, personal communication). The effect of debris on larger fish is therefore an open and interesting question.

The propensity of fish to pursue debris might also be increased by pressure from competitors. Pursued items were often detected at distances greater than half the mean distance between each fish and its nearest neighbor (Table 2.2), although not always in the direction of the nearest neighbor. This partial overlap of detection volumes led to very rare conflicts (four total observed) in which two fish pursued the same item simultaneously. The rarity of these conflicts, and the similar frequency of debris pursuits among groups with relatively large (i.e. July 9) and small (i.e. June 11) nearest-neighbor distances, suggest that competition did not greatly influence debris pursuits in our observations. The decision of whether or not to pursue each item was probably pressured more by the risk of the item drifting out of reach than by the risk of the item being captured by a competitor. This tradeoff could change in other groups with tighter spacing relative to individual reaction distances.

Our finding that debris is important even under clear, low-flow conditions suggests significant consequences for drift-feeding fish when disturbances introduce more debris. A high rate of debris pursuits was not detrimental to fish in our study because it was a consequence of a higher overall encounter rate in faster water, which also increased prey encounters. However, some disturbance events might increase debris without a proportional increase in prey, reducing foraging success. In a concurrent diet study of our study population, juvenile Chinook salmon had less food in their stomachs during floods (Gutierrez 2011). Further, Chinook salmon recruitment in the Chena River is significantly worse for year classes that experienced a high median flow during the summer they spent in freshwater, and this effect was not associated with extreme flood events (J. Neuswanger, Chapter 4, this dissertation). The negative effects of prolonged, moderately high water on primary productivity (Benson et al. 2013), foraging conditions (including debris density), or some combination thereof may strongly influence recruitment in this system.



#### **2.5.4 Limited attention and signal detection in drift feeding**

The difficulty experienced by juvenile Chinook salmon in discriminating prey from debris raises questions about the cognitive process of visual attention that controls prey detection and discrimination. Experiments have shown reduction in drift-feeding performance when predation risk (Metcalf et al. 1987), competition (Hazelton and Grossman 2009), or debris (O'Brien and Showalter 1993) compete with food for a fish's visual attention. Here we discuss how limited visual attention might influence the spatial behavior and prey selection tactics of drift-feeding fish and how an understanding of these effects might help resolve recognized problems with current drift-feeding models.

##### **2.5.4.1 Visual attention and the control of reaction volumes**

Empirical observations about the relationship between water velocity, reaction distance, and prey detection probability are central to the predictions of energy intake and habitat selection in drift-feeding models. Reaction volumes narrow as water velocity increases (Hill and Grossman 1993; O'Brien and Showalter 1993; Piccolo et al. 2008a), and detection probability within the reaction volume decreases (Piccolo et al. 2008a; Hazelton and Grossman 2009). When accurate representations of these relationships are needed for specific applications, they may be measured directly in the laboratory (Grossman et al. 2002; Piccolo et al. 2008b). This empirical approach complements theoretical attempts to predict and understand drift feeding more generally using mechanistic models.

In one mechanistic model on which several others have been based, Hughes and Dill (1990) reproduced the relationship between velocity and reaction distance using three restrictive geometric assumptions. Although these assumptions were recognized as unrealistic from the beginning, they were used for lack of plausible alternatives. The model assumed that fish 1) detect prey as soon as it enters their reaction volume, 2) move to intercept it at their maximum sustainable swimming speed, and 3) cannot intercept it if the water velocity is high enough to carry it downstream from their focal point before

they can reach it at that speed. Our results corroborated others (e.g., Hughes et al. 2003) in falsifying all three assumptions. Drift-feeding fish 1) detected prey at many distances and not just on the surface of a reaction volume (Fig. 2.2*c*), 2) intercepted prey at varied speeds (Fig. 2.2*f*), and 3) usually captured prey downstream of the point from which they reacted to it (Fig. 2.2*b*). The consistent failure of the above model's assumptions to match empirical data suggests they do not approximate the correct mechanism and a complete replacement is warranted.

A preliminary replacement model developed by N. Hughes and R. Dukas (unpublished manuscript), summarized by Dukas (2002), used a limit on spatial attention to explain the narrowing of reaction volumes with increased velocity in a manner consistent with several observations that contradicted the previous model. It also explained reduced detection probabilities with increased velocity, and the narrowing of reaction volumes with increased debris density observed in Arctic grayling by O'Brien and Showalter (1993). In their model, discriminating prey from debris was the most difficult (and therefore limiting) part of the visual search for prey. This is consistent with the "set size effect" observed in visual searches by humans and other animals, in which the time required to detect an inconspicuous target among distractors increases linearly with the number of distractors (Wolfe 1998; Nakayama and Martini 2011).

Our observations of frequent reactions to debris show that the ideas Hughes and Dukas explored remain promising, and their work showed that understanding the effects of debris could be critical for understanding the mechanisms underlying drift-feeding behavior. Some of this understanding may already exist from the study of analogous problems using signal detection theory (Wickens 2001), which describes the tradeoffs in searching for a signal amidst noise (e.g., prey amidst debris) and has proven useful for studying foraging on cryptic (Staddon and Gendron 1983), mimetic (Speed and Ruxton 2010), and masquerading prey (Skelhorn et al. 2010).

#### **2.5.4.2 Drift-feeding fish as signal detectors**

Signal detection theory is easily adapted to describe the tradeoffs in prey discrimination for drift-feeding fish (Grubb 2003). If some prey are visually indiscriminable from some debris as perceived by fish, then fish cannot detect all prey while rejecting all debris. They can accept all items of both types, or none of either, but any intermediate strategy involves pursuing the most prey-like debris (false positives), overlooking the most debris-like prey (missed detections), or both.

The discriminability of prey from debris depends on 1) the mean difference in appearance between them, 2) variability in visual characteristics among items within each type, 3) variability in how fish perceive each individual item as it drifts and tumbles through a complex visual field, and 4) the attributes of fish as signal receivers, including both their innate characteristics (e.g., sensory acuity and memory of prey appearance) and their behavioral allocation of time and attention. Fish might improve discriminability by devoting more visual attention to foraging instead of monitoring potential predators or competitors. To reduce perceptual uncertainty, fish might spend more time visually fixating on each item before pursuit, perhaps even foraging in slower current to allow longer fixations. Fish might also improve discriminability for certain types of prey, at the expense of others, by tuning their attention systems to respond more strongly to specific visual characteristics (“feature-based attention”; Carrasco 2011). When discrimination is difficult, individual fish might profitably focus feature-based attention on a single prey type of desirable abundance, energetic value, or conspicuousness, i.e., form a search image (Dukas and Kamil 2001).

Regardless of their behavioral strategies for influencing discriminability, fish must also choose how discriminating to actually be—a threshold level of some visual characteristic (or an analogous boundary for multiple characteristics) above which items are considered prey-like enough to pursue, and below which they are not. The choice of a discrimination threshold reflects a tradeoff between the costs of mistakenly pursuing debris and the costs of failing to detect real prey.

The resolution of signal detection tradeoffs by juvenile Chinook salmon in this study involved numerous false positives and much time spent pursuing debris. However, we qualitatively observed much more debris than the fish actually pursued, so they were not completely indiscriminating. Some studies of larger salmonids observed the opposite strategy—discriminating to the point that some individuals ate only a single type of prey when many others were available (Allen 1941; Bryan and Larkin 1972; Bisson 1978; Ringler 1979; Ringler 1985). Learning why drift-feeding fish resolve discrimination tradeoffs in very different ways might help uncover the mechanisms behind the wide variation in individual diets, prey detection abilities, and other behaviors of drift-feeding fish. Abbott and Sherratt (2013) created a general model applying signal detection theory to speed-accuracy and attention allocation tradeoffs, including many of those described above, and their work would be a useful starting point for modeling specific to drift-feeding fish.

### **2.5.5 Implications for foraging experiments**

Experimenters studying drift-feeding behavior should be aware of the potentially integral role of debris in the mechanisms governing the prey detection, energy budgets, and optimal foraging behavior of drift-feeding fish. Experimental tanks with unnaturally debris-free water might lack a factor central to the mechanisms that produce the behaviors of interest in the wild. Only O'Brien and Showalter (1993) have added natural debris to tanks for foraging experiments (as a treatment variable, with multiple significant effects). Our observation of strong debris effects under clear, low-flow conditions suggests that some baseline level of debris might actually be the natural “control” state to reproduce in experiments involving processes affected by debris. However, as noted above, adding realistic debris would require more cautious interpretations of foraging attempts as indicators of foraging success.

## 2.6 Conclusions

Drift-feeding juvenile Chinook salmon in the wild spent most of their foraging time and attempts pursuing and sampling debris items they did not ingest. The proportion of failed subsurface foraging attempts greatly exceeded that observed in previous studies of still-water brook trout; this is consistent with the greater challenge of identifying drifting targets quickly. For some fish, especially in fast water, drift feeding was an almost continuous process of investigating and sampling debris in search of prey. This has direct theoretical implications as a previously overlooked part of a drift-feeding fish's time and energy budgets. It also provides reasons to rethink drift feeding as a process in which energy intake and optimal behavior are controlled not only by physical limitations, but also by cognitive limitations on the use of visual attention for the signal detection task of discriminating prey from debris.

## 2.7 Acknowledgments

This work was supported by the Arctic-Yukon-Kuskokwim Sustainable Salmon Initiative, the Institute of Arctic Biology, Alaska EPSCoR NSF award #OIA-1208927 and the state of Alaska, and the Department of Biology and College of Natural Sciences and Mathematics at the University of Alaska Fairbanks. David Neuswanger, Milo Adkison, and three anonymous reviewers helpfully critiqued this manuscript. This work was conducted under IACUC protocols #134754-1 and #175627-1. Any use of trade, product, or firm names in this publication is for descriptive purposes only and does not imply endorsement by the U.S. Government.

## 2.8 References

Abbott KR, Sherratt TN (2013) Optimal sampling and signal detection: unifying models of attention and speed-accuracy trade-offs. *Behav Ecol* 24: 605-616.  
doi:10.1093/beheco/art001

Allen KR (1941) Studies on the biology of the early stages of the salmon (*Salmo salar*). J Anim Ecol 9: 47-76

Bachman RA (1984) Foraging behavior of free-ranging wild and hatchery brown trout in a stream. Trans Am Fish Soc 113: 1-32

Benson ER, Wipfli MS, Clapcott JE, Hughes NF (2013) Relationships between ecosystem metabolism, benthic macroinvertebrate densities, and environmental variables in a sub-arctic Alaskan river. Hydrobiologia 701: 189-207. doi:10.1007/s10750-012-1272-0

Biro PA, Ridgway MS, McLaughlin RL (1996) Does the rate of foraging attempts predict ingestion rate for young-of-the-year brook trout (*Salvelinus fontinalis*) in the field? Can J Fish Aquat Sci 53: 1814-1820

Bisson PA (1978) Diel food selection by two sizes of rainbow trout (*Salmo gairdneri*) in an experimental stream. J Fish Res Board Can 35: 971-975

Bryan JE, Larkin PA (1972) Food specialization by individual trout. J Fish Res Board Can 29: 1615-1624

Carrasco M (2011) Visual attention: the past 25 years. Vision Res 51: 1484-1525. doi:10.1016/j.visres.2011.04.012

Dukas R (2002) Behavioural and ecological consequences of limited attention. Philos Trans R Soc Lond B Biol Sci 357: 1539-1547. doi:10.1098/rstb.2002.1063

Dukas R, Kamil AC (2001) Limited attention: the constraint underlying search image. Behav Ecol 12: 192-199

Dunbrack RL (1992) Sub-surface drift feeding by coho salmon (*Oncorhynchus kisutch*, Walbaum): a model and test. J Fish Biol 40: 455-464

Elliott JM, Hurley MA (1999) A new energetics model for brown trout, *Salmo trutta*. Freshw Biol 42: 235-246

Fausch KD (1984) Profitable stream positions for salmonids: relating specific growth rate to net energy gain. Can J Zool 62: 441-451

Gowan C, Fausch KD (2002) Why do foraging stream salmonids move during summer? Environ Biol Fish 64: 139-153

Grant JWA, Noakes DLG (1986) A test of a size-selective predation model with juvenile brook charr, *Salvelinus fontinalis*. J Fish Biol 29: 15-23

Grossman GD, Rincón PA, Farr MD, Ratajczak REJ (2002) A new optimal foraging model predicts habitat use by drift-feeding stream minnows. Ecol Freshw Fish 11: 2-10

Grubb TCJ 2003. The mind of the trout: a cognitive ecology for biologists and anglers. University of Wisconsin Press, Madison, WI

Guensch GR, Hardy TB, Addley RC (2001) Examining feeding strategies and position choice of drift-feeding salmonids using an individual-based, mechanistic foraging model. Can J Fish Aquat Sci 58: 446-457

Gutierrez L (2011) Terrestrial invertebrate prey for juvenile Chinook salmon: abundance and environmental controls in an interior Alaskan river. M.S. Thesis, University of Alaska Fairbanks

Harvey BC, Railsback SF (2007) Estimating multi-factor cumulative watershed effects on fish populations with an individual-based model. *Fisheries* 32: 292-296

Hayes JW, Hughes NF, Kelly LH (2007) Process-based modelling of invertebrate drift transport, net energy intake and reach carrying capacity for drift-feeding salmonids. *Ecol Model* 207: 171-188

Hayes JW, Stark JD, Shearer KA (2000) Development and test of a whole-lifetime foraging and bioenergetics growth model for drift-feeding brown trout. *Trans Am Fish Soc* 129: 315-332

Hazelton PD, Grossman GD (2009) The effects of turbidity and an invasive species on foraging success of rosyside dace (*Clinostomus funduloides*). *Freshw Biol* 54: 1977-1989. doi:10.1111/fwb.2009.54.issue-9

Hill J, Grossman GD (1993) An energetic model of microhabitat use for rainbow trout and rosyside dace. *Ecology* 74: 685-698

Hollander M, Wolfe DA 1999. Nonparametric statistical methods. John Wiley & Sons, Inc. USA

Holling CS (1959) Some characteristics of simple types of predation and parasitism. *Can Entomol* 91: 385-398



Hughes NF, Dill LM (1990) Position choice by drift-feeding salmonids - model and test for arctic grayling (*Thymallus arcticus*) in sub-arctic mountain streams, interior Alaska. Can J Fish Aquat Sci 47: 2039-2048

Hughes NF, Hayes JW, Shearer KA, Young RG (2003) Testing a model of drift-feeding using three-dimensional videography of wild brown trout, *Salmo trutta*, in a New Zealand river. Can J Fish Aquat Sci 60: 1462-1476

Hughes NF, Kelly LH (1996) A hydrodynamic model for estimating the energetic cost of swimming maneuvers from a description of their geometry and dynamics. Can J Fish Aquat Sci 53: 2484-2493

Irvine JR, Northcote TG (1982) Significance of sequential feeding patterns of juvenile rainbow trout in a large lake-fed river. Trans Am Fish Soc 111: 446-452

Jenkins AR, Keeley ER (2010) Bioenergetic assessment of habitat quality for stream-dwelling cutthroat trout (*Oncorhynchus clarkii bouvieri*) with implications for climate change and nutrient supplementation. Can J Fish Aquat Sci 67: 371-385.  
doi:10.1139/F09-193

Jenkins TM, Jr (1969) Social structure, position choice, and micridistribution of two trout Species (*Salmo trutta* and *Salmo gairdneri*) resident in mountain streams. Anim Behav Monogr 2: 57-123

Kiflawi M, Genin A (1997) Prey flux manipulation and the feeding rates of reef-dwelling planktivorous fish. Ecology 78: 1062-1077

Kutner MH, Nachtsheim CJ, Neter J, Li W (2005) Applied Linear Statistical Models. 5<sup>th</sup> ed. McGraw-Hill/Irwin. New York

McLaughlin RL, Grant JWA, Noakes DLG (2000) Living with failure: the prey capture success of young brook charr in streams. *Ecol Freshw Fish* 9: 81-89

McNicol RE, Scherer E, Murkin EJ (1985) Quantitative field investigations of feeding and territorial behavior of young-of-the-year brook charr, *Salvelinus fontinalis*. *Environ Biol Fish* 12: 219-229

Metcalfe NB, Huntingford FA, Thorpe JE (1987) Predation risk impairs diet selection in juvenile salmon. *Anim Behav* 35: 931-933

Nakayama K, Martini P (2011) Situating visual search. *Vision Res* 51: 1526-1537.  
doi:10.1016/j.visres.2010.09.003

Nislow KH, Folt CL, Parrish DL (2000) Spatially explicit bioenergetic analysis of habitat quality for age-0 Atlantic salmon. *Trans Am Fish Soc* 129: 1067-1081

O'Brien WJ, Showalter JJ (1993) Effects of current velocity and suspended debris on the drift feeding of Arctic grayling. *Trans Am Fish Soc* 122: 609-615

Palmer J (1995) Attention in visual search: distinguishing four causes of a set-size effect. *Curr Dir Psychol Sci* 4: 118-123

Piccolo JJ, Hughes NF, Bryant MD (2008a) Water velocity influences prey detection and capture by drift-feeding juvenile coho salmon (*Oncorhynchus kisutch*) and steelhead (*Oncorhynchus mykiss irideus*). *Can J Fish Aquat Sci* 65: 266-275

- Piccolo JJ, Hughes NF, Bryant MD (2008b) Development of net energy intake models for drift-feeding juvenile coho salmon and steelhead. *Environ Biol Fish* 83: 259-267
- Ringler NH (1985) Individual and temporal variation in prey switching by brown trout, *Salmo trutta*. *Copeia* 1985: 918-926
- Ringler NH (1979) Selective predation by drift-feeding brown trout (*Salmo trutta*). *J Fish Res Board Can* 36: 392-403
- Skelhorn J, Rowland HM, Speed MP, De Wert L, Quinn L, Delf J, Ruxton GD (2010) Size-dependent misclassification of masquerading prey. *Behav Ecol* 21: 1344-1348. doi:10.1093/beheco/arq159
- Speed MP, Ruxton GD (2010) Imperfect Batesian mimicry and the conspicuousness costs of mimetic resemblance. *Am Nat* 176: E1-14. doi:10.1086/652990
- Staddon JER, Gendron RP (1983) Optimal detection of cryptic prey may lead to predator switching. *Am Nat* 843-848
- Van Winkle W, Jager HI, Railsback SF, Holcomb BD, Studley TK, Balridge JE (1998) Individual-based model of sympatric populations of brown, and rainbow trout for instream flow assessment: model description, and calibration. *Ecol Model* 110: 175-207
- Webster JR, Benfield EF, Ehrman TP, Schaeffer MA, Tank JL, Hutchens JJ, D'Angelo DJ (1999) What happens to allochthonous material that falls into streams? A synthesis of new and published information from Coweeta. *Freshw Biol* 41: 687-705

Wickens TD 2001. Elementary signal detection theory. Oxford University Press

Wolfe JM (1998) What can 1 million trials tell us about visual search? Psychol Sci 9: 33-39

## 2.9 Figures



Fig. 2.1. Videotaping fish amidst debris in clear water. (a) The 0.7-m deep water appears crystal clear from above; however, (b) it carries numerous fine debris particles, evident in comparison to (c) a version of the same image with the debris removed by averaging several video frames.

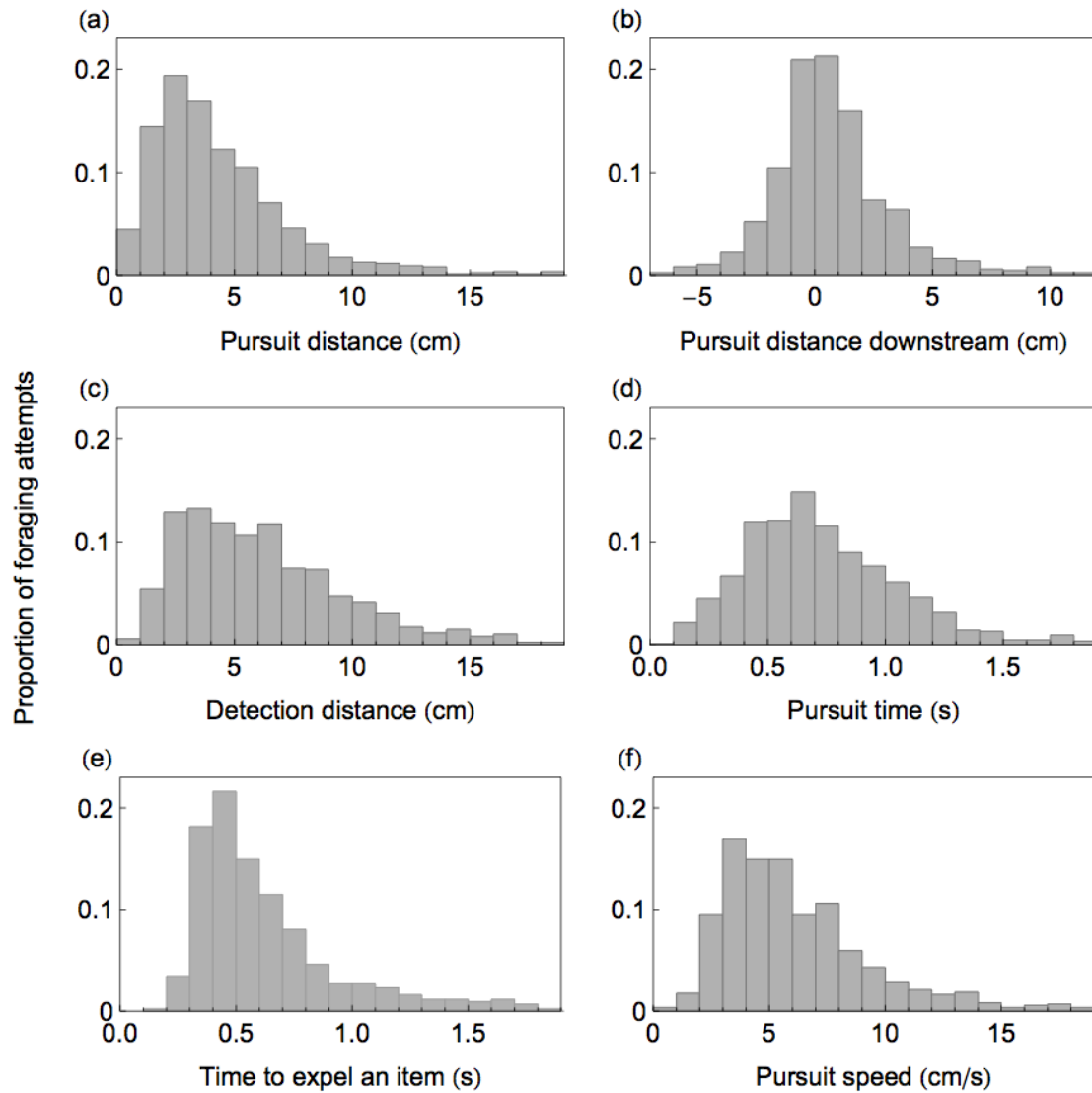


Fig. 2.2. Histograms of foraging summary statistics for all measurement dates combined: (a) the distance a fish moved during its reaction to an item, prior to capture or visual rejection (b) distance from the detection point to the capture or visual rejection point along the upstream-downstream axis (negative values mean the fish moved upstream to capture the item), (c) the estimated distance of an item from the fish's snout when it was detected, under the assumption that reaction immediately followed detection, (d) the time between a fish's initial reaction to an item and capturing or rejecting it, (e) the time to spit an item out after capturing it, and (f) the pursuit distance divided by pursuit time.

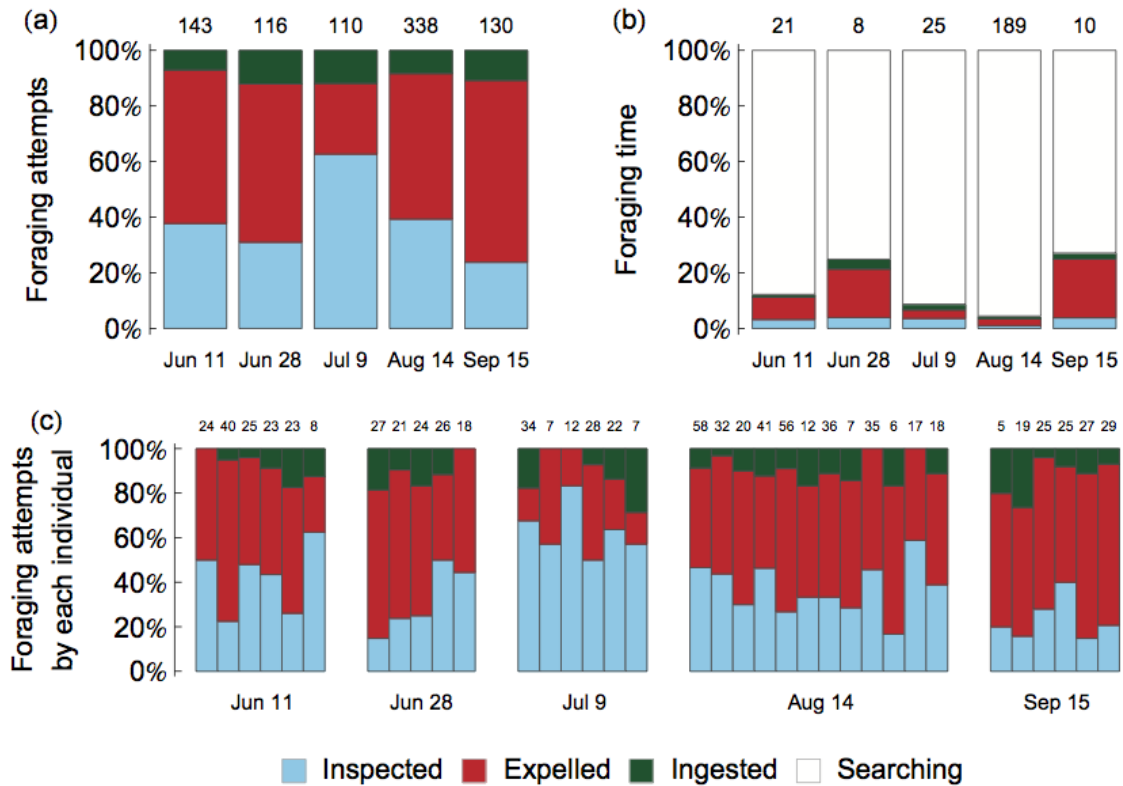


Fig. 2.3. Foraging effort categorized according to whether the item was inspected and rejected, captured and expelled, or captured and ingested. (a) All foraging attempts with clear outcomes by all fish were combined for each date. (b) The total time spent on foraging attempts with each outcome is shown as a percentage of total foraging time observed for all fish. Searching time as used here includes all time not spent pursuing or handling items, including any unmeasured time allocated to competition or watching for predators. (c) The bars from part a are subdivided by individual fish, for comparison of within-group versus among-group variation. Foraging attempts with unclear outcomes (fewer than 15% of attempts on any date) were not included here, and time spent on them (less than 1.5% of total time on any date) was proportionally allocated to the other attempt types for comparison with searching time. Numbers above each bar indicate the number of foraging attempts observed (in a and c) and the number of minutes observed for all fish combined (in b).

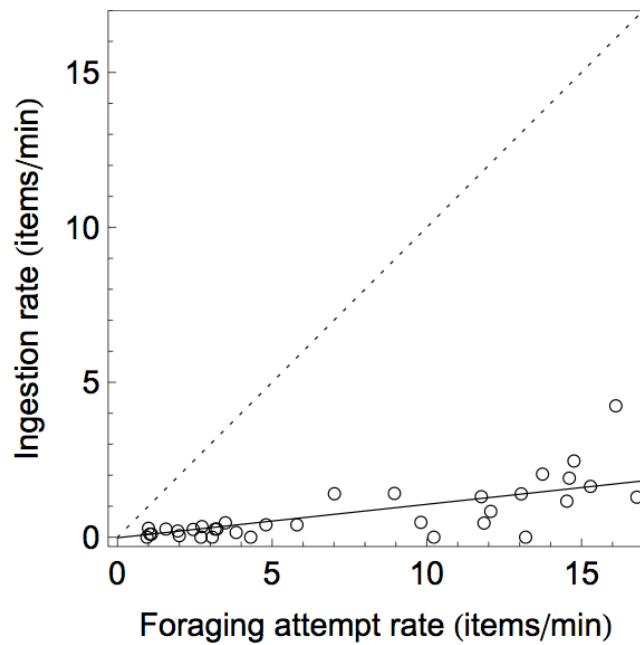


Fig. 2.4. Foraging attempt rate underestimates ingestion rate. A solid line was fitted by distribution-free regression through data points for all fish from all dates (circles), showing that ingestion rate increased slowly but significantly with foraging attempt rate in a highly variable relationship. If all foraging attempts were ingestions, the regression line would overlay the dotted line, which represents a 1:1 relationship.



## 2.10 Tables

Table 2.1 Environmental conditions at five sites observed on separate dates

	Jun 11	Jun 28	Jul 9	Aug 14	Sep 15
Year	2009	2010	2010	2009	2010
Time of day	7:05pm	11:07am	11:11am	1:13pm	12:52pm
Water temperature (°C)	12.1	9.6	Unavailable	9.0	6.1
Stream discharge <sup>a</sup> (m <sup>3</sup> /s)	21.5	12.3	13.6	11.5	20.7
Water velocity (m/s)	0.04	0.15	0.06	0.07	0.10
Water depth (m)	0.25	0.42	0.37	0.46	0.53

<sup>a</sup> The daily median June-September discharge is 25 m<sup>3</sup>/s.

Table 2.2 Fish attributes and foraging behavior for five groups of fish observed on separate dates.

	Jun 11	Jun 28	Jul 9	Aug 14	Sep 15	Overall
Number of fish observed	6	5	6	12	6	35
Fork length <sup>a, d</sup> (mm)	35.2 ± 0.3	49.9 ± 6.1	51.7 ± 4.0	71.4 ± 2.6	61.4 ± 2.3	57.0 ± 13.5
Foraging attempts <sup>a, d</sup> (/ min)	9.0 ± 3.9	16.1 ± 2.7	6.3 ± 4.9	2.2 ± 0.9	12.4 ± 3.1	7.8 ± 5.8
Ingestions <sup>a, d</sup> (/ min)	0.7 ± 0.8	1.8 ± 1.4	0.7 ± 0.8	0.2 ± 0.1	1.6 ± 1.4	0.8 ± 1.0
Time handling all items <sup>b, d</sup> (%)	12.3	24.9	8.7	4.5	27.1	14.0 ± 10.5
Time handling debris <sup>b, d</sup> (%)	11.3	21.4	6.7	3.5	24.9	12.1 ± 9.3
Handling time per item <sup>a, e</sup> (s)	1.0 ± 0.6	0.9 ± 0.8	1.1 ± 1.1	1.3 ± 1.0	1.3 ± 0.7	1.2 ± 0.9
P(capture   attempt) <sup>a, c, e</sup>	0.58 ± 0.15	0.68 ± 0.15	0.37 ± 0.12	0.63 ± 0.11	0.77 ± 0.09	0.61
P(ingestion   capture) <sup>a, c, e</sup>	0.14 ± 0.12	0.16 ± 0.10	0.29 ± 0.28	0.14 ± 0.08	0.16 ± 0.10	0.15
P(ingestion   attempt) <sup>a, c, e</sup>	0.08 ± 0.06	0.11 ± 0.07	0.11 ± 0.11	0.09 ± 0.06	0.13 ± 0.09	0.094
Detection distance <sup>a, e</sup> (cm)	3.8 ± 2.1	7.3 ± 3.8	6.1 ± 3.3	6.6 ± 3.6	7.3 ± 4.4	6.3 ± 3.7
Nearest-neighbor distance <sup>a, d</sup> (cm)	7.4 ± 2.7	16.7 ± 6.2	22.3 ± 8.7	10.6 ± 4.0	16.9 ± 8.4	15.1 ± 8.0

<sup>a</sup> Mean ± 1 standard deviation.<sup>b</sup> Total percent of time observed.<sup>c</sup> P(A | B) denotes the probability that event A occurred, given that event B did.<sup>d</sup> For these rows, overall values are the mean and standard deviation of the values for all individual fish.<sup>e</sup> For these rows, overall values are calculated across all foraging attempts.

## **CHAPTER 3:**

### **Territoriality within schools: dynamic competition of drift-feeding juvenile Chinook salmon in 3-dimensional space<sup>1</sup>**

#### **3.1 Summary**

1. Territoriality is widely reported in drift-feeding salmonids, typically as a broadly spaced 2-D “territorial mosaic.” However, juvenile Chinook salmon in the Chena River, Alaska, feed in schools. We sought to determine whether they exhibit any territorial behaviors despite their schooling.
2. Territoriality is a major cause of density-dependent population regulation in many salmonids. Population data show density dependence is significant in the Chena River, but the mechanisms of this dependence are unclear because juvenile schooling departs from typical territorial behavior. Any indication of territoriality within these schools would be consistent with the attribution of this density dependence to a known mechanism. However, feeding territories within dense animal aggregations and in 3-D configurations would be novel findings not only for salmonids but also for animals in general.
3. We used 3-D video techniques to create fine-scale maps of the foraging and competitive interactions of individual fish within schools; and we developed analytical methods to measure and compare the motion, exclusivity, and size of potential territories in a temporally dynamic 3-D environment.

---

<sup>1</sup> Neuswanger, J., Rosenberger, A.E., Wipfli, M.S., and Hughes, N.F. Territories within schools: the dynamic competition of drift-feeding juvenile Chinook salmon in 3-dimensional space. Prepared for submission in Journal of Animal Ecology.

4. Several fish aggressively defended stationary, exclusive feeding territories within their schools. Many others maintained stationary or semi-stationary, exclusive feeding volumes without overt aggression. Transient floaters frequently passed through schools, stopping briefly to feed before moving on. Aggressive territory holders were among the largest and most dominant individuals.
5. Foraging strategies of exclusive space use, whether by aggressive defense or passive cooperation, were consistent with known mechanisms of density-dependent regulation. Territoriality and aggregation are not mutually exclusive and may be expressed simultaneously with complementary fitness benefits.

### 3.2 Introduction

Drift-feeding salmonids are widely reported as territorial (Mason and Chapman 1965; McNicol and Noakes 1981; Puckett and Dill 1985; Keeley and Grant 1995; Keeley 2000), although space sharing has also been observed (Bachman 1984; Armstrong et al. 1999). Space available for territories can limit population size (Elliott 1990; Grant and Kramer 1990; Steingrímsson and Grant 1999). With some exceptions, the following basic description summarizes their feeding strategy: fish face upstream into the current from a single, stationary “focal point” from which they dart back and forth to intercept drifting prey or repel competitors (Jenkins 1969). Neighboring fish typically establish size-based dominance hierarchies in which the strongest competitors occupy the focal points that provide the greatest net energy intake. From these points, they defend exclusive territories in a two-dimensional (2-D) mosaic spread across the profitable portions of their habitat (Hughes 1992). Individuals that cannot defend a territory exhibit a “floater” strategy, roaming broadly within less energetically profitable habitat and surviving at a lower rate than territorial fish (Elliott 1990).

The Chena River, Alaska, supports a subpopulation of the declining (Schindler et al. 2013) and economically important Yukon River population of Chinook salmon (*Oncorhynchus tshawytscha*). Most of these juvenile salmon spend their first post-emergence summer drift feeding in the mainstem Chena River. The productivity of this population (the number of offspring per spawner that eventually reach adulthood and return to spawn or be harvested) is negatively correlated with spawner density and stream discharge during this period of freshwater residency (J. Neuswanger, Chapter 4, this dissertation). The population-level effect of spawner density is consistent with the mechanism of population regulation through feeding territoriality reported for other juvenile salmonids (Elliott 1990; Grant and Kramer 1990).

However, the behavior of juvenile Chinook salmon (hereafter, “Chinook salmon fry”) in the Chena River is strikingly different from the territorial behaviors commonly

reported for other drift-feeding salmonids. Instead of occupying a territorial mosaic spread widely across the river bottom, Chena River Chinook salmon fry occur in schools<sup>2</sup> numbering from tens to hundreds of fish, inhabiting all levels of the water column, tightly associated with woody debris along the river margins (J. Neuswanger, personal observation). Such schooling behavior is not unique to this system—juvenile Coho salmon (*Oncorhynchus kisutch*) in pool habitats can also form tight groups throughout the water column (Hartman 1965). Both schooling and associating with cover have obvious survival advantages for small fish sharing the moderately large Chena River (median discharge 25 m<sup>3</sup>/s) with piscivores such as common mergansers (*Mergus merganser*) and possibly Arctic grayling (*Thymallus arcticus*). The close proximity of fish within these schools and the relative homogeneity of the habitat on their spatial scale (a fraction of a cubic meter) might weaken the fitness incentives for any fish to hold a stationary focal point or defend the area around it. Nevertheless, Hartman (1965) observed dominant Coho salmon fry competing aggressively for positions near the front of their tight groups. What else might schooling salmon fry have in common with their well-studied counterparts in territorial mosaics?

We sought to determine whether Chinook salmon fry in the Chena River exhibit any of the behavioral patterns associated with population-regulating territoriality in many other salmonids. Our specific objectives were to determine if schooling Chinook salmon fry 1) maintain stationary feeding positions, 2) feed within exclusive spaces, 3) aggressively exclude competitors in accordance with a size-based dominance hierarchy, and 4) derive any observable fitness benefits, such as increased foraging rates, from these behaviors. We also developed new analytical techniques for describing and comparing temporally dynamic, three-dimensional (3-D) space use behavior. We discuss how behaviors measured here compare with those of other territorial animals, and consider

---

<sup>2</sup> We make no distinction in this paper between schooling and shoaling, and use “school” throughout for simplicity. These fish moved as a cohesive unit (a school) when frightened or when moving between pools, and moved independently (like a shoal) but still aligned in the same direction (like a school) while drift feeding.

whether Chinook salmon fry behavior is compatible with the mechanisms of population regulation identified in known territorial salmonids.

### **3.3 Materials and methods**

#### **3.3.1 Study system**

The Chena River is a 5<sup>th</sup>-order stream in the Yukon River drainage in central Alaska. Its median summer discharge was 25 m<sup>3</sup>/s in the study reach, which extended from 100 to 160 km upstream of the confluence of the Chena with the large, glacial Tanana River, which flows into the Yukon River. Chinook salmon fry emerge from the gravel in May and early June, grow and drift feed throughout their first summer in the river, and outmigrate as smolts to the Bering Sea the following spring.

#### **3.3.2 Collection and 3-D measurement of video footage**

We recorded drift-feeding Chinook salmon fry at close range using a stereo pair of wide-angle, high-definition video cameras in underwater housings. The VidSync video analysis program (<http://www.vidsync.org>) allowed measurement of 3-D positions with sub-millimeter precision (J. Neuswanger, Chapter 1, this dissertation). We analyzed three pairs of video recorded in 2009 and 2010, representing a variety of water velocities, water temperatures, and fish sizes. Full details of the filming and study sites (labeled “Jun 11,” “Jul 9,” and “Aug 14”) are described by Neuswanger et al. (2014), who performed different analyses of the same groups of fish (and two others not conducive to the present analysis due to field-of-view and resolution limitations).

We converted all spatial measurements from the arbitrary coordinates of the camera system into a 3-D coordinate system aligned with the stream, where  $x$  = stream-wise, from upstream to downstream,  $y$  = cross-stream, from near to far from the cameras, and  $z$  = vertical from bottom to surface. To find the vertical direction, we measured positions of at least three objects at the water’s surface, fit a plane through them by the

method of least squares, and used a unit vector normal to that plane as vertical direction. To measure the stream-wise direction, we averaged the trajectories of at least five fine drifting debris particles and projected that averaged vector onto the surface plane to get its component perpendicular to the vertical direction (i.e., the downstream direction). The cross-stream unit vector was the cross product of the vertical  $\times$  downstream unit vectors. The above coordinate conversions and all subsequent calculations were performed in Mathematica ® 8.0.1, except where noted.

### 3.3.3 Behaviors recorded

In each video, we measured the relevant actions of all fish—foraging attempts, aggressive acts, and focal point locations at regular intervals—within the region of adequate visibility for both cameras (roughly  $0.2 \text{ m}^3$ ). We used twenty minutes from one pair of videos in high detail for the primary analysis, and we analyzed the other videos for five minutes each to evaluate the generality of observed patterns. We recorded the behavior of every fish that attempted to drift feed within the region of observation during any part of the observation period. In total, we analyzed 77 fish and recorded 3-D coordinates of 1,307 foraging attempts, 4,138 focal point locations, and 54 aggressive acts from the three sites (Fig. 3.1).

We recorded foraging attempts in different ways depending on outcome. Most foraging attempts were investigations of debris particles, which were either captured and expelled or visually inspected without capture (Neuswanger et al. 2014). We analyzed one spatial position associated with each foraging attempt. For captures, this was the tip of the fish's upper jaw at the moment of capture<sup>3</sup>. For visual rejections, it was the tip of the upper jaw in the video frame preceding termination of pursuit. We did not distinguish

---

<sup>3</sup> Foraging attempts on the surface were a small exception, because they often occurred slightly outside the cameras' field-of-view, but were obvious from the fish's rapid acceleration and later ripples on visible parts of the surface. In these cases, the horizontal and time coordinates were set in the last frame in which any part of the fish was visible on both cameras, and the vertical coordinate was set to that of the surface.



between successful and unsuccessful foraging attempts in this study because most fish were too far from the cameras to determine whether they ingested or rejected each item; however, Neuswanger et al. (2014) analyzed the most readily visible subset of the same fish and found that only 9.4 percent of foraging attempts led to ingestion overall, and the overall foraging attempt rate was only moderately correlated with ingestion rate (Kendall's  $\tau = 0.55$ ). The presence of this correlation justified our use of foraging attempt rate as a tentative surrogate for ingestion rate (a presumed correlate of fitness), particularly because it was the only such measure available; however, results based on this surrogate must be interpreted with caution because of the high variability indicated by the low correlation coefficient.

We measured “focal point locations” of fish when they were facing upstream into the current, seemingly watching for food instead of engaging in a foraging attempt or conflict. Past studies treated focal points as approximately stationary; however, we measured them with high frequency (at five-second intervals) and precision to describe their fine-scale motion. We skipped intervals when fish were capturing prey or engaging in aggression, when other fish blocked our view, or when fish were off-screen in both cameras (individuals for which this was common are noted).

We recorded “aggressive acts” between fish by measuring the positions of the tip of the upper jaw of the aggressor (the “initiation point”) and the target (the “provocation point”) at the moment the aggressor initiated an attack. We also recorded the “winner,” which was always clear because one fish maintained its position and the other retreated, albeit sometimes temporarily and not very far. Rare cases in which one fish attacked another multiple times in quick succession, without either fish settling to a docile position in between, were scored as single aggressive acts based on the spatial coordinates from the first pursuit. We did not count certain lesser conflicts as aggressive acts, including events in which one fish yielded to another after mistaking some incidental rapid motion for aggression, and foraging attempts in which two fish pursued the same potential prey item, which were recorded as foraging attempts at the same position for both fish. These

dual foraging attempts were not considered “aggressive acts” because there was no clear aggressor, but they often prompted a threat display (raised dorsal fin) from both fish.

### **3.3.4 The instantaneous region of influence (IROI) of a fish**

We developed new measures to represent the most meaningful types of variation in temporally dynamic, spatially 3-D space use behavior. We began with the observation that, at each instant in time, there must be a limited region of space within which a fish might react to prey or competitors. We term this region the “instantaneous region of influence” (IROI) to distinguish it from the commonly described “home range,” which encompasses all the areas used by an animal over a long period of time, and from “territory,” which implies defense against competitors. These different measures of space use are not mutually exclusive; sometimes an IROI can also be a home range or territory. Like home ranges and territories, the IROI is clearly defined as a broad concept but fuzzier in detail; it may or may not have a sharp boundary, depend on target attributes (e.g., fish moving far to pursue large prey), or be different for foraging and aggression. Rather than making arbitrary simplifying assumptions to assign each IROI hard boundaries with exact sizes and shapes, we developed measures that—despite the definitional uncertainty—provide insight into the IROI’s most important attributes: position, size, motion, and overlap among competitors.

Estimating the motion of the IROI (or lack thereof) requires separating motion of the IROI itself from motion of the fish within it. We represent the center of each IROI as a function of time defining an irregular curve in 3-D space, such that each point in time corresponds to a single 3-D position representing the current center of the IROI. The “IROI movement speed” was the length of this curve divided by the amount of time the fish was observed. For each fish, the IROI center was estimated by combining separate LOESS regressions versus time of the  $x$ ,  $y$ , and  $z$  coordinates of all focal point and foraging attempt measurements. We performed the regression using the “loess” function in R (R Core Development Team 2014) with the family parameter set to “symmetric,”

which uses a robust, iterative procedure that performed much better in the presence of outliers than the alternative least-squares fitting method. The “span” parameter, which controls the proportion of the data used for each local area of the fit, was set to 1 (minimum sensitivity) for fish observed for less than three minutes, and scaled by observation time to represent an approximately three-minute period for fish observed for longer durations. We chose the three-minute period by qualitative examination of model sensitivity, balancing the need to capture real IROI movement against the need to avoid interpreting extensive movement within the IROI as motion of the IROI center (i.e. overfitting). Scaling the span by observation time allowed similar model sensitivity for most fish regardless of how long they were observed, except that the model was unavoidably oversensitive for highly transient fish. The effect of this oversensitivity was to mildly exaggerate the naturally high IROI movement speeds of transient fish with very short observation times (e.g.,  $< 1$  minute); this had little relevance to our inferences because we used rank-based statistics, and these fish would rank among the most mobile by any measure.

We calculated and compared two indices of the size of the IROI, one based on foraging attempts and one on focal points. The “foraging median center distance (MCD)” and the “focal MCD” represented the median distance from an event of each type to the fish’s IROI center at the time of the event. These indices cannot be interpreted as areas or volumes, and they notably reflect median space use rather than outer dimensions.

### **3.3.5 Indices of proximity between competitors**

To measure the extent to which different fish used the same area at the same time, we developed two indices of proximity, based on 1) the distances between IROI centers of two fish at one-second intervals throughout the time period or periods during which the fish were observed simultaneously, and 2) all pairwise distances between the foraging attempts of two fish. To avoid assigning high proximity scores to fish using the same location at different times, proximity was calculated using Euclidean distances between

4-D spatiotemporal  $(x, y, z, V t)$  coordinates, where time  $t$  was multiplied by a constant speed  $V = 1$  cm/s to create a spatial coordinate. This scaling factor was chosen both for ease of interpretation (for example, foraging attempts in the same location 10 s apart would receive the same proximity score as foraging attempts at the same time 10 cm apart) and because 1 cm/s was in the middle of the observed IROI movement speeds for transient individuals, and is therefore within the range of speeds at which one fish might encroach on another's territory.

To combine these distance comparisons into useful indices of proximity, we transformed them using a sigmoid function with exponential decline, which produced indices with three important characteristics: 1) smaller distances between fish had higher proximity scores; 2) the exponential decline toward the lower asymptote assured that a large number of comparisons with irrelevantly distant fish, added together, had little influence on the proximity score; and 3) the upper asymptote guaranteed that single comparisons with very high proximity (e.g., when two fish pursued the same prey item) did not overwhelm all the other data points by approaching infinity.

The starting formula for the proximity score for two points separated by distance  $d$  was a typical sigmoid function:

$$(3.1) \quad X^*(d) = \frac{\rho^*}{1 + e^{\gamma d + \kappa}}$$

Fitting the parameters  $\rho^*$ ,  $\gamma$ , and  $\kappa$  required some objective approximation of the importance of objects at each distance to the fish. Reasoning that fish might be concerned about neighbors pursuing the same prey items, we based our measure of importance versus distance on the histogram of foraging attempt pursuit distances (from the detailed foraging attempt analysis of Neuswanger et al. 2014), multiplied by two to account for the foraging distances of both fish. We used the Levenberg-Marquardt method to fit

Equation (3.1) to the bin heights of the parts of this histogram to the right of its peak<sup>4</sup>. Reassuringly, the shape of this final function also closely matched the distribution of aggression initiation distances. To standardize the vertical scaling of the index (which otherwise depends arbitrarily on the histogram bin widths), we divided the parameter  $\rho^*$  by the total area under the curve,  $\int_0^\infty X^*(u) du$ , to get a new parameter  $\rho$  used in the final formula, in which  $\rho = 9.25$ ,  $\gamma = 28.3 \text{ m}^{-1}$ , and  $\kappa = -3.01$ :

$$(3.2) \quad X(d) = \frac{\rho}{1 + e^{\gamma d + \kappa}}$$

To compare two fish, let  $d_{i,j}$  be the spatiotemporal distance between the  $i$ th foraging attempt out of  $N$  total attempts by fish  $A$  and the  $j$ th attempt out of  $M$  total attempts by fish  $B$ . Let  $T_A$  and  $T_B$  represent the total times each fish was observed. Their foraging proximity index is:

$$(3.3) \quad ForgProx_{A,B} = \frac{1}{T_A T_B} \sum_{i=1}^N \sum_{j=1}^M X(d_{i,j})$$

Let  $d_t$  be the distance between the IROI centers of the two fish at each one-second interval time  $t$  within the time range or ranges (with total duration  $T_{AB}$ ) during which both fish were on-screen together. Their center proximity index is:

$$(3.4) \quad CentProx_{A,B} = \begin{cases} \frac{1}{T_{AB}} \sum_{\text{all } t} X(d_t) & \text{if } T_{AB} > 0 \\ 0 & \text{if } T_{AB} = 0 \end{cases}$$

Total proximity indices for each fish,  $TotForgProx$  and  $TotCentProx$ , were the sums of  $ProxForg$  and  $ProxCent$  from pairwise comparisons of the fish with every other fish in the same video. They represent the total proximity of each fish to all its neighbors combined.

---

<sup>4</sup> We ignored the decline in foraging attempts at distances to the left of the peak because it probably represents an unrelated mechanism, the simple fact that very few items pass through the tiny cross-sectional area at tiny distances from the fish.

### 3.3.6 Statistical analysis

Many of the measures derived above were not distributed compatibly with the assumptions of common parametric statistical tests. Therefore, we used standard nonparametric, rank-based tests (Hollander and Wolfe 1999), including the Wilcoxon signed-rank test for comparing means and Kendall's  $\tau$ -test of association.

## 3.4 Results

Chinook salmon fry exhibited a broad range of movement, exclusivity, and aggression behaviors as indicated by the IROI movement speed, proximity indices, and aggression rate in Table 3.1. Some individuals remained within a fixed volume and successfully excluded competitors via overt aggression. Others moved rapidly through the region of observation, stopping only briefly to attempt to drift feed before moving on. Many fish used intermediate strategies, making somewhat exclusive use of stationary or nearly stationary spaces without overt aggression.

### 3.4.1 Site fidelity and characteristics of the IROI

Representing space use with the instantaneous region of influence (IROI) allowed us to distinguish long-term shifts in a fish's occupied space from its high-frequency movements within that space. The IROI provided an objective measure that agreed with qualitative graphical judgments about the movement of each fish. Nonzero motion of the IROI centers of all fish (Table 3.1) indicated that none of them used a single, fixed focal point indefinitely. However, they did watch for prey from within a shorter distance of their IROI center—represented by the focal “median center distance” (MCD)—than the distance at which they intercepted potential prey items. The mean length by which the foraging MCD exceeded the focal MCD was 1.42 cm on Jun 11 (Wilcoxon signed-rank test,  $p = 0.0001$ ,  $N = 28$ ), 1.45 cm on Jul 9 ( $p = 0.01$ ,  $N = 11$ ), and 2.2 cm on Aug 14 ( $p = 0.0002$ ,  $N = 33$ ).

In the Aug 14 video, the IROI movement speeds of highly stationary fish (e.g., Fig. 3.2a) ranged from 0.01 to 0.04 cm / s, and those of transient floaters were above 0.4 cm / s. Fish exhibiting intermediate levels of movement (range: 0.044 cm / s to 0.16 cm / s) held mostly-stationary positions that sometimes shifted, either gradually or suddenly, in response to distant foraging opportunities, competitor intrusion, or other disturbances. In many cases, a fish returned to its previous position after leaving for a few minutes (e.g., Fig. 3.2c), indicating that stationary behavior was likely due to fidelity to specific locations in space, not aversion to unnecessary movement. In the other two videos, the IROI movements speeds associated with each strategy were slightly higher, but still provided good separation among the different strategies within each video.

IROI movement speed was negatively correlated with fish size in the primary, twenty-minute Aug 11 video analysis (Kendall's  $\tau = -0.50$ ;  $p = 0.00001$ ;  $N = 38$ ). This relationship was largely driven by the fact that the smallest fish (fork length < 67 mm) were almost all floaters. However, the relationship persisted even when all floaters (IROI movement speed > 0.2 cm/s) were excluded from analysis ( $\tau = -0.49$ ;  $p = 0.0005$ ;  $N = 25$ ). No significant relationship between fish size and IROI movement speed was detected in the Jun 11 ( $\tau = -0.06$ ;  $p = 0.66$ ;  $N = 28$ ) or Jul 9 ( $\tau = 0.02$ ;  $p = 0.94$ ;  $N = 11$ ) videos. The range of fish sizes observed was much smaller on Jun 11 (32 to 37 mm) and Jul 9 (47 to 58 mm) than on Aug 14 (56 to 80 mm), which could explain the weakness or absence of size-based relationships earlier in the summer.

We qualitatively observed that the most stationary individuals were closely associated with structure, such as the river bottom or woody debris. They were not necessarily in positions where this structure conferred a fitness advantage (such as a velocity or escape shelter); but having fixed reference points nearby may have helped fish to maintain steady positions.

### 3.4.2 Exclusive use of space

No fish in any of the schools shared largely overlapping spaces for a substantial period of time. The center proximity index and foraging proximity index revealed interesting relationships between neighboring fish. Apart from the obvious cases of consistently distant fish (both indices near zero) or consistently close fish (both indices large), some pairs of fish were usually distant but occasionally foraged in each other's direction (small center proximity index, large foraging proximity index); and other pairs maintained focal positions close together but foraged on opposite sides of a soft boundary (large center proximity index, small foraging proximity index).

Even the competitors in closest proximity by both indices used largely separate spaces (Fig. 3.3). A few used partially overlapping spaces but not concurrently (Fig. 3.4). Some of these pairs had correlated movements over a long time period, suggesting that one or both were consistently adjusting movement in relation to the other—taking up space when the other moved away, or yielding space when the other came too close (Fig. 3.4a).

Cases in which purely spatial data created an illusion of major overlap between two fish were actually cases in which one fish moved out of an area before the other moved in (Fig. 3.4b). Similarly, cases of apparent overlap in a 2-D top view were resolved as fish that were completely separated vertically (Fig. 3.3, top right comparison). In these instances, live viewing and 2-D video footage gave false impressions that adjacent fish were using the same large area without any internal structure. Applying the IROI method to measure spatial patterns in 3-D and their temporal dynamics revealed unexpectedly high exclusivity.

Large foraging proximity indices were much more common in the Jun 11 video than in the Jul 9 or Aug 14 videos, meaning the smaller fish observed on Jun 11 fed closer together. This does not necessarily mean the smaller fish were more prone to encroaching on their neighbors. Instead, they used smaller spaces and could be packed more tightly without encroaching. As in the Aug 14 video, manual inspection of their



pairwise relationships shows the fish in closest proximity to each other used largely non-overlapping spaces (Fig. 3.3).

### 3.4.3 Aggression

Aggressive maneuvers (primarily chases) were observed 22 times in the five-minute Jul 9 video and 31 times in the twenty-minute Aug 14 video (Fig. 3.5). Only one aggressive maneuver was observed in the five-minute Jun 11 video. In all videos, adjacent fish sometimes pursued the same potential prey item and reacted to each other by displaying raised dorsal fins. However, there was no clear aggressor in these conflicts, and no indication whether dominance or luck determined the winner. We also observed fish yield space to competitors that made rapid, aggressive-like motions for other reasons, such as fleeing another fish's aggression or pursuing a prey item with exceptional vigor. These incidental conflicts suggest that many fish maintain their exclusive use of space by means more subtle than fighting.

Just six of the 38 fish observed in the Aug 14 video acted aggressively, and the vast majority (26/31) of aggressive acts were initiated by just two fish (labeled Aug14\_38 and Aug14\_47 in Table 3.1). Despite clear pairwise dominance relationships between aggressive individuals and the targets of their aggression, the low number of aggressors meant a linear dominance hierarchy was not evident. A larger proportion (5/11) of the observed population acted aggressively in the Jul 9 video. There were not enough interactions to fully resolve a linear hierarchy, but the interactions among the individuals that initiated aggression were consistent with such a hierarchy, meaning no fish won a conflict against a fish that had defeated its superior.

In 51 of 54 total aggressive acts, the target of the attack yielded space to the aggressor (i.e., the aggressor “won”). Two of the three aggressors that lost their disputes were smaller than the target; however, in most attacks (41 of the 54) the aggressor was larger than the target. Aggressive fish were among the largest in the Jul 9 video ( $\tau = 0.47$ ,  $p = 0.06$ ,  $N = 11$ ) and the Aug 14 video (Fig. 3.6a;  $\tau = 0.31$ ,  $p = 0.02$ ,  $N = 38$ ). They were

also among the most stationary in the Aug 11 video as indicated by a negative association with the IROI center motion rate (Fig. 3.6*b*;  $\tau = -0.30$ ,  $p = 0.02$ ,  $N = 38$ ), but not in the Jul 9 video ( $\tau = -0.17$ ,  $p = 0.49$ ,  $N = 11$ ). These large, stationary, aggressive fish had medium to low total proximity scores (Fig. 3.6*c*), indicating they occupied mostly exclusive spaces. However, aggression was not the only path to using a moderately stationary and exclusive space; many fish exhibited similar numbers without aggression (Table 3.1).

#### 3.4.4 Foraging attempt rate in relation to space use

If territoriality provides a foraging advantage, we might expect a high foraging attempt rate (relative to competitors in the same school) to correlate with a high aggression rate, large IROI size (focal MCD or foraging MCD), low IROI movement speed, or low total proximity indices. We used Kendall's  $\tau$ -test to search for these relationships that might indicate a foraging advantage to territoriality, and none were significant at the 5% level for any of the three videos (details not reported).

One detected relationship agreed with the above expectations, but not because territorial fish had a foraging advantage. In the Jul 9 video, fish using focal spaces distant from their competitors (low *TotCentProx*) had high foraging attempt rates ( $\tau = -0.78$ ,  $p = 0.0008$ ,  $N = 11$ ). The reason for this correlation was probably that fish close to competitors (high *TotCentProx*) were prone to aggression ( $\tau = 0.72$ ,  $p = 0.004$ ,  $N = 11$ ), and aggressive fish had very low foraging attempt rates ( $\tau = -0.77$ ,  $p = 0.002$ ,  $N = 11$ ). These correlations quantitatively support our qualitative assessment of the Jul 9 video—a few fish spent much of their time attacking other fish throughout a large volume (Fig. 3.5*b*) without settling down to feed, and individuals that avoided conflict were able to better focus on foraging.

Contrary to expectations of a foraging benefit to territoriality, fish that foraged close to competitors (high *TotForgProx*) had significantly higher foraging attempt rates on Jun 11 ( $\tau = 0.47$ ,  $p = 0.0004$ ,  $N = 28$ ), Jul 9 ( $\tau = 0.53$ ,  $p = 0.02$ ,  $N = 11$ ), and Aug 11 ( $\tau = 0.63$ ,  $p = 0.00000004$ ,  $N = 38$ ). This relationship could be explained by the fact that

91% of foraging attempts by Chena River Chinook salmon fry were investigations of inedible debris (Neuswanger et al. 2014). The possibility of being out-raced to prey by a competitor might pressure fish into making exceptionally hasty, inaccurate decisions about whether to pursue each item they detect, causing them to pursue more debris and exhibit higher overall foraging attempt rates than more isolated individuals.

The high proportion of foraging attempts directed at inedible debris might help explain why behaviors associated with territoriality did not have a detectable positive effect on foraging attempt rate. If territoriality does provide a foraging advantage, it might only be detectable in the actual ingestion rate, which could not be estimated for most of the fish we observed due to visual resolution limits.

### **3.5 Discussion**

Although it is intuitive to view territoriality and aggregation as contrary and mutually exclusive behaviors, several individuals within schools of Chinook salmon fry aggressively defended territories (as defined by Wilson 1975: “an area occupied more or less exclusively by an animal or group of animals by means of repulsion through overt defense or advertisement”). Many fry were transient floaters, briefly passing through the window of observation with few or no stops. Other fry used relatively stationary and exclusive spaces without overt defense. Whether to term all these spaces “territories” is open to debate, but their key characteristic—exclusivity—may result in population-regulatory effects similar to those documented for territorial competitors.

Overall, many previously reported attributes of non-schooling, drift-feeding salmonids were present in some form, but there were many interesting differences in detail. Below, we consider how these differences might be adaptive for fish schooling in a dynamic, 3-D environment, and we contrast them with behaviors observed in “2-D environments,” by which we mean those too flat or shallow for individuals to distance themselves vertically, without overlapping, while sharing the same horizontal space.

### **3.5.1 Territoriality while schooling**

Some of the Chinook salmon fry we observed were clearly territorial, exhibiting site fidelity, exclusivity, and aggression. Many other fish could be considered territorial depending on one's definition. These individuals inhabited relatively stationary spaces from which nearby competitors were excluded by unknown means, possibly including past aggression, subtle body language, or cooperation (mere visible presence could be an "advertisement" that the space is occupied). We are not aware of other reports of territoriality within schooling fish. Hartman (1965) observed juvenile Coho salmon competing aggressively for positions near the front of their groups, but did not report the exclusivity or stationarity of individuals within the group. It is intuitive to think of territoriality and schooling as contrary or mutually exclusive, but this study illustrates conditions under which these behaviors appear to be compatible and to confer complementary fitness benefits. In general, animals in risky environments might benefit from territoriality and aggregation simultaneously in cases where economically defendable territories (Brown 1964) can be small and densely aggregated enough to confer safety without sacrificing the energetic benefits of an exclusive feeding space.

The conditions favoring territoriality-while-schooling are present for drift-feeding Chinook salmon fry in the Chena River. They can thrive in relatively small territories because their food supply is rapidly renewed and independent of production within the territory itself. Because the depth of their habitat (25+ cm) greatly exceeds the size of an IROI (roughly 10-15 cm), fry can form 3-D schools with some non-overlapping territories directly above or below others. Compared to 2-D territorial mosaics in which fish cannot separate vertically within the same horizontal space (due to either lack of depth or unsuitable current speed in surface layers), many more fish in these 3-D schools can fit within the same linear distance of each other without exploiting overlapping spaces, thus increasing the safety associated with numbers.

### 3.5.2 Competition in 3 spatial dimensions

The deep-water environment of Chena River Chinook salmon fry (relative to the spatial scale of individual foraging) may explain several differences between their 3-D behavior and that of salmonids in 2-D territorial mosaics. In a 2-D mosaic distributed throughout the bottom of a pool, territories can vary greatly in character because of variation at the full-pool scale in water velocity and velocity shelters, prey density, and proximity to cover (Railsback et al. 1999; Hayes et al. 2000; Guensch et al. 2001). At the scale of a 3-D school of Chinook salmon fry (within a fraction of a cubic meter), habitat characteristics are more uniform, and a fish may have little incentive to prefer one territory instead of an adjacent one, as long as there is room to maintain an exclusive feeding space in either location.

When confronted with crowding from one side at this relatively homogeneous habitat scale, shifting a few centimeters away from an intruder may be energetically preferable to attacking it. This could explain why so many fish used exclusive spaces without overt defense, and why many of those spaces shifted gradually over time. It could also explain why fish sometimes yielded space after mistaking an adjacent fish's rapid motion as an act of aggression. However, the most compelling evidence for this cooperation comes from some fish matching the movements of their neighbors over long time periods, illustrated in Fig. 3.4a. This "cooperative exclusivity" may be favored in 3-D schooling environments more so than in 2-D environments because 3-D schools contain more nearby competitors to distract aggressive individuals (increasing the time and energy costs of an aggressive strategy) and because 3-D space provides more directions in which individuals can yield to light intruder pressure without reducing habitat quality (reducing the cost of cooperation).

A strategy of cooperative exclusivity is consistent with the absence of linear dominance hierarchies, which have been widely observed in drift-feeding salmonids (Jenkins 1969; Bachman 1984; Fausch 1984; Elliott 1990; Hughes 1992; Nakano 1995). In our study, fish that passively avoided each other rather than aggressively disputing

their space could not be ranked in such a hierarchy. Against this field of relatively passive competitors, the individuals that aggressively defended territories almost always won their disputes and maintained relatively high exclusivity despite attempts at intrusion. Aggressive fish were also among the most stationary individuals observed, and their territories were very close to structure (the river bottom or woody debris), which might provide them with several advantages including velocity shelters, reference points for holding position, and the absence of competitors at certain angles. In essence, they found exceptions to the relatively homogeneous habitat occupied by the rest of the school—microhabitat that could be profitable to defend.

### **3.5.3 Population-level implications of the observed behaviors**

Territoriality has been linked to density-dependent population dynamics in the past based on the premise that individuals capable of maintaining exclusive, favorable feeding territories have a survival advantage over those that cannot (Elliott 1990; Grant and Kramer 1990). Elements of this linkage between survival and territorial feeding behavior are surprisingly evident in Chena River Chinook salmon fry, despite schooling. Thus, the density dependence documented in the stock-recruitment relationship of this population ( J. Neuswanger, Chapter 4, this dissertation) could have arisen, at least in part, from well-established mechanisms of territorial feeding behavior. That we do not understand the relative fitness values of observed foraging strategies remains a gap for connecting survival to behavior. Future research could focus on reliably measuring foraging performance (via capture and gastric lavage rather than counting foraging attempts with unknown outcomes) and developing a better theoretical understanding of the shadow of depleted resources created by each fish and cast toward its downstream competitors.

The disparity between competitors using different strategies may also depend on unknown aspects of their ontogeny and environment. Do individuals prefer consistent strategies throughout their drift-feeding lives as a consequence of their metabolic rates

(Millidine, Armstrong, & Metcalfe 2009) or social personalities (Cote, Fogarty, & Sih 2012)? Or do they regularly alternate between multiple strategies depending on disturbances, satiation, group composition, and other factors? The return of many fish to earlier positions after displacement and the prevalence of territoriality among the largest fish together suggest Chinook salmon fry have at least some sustained preference for their observed strategies. However, variation in opportunity or preference over long time periods encompassing major disturbances could change the mixture of strategies expressed in the population. Future work aimed at understanding movement and behavior in response to disturbance and its effect on competitive disparities may help explain why Chena River Chinook salmon productivity is significantly worse in years with high stream discharge (J. Neuswanger, Chapter 4, this dissertation).

### **3.6 Acknowledgements**

This work was supported by the Arctic-Yukon-Kuskokwim Sustainable Salmon Initiative, the Institute of Arctic Biology, Alaska EPSCoR NSF award #OIA-1208927 and the state of Alaska, and the Department of Biology and College of Natural Sciences and Mathematics at the University of Alaska Fairbanks. David Neuswanger helpfully critiqued this manuscript. This work was conducted under IACUC protocols #134754-1 and #175627-1. Any use of trade, product, or firm names in this publication is for descriptive purposes only and does not imply endorsement by the U.S. Government.

### **3.7 References**

Armstrong, J. D., Huntingford, F. A. & Herbert, N. A. (1999) Individual space use strategies of wild juvenile Atlantic salmon. *Journal of Fish Biology*, 55, 1201-1212.

Bachman, R. A. (1984) Foraging behavior of free-ranging wild and hatchery brown trout in a stream. *Transactions of the American Fisheries Society*, 113, 1-32.

Brown, J. L. (1964) The evolution of diversity in avian territorial systems. *The Wilson Bulletin*, 76, 160-169.

Cote, J., Fogarty, S. & Sih, A. (2012) Individual sociability and choosiness between shoal types. *Animal Behaviour*, 83, 1469-1476.

Elliott, J. M. (1990) Mechanisms responsible for population regulation in young migratory trout, *Salmo trutta*. III. The role of territorial behavior. *Journal of Animal Ecology*, 59, 803-818.

Fausch, K. D. (1984) Profitable stream positions for salmonids: relating specific growth rate to net energy gain. *Canadian Journal of Zoology*, 62, 441-451.

Grant, J. W. A. & Kramer, D. L. (1990) Territory size as a predictor of the upper limit to population density of juvenile salmonids in streams. *Canadian Journal of Fisheries and Aquatic Sciences*, 47, 1724-1737.

Guensch, G. R., Hardy, T. B. & Addley, R. C. (2001) Examining feeding strategies and position choice of drift-feeding salmonids using an individual-based, mechanistic foraging model. *Canadian Journal of Fisheries and Aquatic Sciences*, 58, 446-457.

Hartman, G. F. (1965) The role of behavior in the ecology and interaction of underyearling coho salmon (*Oncorhynchus kisutch*) and steelhead trout (*Salmo gairdneri*). *Journal of the Fisheries Board of Canada*, 22, 1035-1081.



Hayes, J. W., Stark, J. D. & Shearer, K. A. (2000) Development and test of a whole-lifetime foraging and bioenergetics growth model for drift-feeding brown trout. Transactions of the American Fisheries Society, 129, 315-332.

Hollander, M. & Wolfe, D. A. (1999) Nonparametric statistical methods. John Wiley & Sons, Inc. USA.

Hughes, N. F. (1992) Ranking of feeding positions by drift-feeding arctic grayling (*Thymallus arcticus*) in dominance hierarchies. Canadian Journal of Fisheries and Aquatic Sciences, 49, 1994-1998.

Jenkins, T. M., Jr (1969) Social structure, position choice, and micridistribution of two trout species (*Salmo trutta* and *Salmo gairdneri*) resident in mountain streams. Animal Behaviour Monographs, 2, 57-123.

Keeley, E. R. (2000) An experimental analysis of territory size in juvenile steelhead trout. Animal Behaviour, 59, 477-490.

Keeley, E. R. & Grant, J. W. A. (1995) Allometric and environmental correlates of territory size in juvenile Atlantic salmon (*Salmo salar*). Canadian Journal of Fisheries and Aquatic Sciences, 52, 186-196.

Mason, J. C. & Chapman, D. W. (1965) Significance of early emergence, environmental rearing capacity, and behavioral ecology of juvenile coho salmon in stream channels. Journal of the Fisheries Board of Canada, 22, 173-190.

McNicol, R. E. & Noakes, D. L. G. (1981) Territories and territorial defense in juvenile brook charr, *Salvelinus fontinalis* (Pisces: Salmonidae). Canadian Journal of Zoology, 59, 22-28.

Millidine, K. J., Armstrong, J. D. & Metcalfe, N. B. (2009) Juvenile salmon with high standard metabolic rates have higher energy costs but can process meals faster. Proceedings of the Royal Society B - Biological Sciences, 276, 2103-2108.

Nakano, S. (1995) Competitive interactions for foraging microhabitats in a size-structured interspecific dominance hierarchy of two sympatric stream salmonids in a natural habitat. Canadian Journal of Zoology, 73, 1845-1854.

Neuswanger, J., Wipfli, M. S. & Hughes, N. F. (2014) Mechanisms of drift-feeding behavior in juvenile Chinook salmon and the role of inedible debris in a clear-water Alaskan stream. Environmental Biology of Fishes, 97, 489-503.

Puckett, K. J. & Dill, L. M. (1985) The energetics of feeding territoriality in juvenile Coho salmon (*Oncorhynchus kisutch*). Behaviour, 92, 97-111.

R Core Development Team (2014) R: A language and environment for statistical computing. R Foundation for Statistical Computing, Vienna, Austria.

Railsback, S. F., Lamberson, R. H. & Duffy, W. E. (1999) Movement rules for individual-based models of stream fish. Ecological Modelling, 123, 73-89.

Schindler, D., Krueger, C., Bisson, P., Bradford, M., Clark, B., Conitz, J., Howard, K., Jones, M., Murphy, J., Myers, K., Scheuerell, M., Volk, E., & Winton, J. (2013) Arctic-Yukon-Kuskokwim Chinook salmon research action plan: Evidence of decline of Chinook salmon populations and recommendations for future research. Prepared for the AYK Sustainable Salmon Initiative (Anchorage, AK). v + 70 pp.

Steingrímsson, S. O. & Grant, J. W. A. (1999) Allometry of territory size and metabolic rate as predictors of self-thinning in young-of-the-year Atlantic salmon. *Journal of Animal Ecology*, 68, 17-26.

Wilson, E. O. (1975) *Sociobiology: The new synthesis*. Harvard University Press.

3.8 Tables

Table 3.1 Foraging and territorial behavior of Chinook salmon fry

Label	Fork length (mm)	IROI speed (cm/s)	Foraging rate (attempts/min)	Location proximity (unitless)	Foraging proximity (unitless)	Foraging MCD (cm)	Focal MCD (cm)	Aggression (attacks/min)	Observation duration (s)
Aug14_02	73.9	0.07	3.2	26.3	0.0010	5.1	3.5	0.05	1159
Aug14_03	72.3	0.08	2.1	47.5	0.0008	4.1	2.3	0	1201
Aug14_04	71.2	0.07	1.7	24.0	0.0003	3.1	3.1	0	278
Aug14_05	72.1	0.04	1.1	72.6	0.0006	2.5	1.6	0	1201
Aug14_36	69.5	0.14	2.7	42.8	0.0014	4.6	4.7	0	176
Aug14_37	67.3	0.06	3.4	54.5	0.0019	4.5	2.4	0	1139
Aug14_38	74.0	0.02	2.4	36.6	0.0009	3.7	1.1	0.70	1201
Aug14_39	74.9	0.04	1.1	58.1	0.0005	4.2	1.7	0	1195
Aug14_40	70.7	0.16	3.1	37.3	0.0017	4.4	3.7	0	411
Aug14_41	72.9	0.03	1.9	52.3	0.0012	4.3	1.3	0	1201
Aug14_44	71.4	0.06	2.7	24.6	0.0007	4.5	1.6	0	1201
Aug14_45	66.4	0.07	1.1	69.5	0.0006	3.4	2	0	1201
Aug14_46	67.6	1.34	1.2	26.8	0.0004	11.3	8.6	0	52
Aug14_47	80.4	0.01	2.0	2.3	0.0000	15.6	0.6	0.60	1201
Aug14_48	75.9	0.02	3.1	32.5	0.0008	8.4	1.2	0.05	1201

Table 3.1 continued...

Aug14_49	70.9	0.12	5.2	18.9	0.0015	9.2	6.6	0	252
Aug14_50	75.0	0.09	1.5	31.1	0.0005	3.4	1.1	0	1054
Aug14_51	68.2	0.05	1.6	53.0	0.0009	3.7	1.1	0	1201
Aug14_52	75.5	0.05	1.3	73.0	0.0008	3.2	1.7	0	947
Aug14_53	70.1	0.13	2.5	39.9	0.0011	10.1	4.3	0	169
Aug14_54	73.4	0.03	0.6	26.2	0.0000	3.1	1.5	0	568
Aug14_55	72.0	0.07	3.4	40.3	0.0012	2.8	2.1	0	488
Aug14_56	70.2	0.13	1.7	32.4	0.0011	6	2.7	0	181
Aug14_57	73.6	0.45	0.0	32.4	0.0000	n/a	0.9	0	38
Aug14_58	77.1	0.03	2.7	32.5	0.0013	3.8	1.2	0.10	1201
Aug14_59	61.2	0.81	8.6	4.4	0.0010	3.1	3	0	35
Aug14_61	66.4	3.21	4.9	23.5	0.0016	4.9	1.6	0	12
Aug14_62	63.8	3.30	0.0	11.8	0.0000	n/a	2.9	4.00	15
Aug14_63	56.2	4.28	0.0	18.5	0.0000	n/a	1.9	0	14
Aug14_64	74.0	1.42	1.5	18.9	0.0001	0.4	3.2	0	40
Aug14_65	70.6	0.81	5.2	13.3	0.0007	2.7	2.1	0	46
Aug14_66	56.1	1.35	0.0	13.1	0.0000	n/a	1.7	0	32
Aug14_67	63.6	0.12	4.9	36.7	0.0023	5.2	2.6	0	304
Aug14_68	65.9	0.57	3.7	43.6	0.0032	3.2	1.3	0	48
Aug14_69	60.2	1.49	5.6	21.8	0.0020	7.4	1.2	0	21
Aug14_70	68.1	0.11	2.5	31.2	0.0012	4.9	3	0	428
Aug14_74	69.3	1.38	1.2	18.5	0.0003	2.6	5.7	0	51

Table 3.1 continued...

Aug14_75	73.0	1.22	2.4	18.8	0.0013	3.4	5.9	0	50
Jul9_01	58.1	0.25	0.8	10.4	0.0002	7.3	6.6	1.00	300
Jul9_02	52.4	0.12	5.8	7.2	0.0035	6.6	6.4	0.20	300
Jul9_03	54.0	0.26	3.8	7.5	0.0019	8.7	7.9	3.45	157
Jul9_05	48.9	0.06	4.3	5.6	0.0026	8.2	2.6	0.68	265
Jul9_06	49.8	0.14	9	5.5	0.0090	6.7	4	0	255
Jul9_07	46.9	0.27	15.2	0.4	0.0025	8.8	5	0	94
Jul9_11	49.3	0.42	12.6	4.0	0.0291	2.5 <sup>a</sup>	2.3	0	29
Jul9_12	53.2	1.00	1.7	8.4	0.0000	4.7	3.2	6.68	36
Jul9_33	51.5	0.33	16.4	2.5	0.0288	1.1	1.5	0	22
Jul9_35	51.0	0.67	13.8	1.3	0.0029	5.3	4.4	0	61
Jul9_36	50.7	3.73	6.2	1.6	0.0012	0.1	0	0	10
Jun11_03	35.7	0.04	3.8	88.7	0.0473	2.9	2.1	0	300
Jun11_04	35.0	0.04	8.6	98.8	0.1513	3.5	2.2	0	300
Jun11_05	35.1	0.08	12.7	39.5	0.1399	3.8	2.7	0	119
Jun11_06	35.2	0.07	12.1	78.3	0.1205	5.5	4.6	0	292
Jun11_07	35.4	0.06	5	91.8	0.0721	4.4	2.3	0	300
Jun11_08	34.9	0.19	13.9	42.4	0.1195	7.1	5.4	0	138
Jun11_10	35.0	1.54	7.4	31.0	0.0823	3.2	2.9	0	24
Jun11_11	35.7	0.46	7.8	27.8	0.0798	1.7	1.6	0	46
Jun11_12	33.7	0.72	7.7	25.8	0.0678	2.8	2.2	0	55

Table 3.1 continued...

Jun11_T3	35.5	0.19	11.5	58.6	0.1453	5.5	4.2	0	120
Jun11_35	35.2	1.10	7	26.7	0.0455	2.2	0.6	0	17
Jun11_36	35.5	11.12	7.3	10.9	0.0432	0.4 <sup>a</sup>	0	0	16
Jun11_37	36.7	4.50	11.7	24.0	0.0686	2.3	0.6	0	5
Jun11_38	36.0	1.88	5.6	20.3	0.0405	2.4 <sup>a</sup>	0.7	0	22
Jun11_39	35.6	0.60	17.5	24.0	0.0901	0.5	0.9	0	14
Jun11_40	34.5	0.27	5.7	26.4	0.0383	4.3	5.1	0	84
Jun11_41	35.7	0.20	6.2	33.1	0.0524	4.7	1.8	0.34	176
Jun11_42	35.3	0.13	14.2	45.4	0.1449	3.6	2.8	0	93
Jun11_43	31.8	7.79	11.5	25.4	0.0753	4.6 <sup>a</sup>	0.4	0	5
Jun11_44	35.1	0.13	12.7	35.8	0.1275	4.5	2.9	0	90
Jun11_45	34.6	1.24	3.2	27.3	0.0592	2.3	3.2	0	38
Jun11_46	35.9	0.91	9.8	37.2	0.1507	3.4	3.3	0	37
Jun11_47	33.9	0.04	6.1	38.9	0.0452	2.5	2.4	0	228
Jun11_48	33.8	2.05	11.4	29.8	0.0879	0.6 <sup>a</sup>	0.8	0	16
Jun11_49	34.7	0.85	5.7	38.2	0.1010	2.7	1.9	0	32
Jun11_50	34.6	0.14	7.9	24.5	0.0389	3.9	1.9	0	68
Jun11_51	34.2	1.40	3.6	18.3	0.0103	14.5	2.1	0	17
Jun11_52	34.8	0.21	5.1	11.2	0.0281	4.6 <sup>a</sup>	2.7	0	47

<sup>a</sup> The foraging MCDs of these fish were likely underestimated because 30% or more of their foraging attempts occurred off-screen in one of the cameras. Such foraging attempts were included for calculation of foraging attempt rates.

### 3.9 Figures

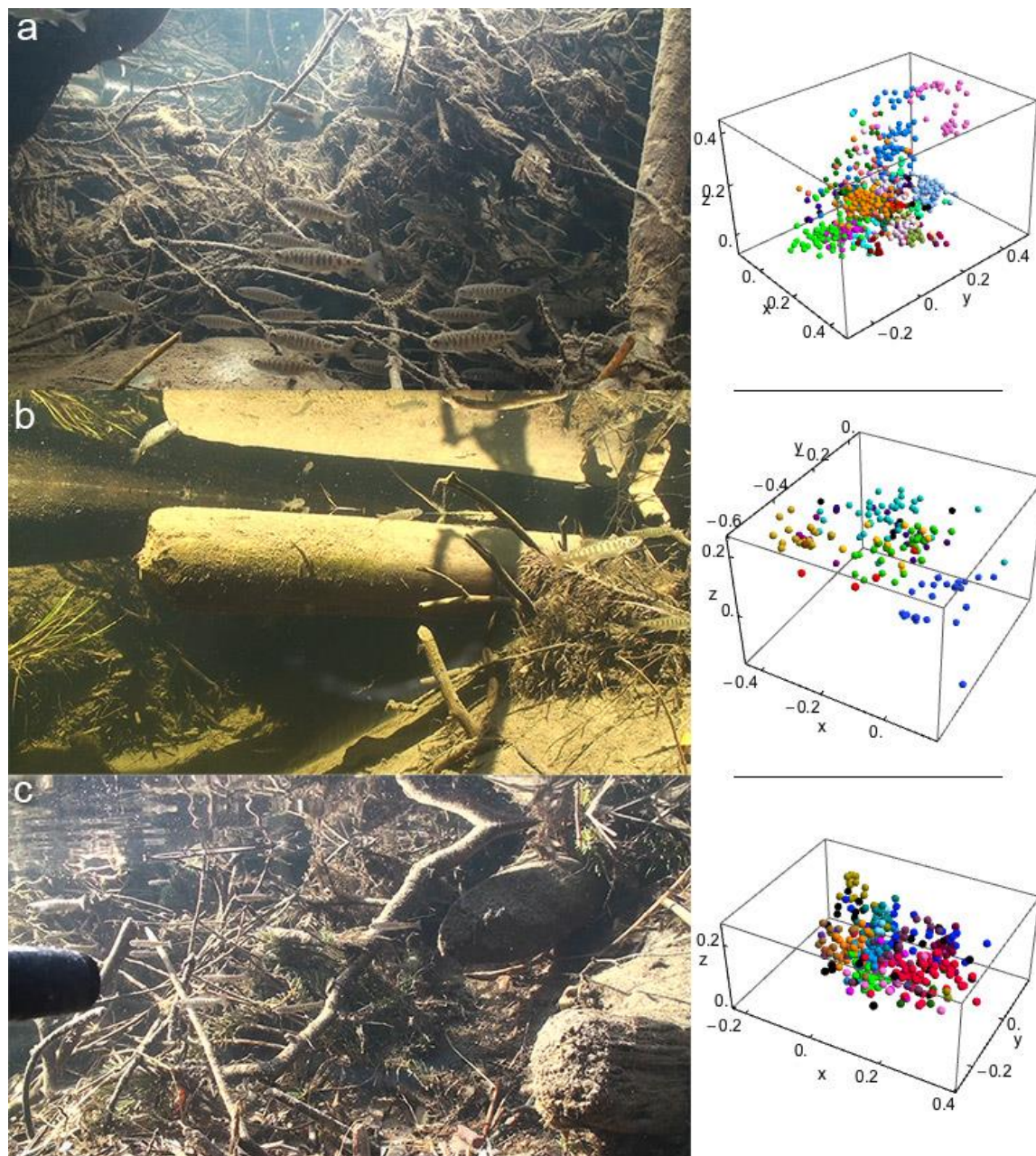


Fig. 3.1. Single camera view of sites from (a) Aug 14, 2009, (b) Jul 9, 2010, and (c) Jun 11, 2009. Adjacent are 3-D foraging attempt positions from all fish in each video over a twenty-minute period in a and five-minute periods in b and c. Each color represents an individual fish, with the exception of black, which represents any of several transient “floater” individuals.



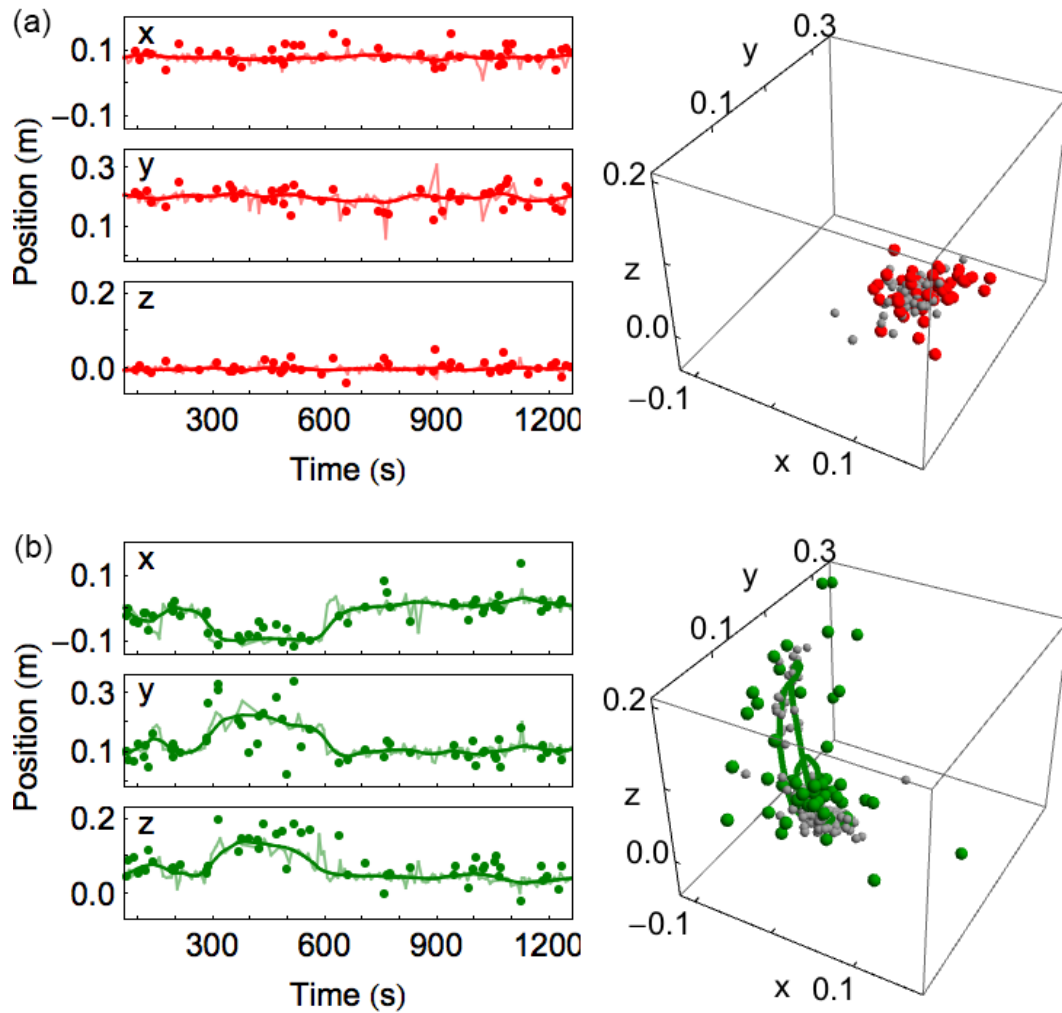


Fig. 3.2. Example 2-D (left) and 3-D (right) IROI representations of (a) a highly stationary fish (Aug14\_38) and (b) a moderately stationary fish (Aug14\_44), which gradually shifted to a distant position and then returned to its earlier location. Colored points on both plots indicate foraging attempt positions. Focal point positions recorded at five-second intervals are indicated by gray points on 3-D plots and faint lines on 2-D plots. Dark lines in all plots indicate the IROI centers calculated by LOESS regression.

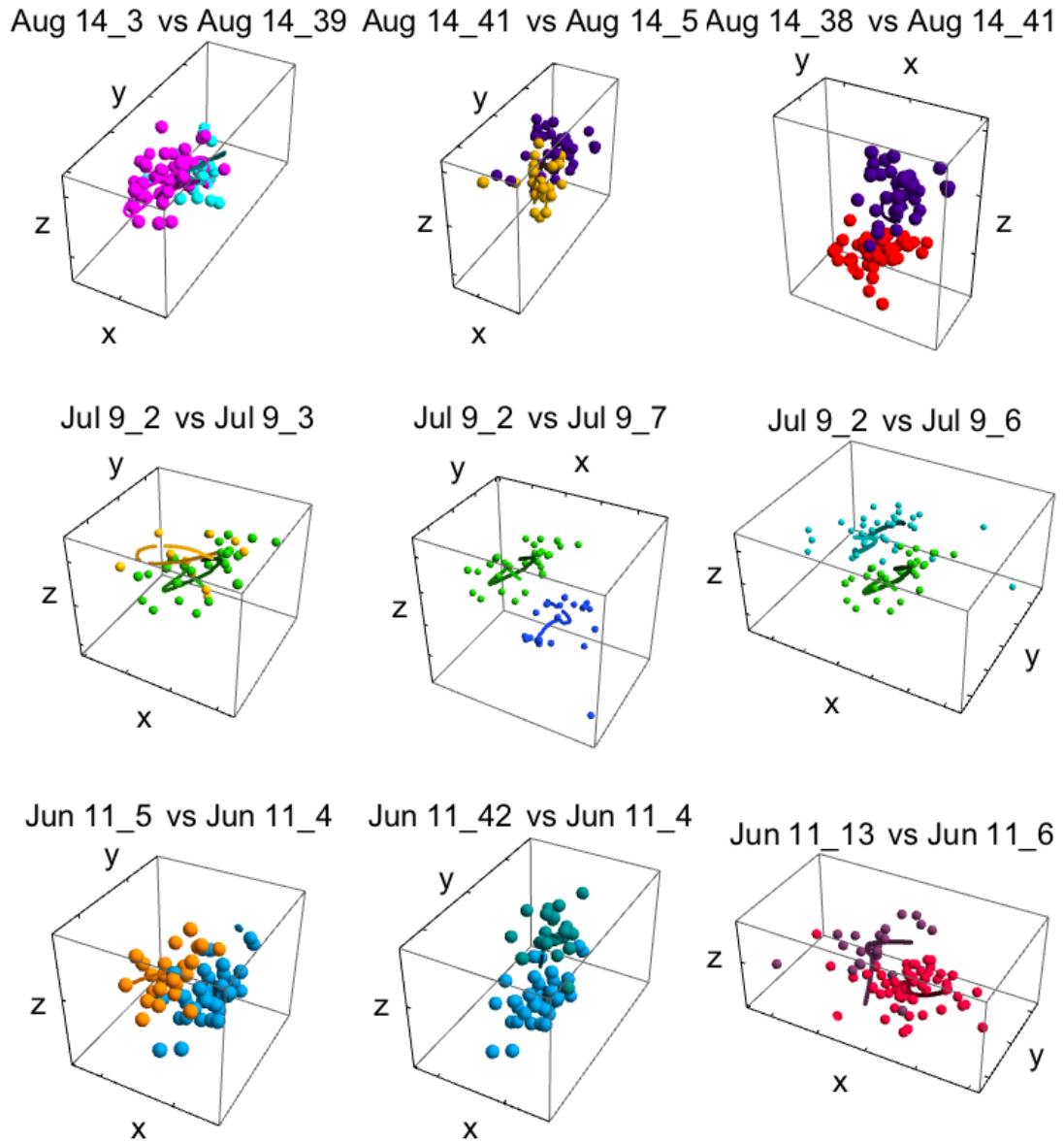


Fig. 3.3. 3-D plots of foraging attempts (spheres) and IROI centers (lines) for the three pairs of fish in closest proximity to each other (highest-ranking *ForgProx* and *CentProx*) on each observation date, excluding pairs with less than 600 seconds (Aug 14) or 90 seconds (Jul 9 and Jun 11) of concurrent observation time. Lines are shaded to represent early (light) versus later (dark) observations. Tick marks on axes indicate 0.1-m intervals. The x-axis from left to right is downstream; the z-axis is vertical.

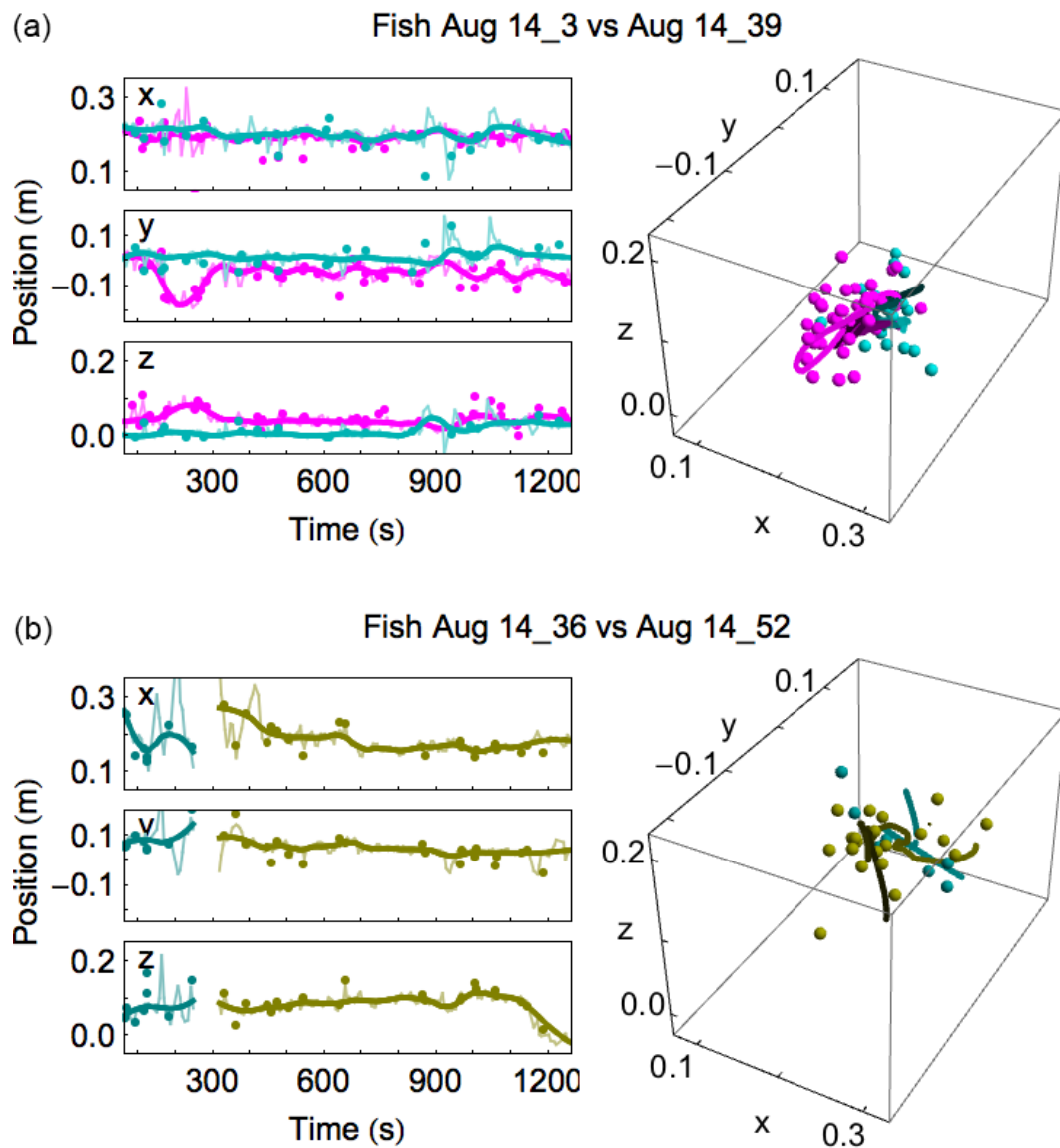


Fig. 3.4. 2-D and 3-D plots that illustrate examples of two different pairs of fish from the Aug 14 video that (a) remained in close proximity to each other with some synchronous movement, and (b) used the overlapping space but at different times. Dots represent foraging attempts, thick lines IROI centers, and thin lines direct interpolations of each fish's recorded focal points. The 3-D plots on the right provide a combined spatial view of the pattern in movement over time evident in the 2-D plots of the  $x$  (streamwise),  $y$  (cross-stream), and  $z$  (vertical) coordinates.

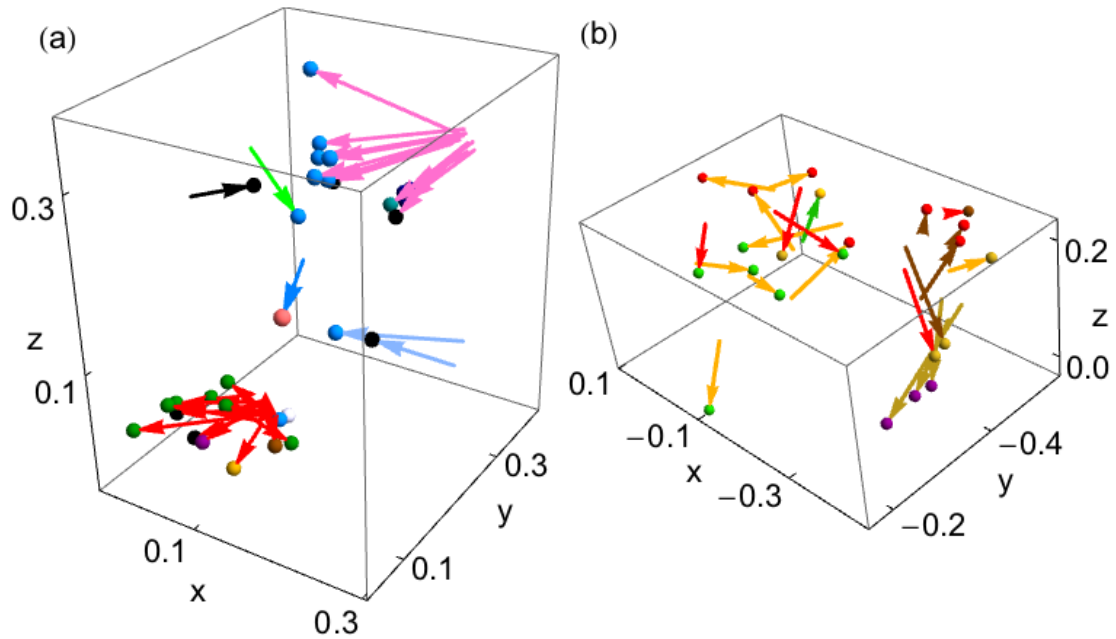


Fig. 3.5. Spatial plots of aggression displayed by Chinook salmon in the (a) Aug 14 video (twenty minutes of footage) and (b) Jul 9 video (five minutes of footage). Coordinates are shown in meters along the  $x$  (streamwise),  $y$  (cross-stream) and  $z$  (vertical) directions. Arrows point from the position of the aggressor to the position of the target at the moment the aggressor began the attack. Each color represents an individual fish, with the exception of black, which represents any of several transient "floater" individuals. Colored spheres at the ends of arrows indicate the identity of the fish targeted by the aggression.

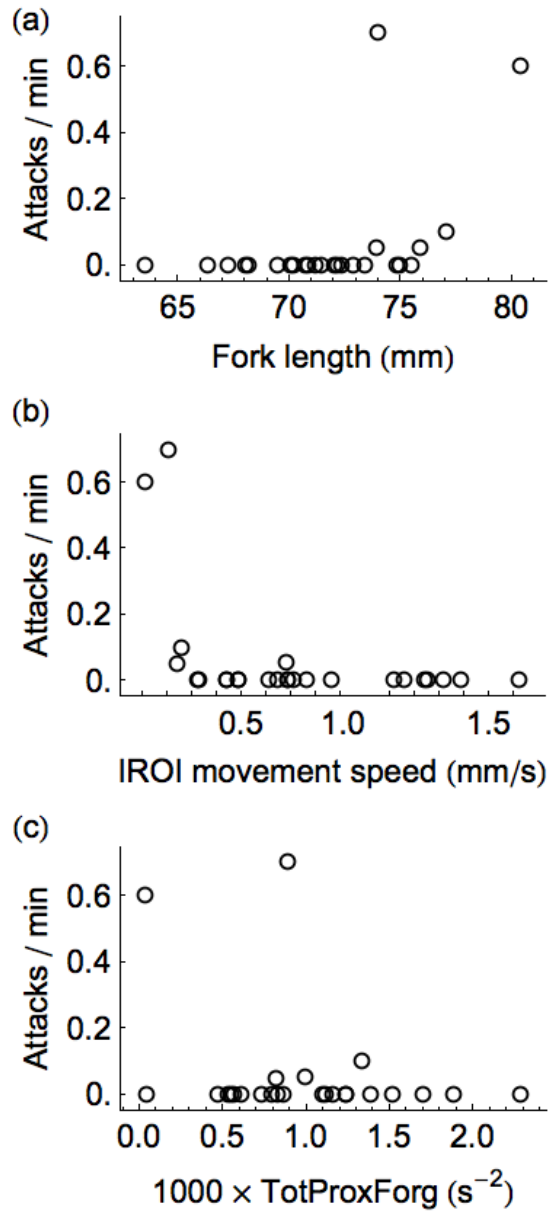


Fig. 3.6. Relationships between aggression rate in the Aug 14 video and the aggressor's (a) fork length, (b) IROI movement speed, an indicator of long-term motion of the space the fish is using, and (c) total foraging proximity index, an indicator of the spatiotemporal proximity of its foraging attempts to those of its neighbors. Fish observed for less than one minute are not included.



## CHAPTER 4:

### **Low productivity of Chinook salmon strongly correlates with high summer stream discharge in two Alaskan rivers in the Yukon drainage<sup>1</sup>**

#### **4.1 Abstract**

Yukon River Chinook salmon populations are declining for unknown reasons, creating hardship for thousands of stakeholders in subsistence and commercial fisheries. An informed response to this crisis requires understanding the major sources of variation in Chinook salmon productivity. However, simple stock-recruitment models leave much of the variation in this system's productivity unexplained. We tested adding environmental predictors to stock-recruitment models for two Yukon-drainage spawning streams in interior Alaska—the Chena and Salcha rivers. Low productivity was strongly associated with high stream discharge during the summer of freshwater residency for young-of-the-year Chinook salmon. This association was more consistent with the hypothesis that sustained high discharge negatively affects foraging conditions than with acute mortality during floods. Productivity may have also been reduced in years when incubating eggs experienced major floods or cold summers and falls. These freshwater effects—especially density dependence and high discharge—helped explain population declines in both rivers. They are plausible as contributors to the decline of Chinook salmon throughout the Yukon River drainage.

---

<sup>1</sup> Neuswanger, J., Wipfli, M.S., Evenson, M.J., Hughes, N.F., and Rosenberger, A.E. Low productivity of Chinook salmon strongly correlates with high summer stream discharge in two Alaskan rivers in the Yukon drainage. Prepared for submission in Canadian Journal of Fisheries and Aquatic Sciences.

## 4.2 Introduction

In most years since 1998, the abundance of Chinook salmon (*Oncorhynchus tshawytscha*) in the Yukon River drainage has been low compared to historical averages (Schindler et al. 2013), similar to patterns in many drainages throughout Alaska (ADF&G 2013). Harvest restrictions prompted by declining stocks have caused severe hardship for thousands of stakeholders in commercial and subsistence fisheries. This problem has elicited disaster declarations and nationwide media attention (Milkowski 2009). Despite commercial fishery closures and restriction of subsistence harvest to levels below the “amount necessary for subsistence” (as designated by the Alaska Board of Fisheries), escapement up the Yukon River into Canada has failed in recent years to reach the minimum required by international treaty (Schindler et al. 2013). An informed response to this crisis requires that we identify the major drivers of salmon productivity in these systems.

To facilitate management decisions and investigate population trends, the dynamics of salmon populations can be summarized using stock-recruitment models (Quinn and Deriso 1999) that relate the estimated spawning stock in each brood year (the number of adult fish, of mixed age, that escape the fishery to spawn in that year; i.e., escapement) with the number of recruits produced (the total number of offspring from that brood year that eventually returned, over multiple years, to be harvested or spawn themselves). The ratio of recruits per spawner in a given brood year, termed “productivity,” must be at least one for the spawners to fully replace themselves.

Commonly used stock-recruitment models such as the Ricker (1954) model describe the productivity of a population using a constant “productivity parameter” and one or more “density dependence” parameters, which represent the effects of intra-specific competition and any other mechanisms by which the number of spawners affects the number of recruits *per* spawner. These models often leave a large portion of the variation in productivity unexplained. For the stream-type Chinook salmon of the Yukon



River drainage, the unexplained variation might be attributed to any of the natural and anthropogenic factors affecting stream-type Chinook salmon in freshwater streams during their first year, in estuarine or near-shore ocean habitats during their second year, in the off-shore ocean environment thereafter, or in the rivers hosting their long-distance migrations as smolts and returning spawners.

Processes acting on juvenile salmonids during their first few months in freshwater can determine much (often more than half) of the variation in productivity (Elliott 1989b; Bradford 1995; Keeley 2001). This may be true even if mortality rate later in life is high, provided it is less variable than juvenile mortality in freshwater. For example, only an estimated 6% of juvenile Canadian-origin Yukon drainage Chinook salmon, captured during their first few months at sea by the Bering-Aleutian Salmon International Survey, survived to maturity. Despite this low marine survival rate, juvenile abundance was highly correlated ( $r = 0.89$ ) with the eventual recruitment of their brood year (Murphy et al. 2013). Thus, most of the variation in recruitment was probably generated during the freshwater stage (including the spawning success of the parent stock and juvenile survival) or the first few months at sea.

The density-independent variables of stream discharge and temperature are also important determinants of salmonid productivity because of their significant ecological and physiological effects. Temperature controls the rate of development and emergence times of juveniles from spawning grounds (From and Rasmussen 1991), and it mediates the relationship between food consumption, growth, and body condition (Elliott and Hurley 1999). Patterns in stream discharge affect salmonids in diverse ways. Water that is flowing faster, is more turbid, or carries more debris than normal may reduce foraging success in sight-feeding fishes (O'Brien and Showalter 1993; Piccolo et al. 2008; Neuswanger et al. 2014). Turbidity associated with high discharge inhibits primary production (Benson et al. 2013). Large floods can kill incubating embryos in the spawning gravel (Healey 1991; DeVries 1997) or displace fry from desirable habitats (Ottaway and Clarke 1981). However, moderately high discharge also creates more

wetted habitat for primary productivity and occupation by fishes, and high-discharge events can entrain more invertebrate prey for fish (Gibbins et al. 2007).

Because the potential effects of discharge and temperature are so diverse, understanding how they affect a particular salmon run requires direct study of that population or representative sub-populations. In this study, we examine the effects of stream discharge and other environmental factors on Chinook salmon productivity in the Chena and Salcha rivers, tributaries of the Tanana River in the Yukon River drainage in central Alaska. Specifically, we sought to 1) test the relationship between stream discharge and productivity, 2) determine whether the discharge-productivity relationship is sensitive to the choice of a specific discharge statistic or time period, 3) determine whether the relationship explains the decline in Chinook salmon productivity in the Chena and Salcha rivers, and 4) search for other relationships with discharge and temperature during both the spawning and rearing periods. We integrate our findings with those of previous ecological studies on the Chena River to identify the most plausible mechanisms behind a discharge-productivity relationship and to identify priorities for new research on both population dynamics and ecological mechanisms affecting individual fish directly.

## **4.3 Methods**

### **4.3.1 Study rivers**

We analyzed twenty years (1986-2005) of Chinook salmon stock-recruitment data for the Chena River and nineteen years (1987-2005) for the Salcha River. These were the only individual spawning streams in the Yukon River drainage for which data were available for long-term run reconstructions. These fifth-order tributaries of the glacial Tanana River in interior Alaska lie in geographically similar, adjacent watersheds, and they join the Tanana 56 km apart (WGS84 coordinates 64°47'52"N 147°54'43"W for the Chena River outlet, and 64°29'15"N 146°59'13"W for the Salcha River outlet). Median

discharge during the open-water season<sup>2</sup> was 47 m<sup>3</sup>/s near the mouth of the Chena River and 59 m<sup>3</sup>/s near the mouth of the Salcha River. We developed stock-recruitment models using the Chena River data, and we tested the same models in a strictly confirmatory analysis of the Salcha River data. However, data for the Salcha River were not completely independent of those for the Chena River because of the proximity of the rivers, the similarity of their watersheds, and the fact that the non-recreational harvest portions of their recruitment estimates were both proportional to a single, middle-Yukon harvest estimate that could not be resolved to the level of individual-river stocks.

#### **4.3.2 Salmon run reconstructions**

Available estimates of in-river harvest, spawner abundance (also termed escapement), and spawner age composition were used to generate age-structured run reconstructions—paired estimates of spawning stock from each brood year and the number of recruits they produced (Table 4.1). Escapement of adult Chinook salmon was estimated annually in the Chena River from 1986 through 2010 and in the Salcha River from 1987 through 2010 using either mark-recapture or counting tower techniques (Savereide 2012). Mark-recapture estimates in the Chena River were thought to underestimate total escapement; therefore all mark-recapture estimates were increased by a factor of 1.24 based on a single-year calibration (ratio of the two estimates) in 1997 when both methods were used (Stuby and Evenson 1998). Age compositions of the escapements were estimated annually in each river from scale samples collected from carcasses recovered from spawning grounds.

---

<sup>2</sup> “Median discharge” was the median of the annual values (from 1986 to 2006) of the median of the daily mean discharge values (from April 26 to September 30). The number from the Chena River gaging station is taken from station 15514000 in Fairbanks near the outlet (for size comparison with the Salcha River), whereas the later analysis of Chena River discharge as an environmental correlate refers to a gaging station farther upstream in an area inhabited by more juvenile Chinook salmon.

Commercial and subsistence fishing occur on a mixture of spawning stocks in the main stem Yukon and Tanana rivers as Chinook salmon are en route to their spawning grounds. Total annual commercial harvests by fishing district were estimated from mandatory returns of fish tickets and were considered censuses of total harvest. Subsistence harvests by district were determined from household surveys and considered a census of total harvest. Age compositions of the commercial and subsistence catches were determined from analysis of scales collected from a sample of the harvest in each district. Identification of specific spawning stocks in the commercial and subsistence harvest was not possible. However, scale pattern analysis was used from 1986-2003 and genetic methods have been used since 2004 to identify run of origin from the commercial and subsistence catch (e.g., Dubois et al. 2009). Runs were identified as lower (below river km 1000), middle (between river km 1,000 and 2,000), and upper (above river km 2,000) river stocks. Chinook salmon bound for the Chena and Salcha Rivers comprise a portion of the middle run harvest in each fishing district.

Small recreational fisheries occur in the lower 3 km of the Salcha River and in the lower 72 km of the Chena River. Estimates of total annual recreational harvest in these rivers are obtained through an annual statewide mail-out harvest survey (e.g., Jennings et al. 2010). Age and sex composition of the recreational harvest is not known. Since 1986, annual harvests of Chinook salmon have ranged from 39 to 1,280 in the Chena and 47 to 1,448 in the Salcha. To estimate age-specific harvest in each river, we assumed age composition of the recreational harvest was equivalent to that of escapement.

We could not directly estimate the proportion of middle-run harvest by commercial and subsistence fishers that was comprised of Chinook salmon from the Chena and Salcha rivers. Results from a three-year Yukon River Chinook salmon radiotelemetry study estimated that fish heading upstream to the Chena and Salcha rivers comprised an average of 0.427 of middle-run stocks present in the lower Yukon River during 2002-2004, respectively (Eiler et al. 2004, 2006a, 2006b). This proportion was used to apportion middle-run harvest to Chena *and* Salcha river stocks for all years in the

data set. Harvest was further apportioned to Chena *or* Salcha river stocks for each age class each year based on the relative proportional escapement of each stock (e.g., ratio of Chena escapement in year  $y$  to Chena plus Salcha escapement in year  $y$ ).

Complete recruitment estimates (for ages 3-8) were available for years 1986-2002 for the Chena River and 1987-2002 for the Salcha River. For age-8 fish from the 2003 brood year, ages 7-8 fish from the 2004 brood year, and ages 6-8 fish from the 2005 brood year, recruitment was extrapolated from a) the average proportion of fish returning at each age in past years, and b) the known returns (in previous years) of younger fish from each brood year.

Recruitment of each age class from a given brood year was estimated as the sum of escapement  $\hat{N}_{a,y+a}$  by age and harvest ( $\hat{H}_{river,a,y+a}$ ) by age within a calendar year:

$$(4.1) \quad \hat{R}_{a,y} = \hat{N}_{a,y+a} + \hat{H}_{rec,a,y+a} + \hat{H}_{river,a,y+a}$$

where  $y$  denotes year class and  $y + a$  the calendar year. Total recruitment for each year class in the data set was estimated as the sum of recruitment over all age classes:

$$(4.2) \quad \hat{R}_y = \sum_{a=3}^8 \hat{R}_{a,y}$$

### 4.3.3 Stream discharge and temperature data sources

We calculated environmental variables from publically available stream discharge and temperature records, including daily discharge data from online records of USGS hydrographs on both the Chena River (station number 15493000) and the Salcha River (station number 15484000). To estimate daily mean water temperature from 1986 to 2006, we used the only available water temperature records from the same gaging station on the Chena (2007 to 2011) to parameterize a non-linear regression predicting daily mean water temperature from the daily mean air temperature at Fairbanks International Airport (FAI). Water temperature at this station was most strongly correlated with the previous day's air temperature ( $r = 0.86$ ; time lags of zero to four days were examined).

We used a non-linear regression model (van Vliet et al. 2011) developed for predicting river water temperature  $T_{water}$  from air temperature  $T_{air}$  and stream discharge; however, the stream discharge term did not improve the model's explanatory power enough to justify an extra parameter, so we excluded it in a simplified model:

$$(4.3) \quad T_{water} = \mu + \frac{\alpha - \mu}{1 + e^{\gamma(\beta - T_{air})}} + \varepsilon \text{ where } \gamma = \frac{4 \tan \theta}{\alpha - \mu}$$

The lower bound on water temperature was  $\mu = 0$  °C, and  $\varepsilon$  represents random error. Fitted parameters for the Chena were  $\alpha = 11.45$ ,  $\theta = 0.5524$ , and  $\beta = 11.86$ . This relationship explained most of the variation in water temperature ( $R^2 = 0.95$ ), with the greatest discrepancies during ice-out. Separate water temperature data were not available for the Salcha River, so we assumed it was the same as in the nearby Chena River.

#### 4.3.4 Stock-recruitment models and environmental predictors

We used generalized versions of the Ricker (1954) stock-recruitment model to investigate patterns of productivity in relation to several measures of stream discharge and temperature. We present detailed results from three variants of the model: 1) the “basic model,” meaning the original Ricker model; 2) the “discharge model,” which was used for confirmatory analysis of an *a priori* hypothesis that poor recruitment is associated with high stream discharge during the summer the juveniles spent in freshwater; and 3) the “full model,” the version most strongly favored by an objective model selection process in an exploratory analysis of the Chena River data using the twelve possible predictors listed in Table 4.2.

The basic model related recruits  $R$  to spawners  $S$  with fitted parameters  $\alpha$  representing productivity (recruits per spawner) in the absence of density dependence,  $\beta$  representing the magnitude of density dependence, and random error  $\varepsilon$ .

$$(4.4) \quad R = \alpha S e^{-\beta S} e^{\varepsilon}$$

Environmental predictors were represented as additional terms in the exponent of the model, following the description of the “generalized Ricker model” in Quinn and Deriso (1999):

$$(4.5) \quad R = \alpha S e^{-\beta S + \gamma_i X_i} e^{\varepsilon}$$

Here,  $X_i$  represents the value of the  $i$ th environmental predictor, and  $\gamma_i$  is the fitted parameter scaling its effect on the model.

The discharge model incorporated one environmental predictor, an indicator variable equal to 0 when discharge was high during the summer growing season and 1 when discharge was low. The summer growing season was defined *a priori* to extend from April 26 (mean date of spring break-up from 1968 to 2010 on the Chena) to September 30 (an approximation of when the Chena River begins to freeze, based on personal field observations). The threshold separating high- and low-discharge years, selected by graphical examination of the residuals from the basic model, was counted as an additional fitted parameter occupying one degree of freedom in calculations of model quality measures. This threshold allows the model to approximate a sigmoid relationship with one less parameter, reducing the risk of overfitting. Unlike linear regression, this model captures a realistic feature of our biological hypothesis that discharge affects recruitment in high-discharge years but does not substantially affect differences in recruitment among low- to medium-discharge years.

In a separate, exploratory analysis, we compared models of every possible combination of the eleven environmental variables in Table 4.2, with or without  $S$ . Interaction terms were not included. All variables were modeled as simple linear effects, except that median discharge over the summer growing season was modeled with a threshold effect using the threshold selected for the discharge model. Some variables were considered in each of three periods of interest: 1) the summer growing season; 2) the “critical emergence period” from May 15 to June 15 when newly emerged fry might be most sensitive; and 3) “spawning and incubation period,” defined *a priori* to span the pre-winter portion of incubation time from July 20 (the earliest date spawning is typically

observed) to October 25 (the last date water temperature differed appreciably from mid-winter levels during 2007-2011 when instrumental water temperature data were available). Temperature was expressed as total degree-days in °C over the period of interest. We used the Richards-Baker Flashiness Index (Baker et al. 2004) to represent the variation in discharge within each period. Although flashiness is typically used to compare the hydrology of different streams over multi-year time scale, we chose it as a potentially useful descriptor of intra-annual variation in discharge because it incorporates both the frequency and magnitude of fluctuations in discharge into a single statistic.

#### **4.3.5 Model fitting and assumptions**

All models were fit using least squares linear regression on log productivity (the natural logarithm of recruits per spawner). The regression assumption that residuals were normally distributed was met for all models presented here (Kolmogorov-Smirnov test,  $p > 0.23$  indicating failure to reject the null hypothesis of normality at the 5% significance level). Homogeneity of variance was established by graphical examination of residuals. Residuals from the basic model were also checked for first-order temporal (i.e., one-year lag) autocorrelation using the Durbin-Watson test (Durbin and Watson 1950). The Durbin-Watson  $D$  statistic for the Chena River residuals was 2.30, indicating the absence of significant autocorrelation (the null hypothesis that the data were not autocorrelated was not rejected at the 5% significance level). The Salcha River residuals showed minor, negative first-order autocorrelation ( $D = 2.86$ , marginally significant at the 5% level). Positive autocorrelation indicating streaks of good or bad years is commonly problematic for stock-recruitment models (Quinn and Deriso 1999); however, minor negative autocorrelation is less troubling. It may be spurious, or a weak sign of some alternating-year biological process, but it should not influence our limited inferences from the Salcha models.



#### 4.3.6 Model selection and evaluation

We used the information-theoretic approach (Burnham and Anderson 2002) to evaluate the performance of models and importance of variables. These analyses are based on Akaike's Information Criterion adjusted for finite sample sizes (AICc), which reflects on whether the inclusion of extra parameters in a model improves the model's likelihood sufficiently to justify the extra parameters. AICc is interpreted not according to its literal value, but by comparing it among alternative models of the same data; a difference in AICc (denoted  $\Delta\text{AICc}$ ) of two or more is conventionally interpreted to indicate that the model with the lower AICc better balances explanatory power against the possibility of spurious model parameters. The Akaike weight, calculated from AICc, reflects the relative weight of evidence in the data for each model in a set of candidate models. The relative importance of individual variables is expressed by adding the Akaike weights of all the models containing each variable (provided each variable appears in the same number of models, which was the case in our exploratory analysis).

The basic and discharge models were selected for detailed reporting for qualitative reasons: the basic model because it is widely used for management, and the discharge model for evaluation of the *a priori* hypothesis that high discharge reduces recruitment. The full model was selected as the "best" model for the Chena River data, based on several criteria described below, including the lowest AICc in the exploratory analysis. To estimate the explanatory power of the models we selected, we used the coefficient of determination adjusted for the number of parameters, denoted  $R_a^2$ , which reflects the proportion of variation in log productivity that could be explained by the model (standard  $R^2$ ), adjusted downward to account for the expected reduction in variability with the addition of any parameter, even uninformative ones.

#### 4.3.7 Explanation of the population decline

To determine whether the effects we detected could potentially explain the decline in Chinook salmon productivity, we plotted log productivity versus time and

compared against the residual log productivity versus time from the basic Ricker model, the discharge model, and the full model. If the visible decline in log productivity was reduced in a model's residuals, we cautiously inferred that the model provides one plausible explanation for part of the decline.

#### **4.3.8 Sensitivity analysis**

We graphically examined the model's sensitivity to our choice of discharge statistics. To determine whether the whole-season discharge effect we observed might be a signature of a stronger effect during a specific critical time period, or a spurious artifact of the period we selected, we plotted the likelihood of the discharge model for all possible time periods ranging from seven days in duration to the entire open-water season. We also examined the effects of using a different discharge statistic (e.g., some other quantile of discharge instead of the median, or the number of days with discharge below a given threshold) to evaluate the sensitivity of the discharge effect to our particular choice of summary statistic. Our twenty-year data set was too small to treat these values as model parameters without risk of overfitting, but the patterns evident in the post-hoc graphical analysis are helpful for interpreting the model results.

### **4.4 Results**

#### **4.4.1 Basic model and its residuals**

The basic Ricker model explained a substantial portion of the variation in log productivity in the Chena River (Fig. 4.1*a*;  $R_a^2 = 0.50$ ) and the Salcha River (Fig. 4.1*b*;  $R_a^2 = 0.70$ ). The residuals from this model (the unexplained portion of log productivity) were inversely related to median discharge during the summer growing season in both the Chena River (Fig. 4.2*a*) and the Salcha River (Fig. 4.2*b*), meaning both rivers produced more recruits per spawner than the model predicted during low-discharge years and fewer during high-discharge years. Compared to linear regression, this relationship was better

described by an ANOVA model with a “threshold” effect of a categorical variable indicating whether median discharge did or did not exceed 27.2 m<sup>3</sup>/s in the Chena River ( $\Delta\text{AICc} = 6.4$ ) or 70.8 m<sup>3</sup>/s in the Salcha River ( $\Delta\text{AICc} = 1.2$ ).

The relationship between discharge and the basic Ricker model residuals was not limited to our arbitrarily chosen summary statistic, the median summer discharge. The large region of separation in Fig. 4.3a between high discharge / low productivity years and low discharge / high productivity years shows the discharge effect in the Chena River could be captured by many different summary statistics, including quantiles of discharge such as the median or threshold exceedance statistics (e.g., number of days with discharge greater than 25 m<sup>3</sup>/s). The discharge effect is similarly flexible in the Salcha (Fig. 4.3b), except that one high-discharge year (2001) was anomalously productive.

#### 4.4.2 Discharge model and its residuals

We compared four possible linear models containing spawner density ( $S$ ), the categorical discharge effect ( $DISCH$ ), or their interaction, in a confirmatory analysis to evaluate the previously suspected relationship between discharge and recruitment (Table 4.3). The “discharge model,” containing main effects of the categorical discharge variable and spawner density, outperformed the basic Ricker model (which only included spawner density) in both the Chena River ( $\Delta\text{AICc} = 13.83$ ) and Salcha River ( $\Delta\text{AICc} = 6.52$ ). The improvement provided by this model is graphically apparent by comparing the main curves in Fig. 4.3 to basic Ricker model in Fig. 4.1. This model also had more explanatory power for both the Chena River ( $R_a^2 = 0.79$  versus 0.50 for the basic model) and the Salcha River ( $R_a^2 = 0.82$  versus 0.70 for the basic model). An interaction term between discharge and spawner density did not improve the model for either river, which may imply that the effect of discharge arises by some mechanism other than discharge-dependent changes in density-dependent, intra-specific competition.

Variants of the discharge model for the Chena River, calculated using different time periods for median discharge, were used to graphically investigate the sensitivity of

the discharge effect to the time period (Fig. 4.5). The large, darkly shaded area in the top left corner of the figure indicates that model performance was relatively strong across a broad range of potential time periods beginning in late spring or early summer and ending in late summer or early fall. The time period we chose *a priori* for the discharge model (April 23 to September 30) was located within this large region, but its AICc (29.7) was not the smallest in the set. The best models (AICc = 21.0) mostly used a range of dates beginning from late April to mid-May, and ending from late August to early September, visible as a large dark-colored streak in Fig. 4.5. This means that a model within those date ranges (e.g. May 1 to August 31) would best represent the effect of discharge. We did not adjust the date range for our model accordingly, because this would effectively add two more parameters and risk overfitting; however, future researchers analyzing other rivers in the region are encouraged to choose an *a priori* range of approximately May 1 to August 31 to determine a discharge effect.

#### 4.4.3 Exploratory analysis of other environmental variables to select the full model

In addition to the variables included in the discharge model, we considered ten other environmental variables derived from discharge and temperature records (Table 4.2) in an exploratory analysis. The top models (ranked by  $\Delta\text{AICc}$  relative to the model with the lowest AICc) from the set of all linear models of any of the twelve predictors are listed in Table 4.4. The two main predictors selected *a priori* for the discharge model, spawner density and the threshold effect of median discharge during the summer growing season, were by far the strongest supported in this broader analysis for both rivers; both appeared in nearly all models with substantial Akaike weights, so their total variable weights (Table 4.2) were very close to 1 (both  $>0.999$  in the Chena River and  $>0.976$  in the Salcha River).

Temperature (degree-days) during the July 20 – October 25 spawning and incubation period was the third-highest-weighted variable for the Chena River (0.797) and was also included, along with the two variables from the discharge model, in the

model with the lowest AICc for the Chena River (Table 4.4). Comparison of this variable against the residuals from the Chena River discharge model (Fig. 4.6a) shows that its effect is driven by a much lower productivity than predicted in the three years with the lowest temperature during this period. Because of the biological plausibility of a negative temperature effect in the coldest years near the northern edge of the species' range, in combination with the relatively strong weight of this variable, we included it in the “full model” along with the variables from the discharge model. The full model was a modest improvement over the discharge model for the Chena River ( $\Delta\text{AICc} = 4.93$ ;  $R_a^2 = 0.85$  versus 0.79 for the discharge model). Its predictions are shown as vertical projections from the curves that represent discharge model predictions in Fig. 4.3a.

The three next highest-ranked variables for the Chena River were too weakly supported for inclusion in the full model, but we plotted them against the residuals from the discharge model to identify trends that might be worth revisiting in future analyses. Productivity was lower than the discharge model predicted during most years with a flood peaking above 200 m<sup>3</sup>/s during the spawning and incubation period (variable weight 0.347; Fig. 4.6b). A slight positive effect of the maximum flood peak during the summer growing season (variable weight 0.327; Fig. 4.6c) seems biologically unrealistic and probably spurious. A slight negative effect of flashiness during the May 15 – June 15 critical emergence period (variable weight 0.266; Fig. 4.6d) is plausible, but it was not supported strongly enough to include in the full model.

The exploratory analysis focused on the Chena River, and was repeated for the Salcha River for the purpose of partially confirming the effects detected on the Chena. The selected full model also performed well on the Salcha River (see vertical projections in Fig. 4.3b), ranking fifth highest by AICc out of 4,095 possible models. However, it was only a slight improvement over the discharge model ( $\Delta\text{AICc} = 0.18$ ;  $R_a^2 = 0.85$  versus 0.82 for the discharge model). The three highest-ranked models for the Salcha River (Table 4.4) included a positive effect of the average duration of floods above seven times the median flow (variable weight 0.452); however, this weakly supported,

biologically implausible effect was not present in the Chena (variable weight only 0.111) and was probably spurious. The effect of temperature during spawning and incubation, included in the full model, ranked fourth highest in the Salcha (0.316), consistent with our conclusion from the Chena River that it might be a real, minor effect. The next three highest-ranked exploratory variables from the Chena River (maximum flood peak during spawning and incubation, maximum flood peak during the summer growing season, and flashiness during the critical emergence period) ranked poorly for the Salcha, corroborating our conclusion that they do not have substantial effects.

#### **4.4.4 Explaining the decline in productivity**

Log productivity declined sharply in the Chena River from 1986 to 2005 (Fig. 4.7a), and the slope of this decline was increasingly reduced in the residuals from the basic model (Fig. 4.7b), discharge model (Fig. 4.7c), and full model (Fig. 4.7d). A similarly sharp decline in the Salcha River (Fig. 4.7e) was absent from the residuals of the basic, discharge, and full models (Fig. 4.7f-h). This suggests that the basic model based on density dependence alone was sufficient to explain the decline in the Salcha River, but incorporating the effect of discharge was necessary to explain the decline in the Chena River.

#### **4.5 Discussion**

Variation in Chinook salmon productivity in the Chena and Salcha rivers was explained primarily by negative density dependence (as represented in the basic Ricker model) and secondarily by a strong negative effect of high stream discharge during the juveniles' first summer in the river. Weaker evidence linked low productivity to cold water during the pre-winter period of egg incubation. Combined, these factors provided plausible explanations for the recent declines in Chinook salmon productivity in the Chena and Salcha rivers. In this discussion, we reason that our detections are probably

not spurious, but rather are ecologically credible through a variety of possible mechanisms likely relevant to broader Chinook salmon declines.

#### **4.5.1 Strength of evidence for the detected effects**

Analyses relating stock-recruitment data to environmental factors have been criticized in general because it is easy to mine data in an exploratory fashion and find some correlate that appears significant and then imagine a post-hoc mechanistic explanation for any such relationship (Hilborn and Walters 1992). Thus, many published environmental correlations with productivity have failed when re-tested with new years of data (Myers 1998). This criticism casts doubt not on the role of the environment in causing variability in productivity, but instead on the modeling practices used to detect such relationships. Myers (1998) prescribed several guidelines for avoiding the methodological pitfalls that lead to spurious detections. We followed these when applicable, including: 1) carefully separating confirmatory and exploratory analysis, 2) honestly reporting the number of possible correlates investigated in exploratory analysis, 3) correcting for—or in our case confirming the insignificance of—temporal autocorrelation, 4) testing results in multiple systems, and 5) accounting for spawner abundance.

By these standards, our confirmatory analysis provides strong evidence that high discharge negatively affects Chinook salmon productivity in the Chena and Salcha rivers. The fact that a similarly strong effect can be observed across a broad range of discharge summary statistics (Fig. 4.3) and over a broad range of time periods (Fig. 4.5) suggests that the effect is not spurious. The Salcha River data are not completely independent of the Chena River data because environmental conditions and recruitment estimates for these nearby rivers covary (see methods), but the combined data still constitute stronger evidence than the Chena River data alone. It is encouraging that our model correctly predicts different population responses in the only year in which the qualitative discharge variable differed between the two rivers: the 2005 brood year experienced a high-

discharge year in the Chena with correspondingly low productivity, and a low-discharge year in the Salcha with correspondingly high productivity (Fig. 4.3).

We tentatively concluded that the variables we modeled – especially density dependence and discharge – explained the recent decline in Chinook salmon in the Chena River. Density dependence alone explained the smaller decline in the Salcha River’s productivity, although the discharge effect was still useful for explaining other inter-annual variation in the Salcha. Inferences about “explaining the decline” are drawn from the fact that the decline is present in log productivity, but not in residual log productivity, from our full model. This is not conclusive evidence that we have a correct or complete explanation of the decline; instead, it means the data are consistent with the possibility of a causal relationship. This is the only group of variables so far identified as having appropriately large effects in the specific years necessary to explain the decline.

The marginally significant negative effect of cold water during the spawning and pre-winter incubation period (Fig. 4.6a) was identified from exploratory analyses of the Chena River data that included nine other exploratory variables. This effect was also detectable, but weaker, in the Salcha River. Because large exploratory analyses are likely to identify some effects by coincidence, the evidence for this effect is not as strong as the model weights suggest. The effect also may not be well represented by a straight-line model, which might allow many moderate-to-warm years to mask the significance of an effect only important in the coldest years. The temperature effect is biologically very plausible because these rivers are near the northern edge of the range of Chinook salmon, and temperatures can decrease the rate of development of fish eggs and individual weight at hatching (From and Rasmussen 1991), so the coldest years might produce relatively weak or late-emerging fry. The weakly supported, possible negative effect of large floods during spawning and incubation (Fig. 4.6b) might also have been masked by the majority of years without such floods, but it is worth considering because redd damage during floods (from scouring or siltation or both) is a primary cause of poor egg-to-fry survival



in Chinook salmon (Healey 1991; Greene et al. 2005). Our main conclusion regarding the negative effects of both low temperature and large floods during spawning and incubation, given the inconclusive evidence but high plausibility, is that they are worthy of continued investigation when new data are available.

#### **4.5.2 Possible mechanisms by which discharge might affect productivity**

Although stock-recruitment analysis is correlative and does not conclusively demonstrate cause-and-effect relationships, the strong association we detected warrants serious consideration of the possibility that variation in discharge causes the associated variation in productivity. For purposes of discussion, let us assume the relationship is causal as we evaluate ideas about the nature of the relationship using post-hoc pattern analyses of the present study, as well as other findings on the life history, behavior, and environment of Yukon drainage Chinook salmon.

In many anadromous salmonid populations, density-dependent mortality regulates the population during a critical period ranging from several days to several weeks after the yolk is absorbed and exogenous feeding begins (Elliott 1989a). We cannot test for a critical period with regard to density dependence in the Chena because no within-year survival estimates are available. However, during mechanistic studies on the Chena River from 2007 through 2010, we qualitatively observed that abundance peaked in June and declined rapidly for several weeks before stabilizing sometime in late July or August (J. Neuswanger, personal observation). This is consistent with a critical period for density-dependent mortality, which raises the question of whether the effect of discharge is also exerted during a specific critical period, such as the first weeks after emergence when the swimming ability of the fry is weakest and they might be more susceptible to floods. However, the AICc plot of our discharge model with different start and end dates (Fig. 4.5) provides evidence that the discharge effect is strongest when the median discharge is calculated over the entire summer, not a briefer critical period. If this inference is correct, it greatly constrains the mechanisms to which we might attribute the discharge effect.

Mechanistic hypotheses are further constrained by the lack of a significant interaction term between discharge and density dependence. In both rivers, the effect of discharge did not depend on population density, and (equivalently) the density dependence of productivity was similar in high- and low-discharge years. The absence of an interaction between these terms tentatively rules out some otherwise promising mechanistic explanations that relate stream discharge to the carrying capacity of the system, because a difference in carrying capacity between high- and low-discharge years should manifest itself as a substantial interaction term.

The most plausible explanations for the discharge effect probably involve the long-term effects of numerous, sustained, moderate- to very-high discharge periods on fish survival, not the short-term effects of catastrophic floods. The first argument to support this claim is that a threshold relationship described the discharge effect much better than a linear relationship, suggesting that it matters whether discharge is generally low or generally high, but not *how* low or *how* high it is. Second, variables pertaining to individual flood severity (including the maximum flood peak, flashiness, and frequency and duration of large floods) were not significant.

One plausible mechanism by which prolonged periods of high discharge could inhibit salmon survival is by increasing depth and turbidity, thereby reducing the amount of photosynthetically active radiation reaching the substrate. This causes a sharp decline in primary production in the Chena River at a discharge of about 1024 ft<sup>3</sup>/s (29 m<sup>3</sup>/s) (Benson et al. 2013), close to the 960 ft<sup>3</sup>/s (27.2 m<sup>3</sup>/s) median discharge threshold that separated years of high and low salmon productivity. A prolonged reduction of primary production would reduce the system's carrying capacity for aquatic invertebrates. However, the timing of any food limitation bottlenecks for these aquatic insect populations is unknown, as is the time lag between a reduction in primary productivity and a reduction in invertebrate populations sufficient to affect the prey density encountered by drift-feeding Chinook salmon. Low primary production early in the summer might affect prey abundance throughout the season. However, the discharge

effect we seek to explain is most likely a whole-summer effect, and it is unlikely that late-summer fluctuations in primary production would have enough time to influence drift-feeding fish before winter. Insect abundance is probably controlled at an earlier date, and Chena River Chinook salmon consume a large number of terrestrial insects late in the summer that might compensate for such reductions (Gutierrez 2011).

A prolonged decrease in primary production is just one threshold-exceeding process that may have triggered a decline in salmon productivity; another might be a shift in salmon behavior in response to the difficulty of foraging during high-discharge periods. Chinook salmon fry in the Chena River are primarily drift feeders, meaning they face upstream into the current from a stationary position and dart back and forth to intercept items of food (Jenkins 1969; Piccolo et al. 2014). Turbidity caused by extremely high discharge inhibits such visual feeding; however, Chinook fry in the Chena River feed mostly on items detected within 10 cm of their positions (Neuswanger et al. 2014), and the river becomes turbid enough to inhibit detection at that distance only briefly during floods. A more likely hindrance to foraging during sustained, moderately-high discharge periods is an increased density of small particles of drifting debris that fish can mistake as prey. Such debris is common in the Chena (and most other rivers) even during low-discharge periods when the water is very clear. During low-discharge periods on the Chena, Chinook fry spent up to 25% of their overall foraging time pursuing debris items they eventually rejected (Neuswanger et al. 2014), which corresponds to a 25% decrease in energy intake rate. Drift net samples in the Chena River and elsewhere show that the density of this debris greatly increases during high-discharge periods, possibly without a proportional increase in prey (M. Wipfli, personal observation). Therefore, debris could cause a population-wide, density-independent reduction in foraging success during high-discharge years. Another aspect of high discharge that can reduce drift-feeding success is increased water velocity (O'Brien and Showalter 1993; Grossman et al. 2002; Piccolo et al. 2008). Sufficiently large increases in discharge might cause widespread increases in water velocity, reduce the availability of safe habitat with optimal velocities for drift

feeding along the margins of the stream. Probably as a consequence of these effects (turbidity, debris, velocity), prey mass consumed by Chinook fry in the Chena River in 2008 and 2009 was negatively correlated with discharge (Gutierrez 2011).

Although high discharge reduces foraging success, that reduction must also increase mortality if it is to explain the population-level association between discharge and productivity. This would obviously happen if fish with reduced foraging success die of starvation. However, at a water temperature typical of the Chena River (12 °C), juvenile Chinook salmon slightly larger than those in the Chena (92.5 mm mean length) survived experimental starvation for up to 6 weeks with minimal loss of condition and no mortality (Snyder 1980), and smaller brown trout have been shown to survive starvation for three weeks without adverse health effects (Sundstrom et al. 2013). It is possible that starvation occurs during a critical period for density-dependent mortality in the few weeks immediately following the transition of fry to exogenous feeding (Kennedy et al. 2008); however, starvation seems to be an unlikely explanation for the effect of discharge throughout the entire summer. High-discharge periods reduce foraging success, rather than eliminating it completely. Given the long survival times under experimental conditions of complete starvation, Chinook fry can probably avoid dying of starvation on reduced-but-positive rations for a very long time. Instead, it is more plausible that these fish, seeking long-term growth, would take more risks to seek better habitat and expose themselves to predation long before they succumb to starvation.

We do not know which predators might be responsible for juvenile salmon mortality in the Chena River, or when that mortality would occur. The piscivorous ducks *Mergus merganser* (common merganser) and *Bucephala clangula* (common goldeneye) raise broods on the Chena and we have observed them targeting Chinook fry. If Chinook fry are a major part of the diet of these ducks, as seems likely, then the number of fry consumed by ducks should be largely determined by the initial population of ducks each summer and their energy needs, and it is unclear how their consumption of Chinook fry would be dramatically higher during high-discharge years. The difference between high-

and low-discharge years would be more consistent with predation by a species that is normally supported at high densities by other foods, but can prey heavily on Chinook fry during high-discharge years. We speculate that Arctic grayling (*Thymallus arcticus*) might fill this role. Although grayling are the quintessential insectivorous drift-feeders (Hughes and Dill 1990), they can be piscivorous in certain situations (Stewart et al. 2007). We do not know of conclusive evidence for or against the hypothesis that grayling sometimes prey on Chinook fry in the Chena River. We have often observed adult grayling drift feeding in close proximity to Chinook fry without acting aggressively. However, grayling are so abundant that even a small minority of individuals feeding on Chinook fry under very specific conditions might still inflict high mortality on the Chinook population.

Predation by grayling might occur during high-discharge periods if the Chinook fry, in search of better foraging conditions, migrate downstream in the main current of the river and temporarily become a part of the “drift” upon which grayling are already feeding. Chinook fry are capable of long-distance downstream and upstream migrations, as evidenced by the Canadian-origin Chinook fry that leave their natal streams and colonize small tributaries of the Yukon far downstream in Alaska (Bradford et al. 2001; Daum and Flannery 2011). In years with sustained high discharge, Chinook fry in the Salcha River system have been found in small tributaries farther upstream and in greater numbers than in low- to medium-discharge years, and fewer fry were observed in the main river during high-discharge years (Chris Stark, Bering Sea Fishermen’s Association, personal communication). These Alaskan Chinook fry are not known to emigrate from their natal river system like their Canadian counterparts, but not enough sampling has been done to rule out the possibility that Alaskan Chinook fry make such movements under certain circumstances, such as during prolonged periods of high discharge. Chinook fry emigrating from the Chena or Salcha rivers would be susceptible to a wider range of predators including northern pike (*Esox lucius*), burbot (*Lota lota*), and sheefish (*Stenodus leucichthys*). These piscivores are present, though uncommon, in the lower

Chena and Salcha rivers and their off-channel sloughs, so extensive within-system movement of Chinook fry might increase predation risk to an unknown extent.

Based on all the constraints developed above, one hypothesis for the discharge effect emerges as the most consistent with available evidence: Frequent or prolonged periods of at least moderately high discharge reduce foraging success (particularly because of increased water velocity and debris density), which compels Chinook fry to migrate more extensively within their natal stream, or to emigrate from it, thereby exposing themselves to predators they would not otherwise encounter very often (grayling within the stream, or burbot and northern pike if they emigrate) and creating a density-independent difference in predation mortality between low- and high-discharge years. This highly testable hypothesis is very tentative, because only weak evidence is available to exclude other plausible explanations, including starvation mortality and the effects of discharge on primary production and habitat carrying capacity. Nevertheless, given the vast number of possibilities, this relatively narrow hypothesis may prove useful as a starting point for future mechanistic research. Such work could investigate 1) direct negative impacts of high discharge on individual foraging and growth; 2) movement within and emigration from the natal river system in response to changes in discharge, particularly with a contrast between low- and high-discharge years; and 3) the timing, location, and proximate causes of mortality, considering both starvation and predation.

#### **4.5.3 Implications for broader Yukon River and Alaska Chinook salmon populations**

Our analysis offers positive direction to future research into the worrisome decline in Chinook salmon runs throughout the Yukon River drainage. In addition to the freshwater density dependence and habitat variables we examined, several other potential mechanisms for the decline have been investigated (summarized by Schindler et al. 2013), including 1) anthropogenic and natural changes in ocean conditions, such as the Pacific Decadal Oscillation; 2) marine bycatch of salmon by the commercial groundfish

fleet; 3) poor escapement quality because of harvest methods that disproportionately target the largest spawners; and 4) pathogens such as *Ichthyophonus*. Although none of these factors are fully understood, to our knowledge no other study has identified a mechanism by which any of them, alone or in combination, seems to convincingly explain the recent Chinook salmon decline. Our analysis shows that freshwater environmental variables, normally associated with uninformative inter-annual “noise” in productivity, have aligned—either coincidentally or as a consequence of climate change—in a way that could have caused the long-term pattern of reduced productivity in the Chena and Salcha rivers. It is plausible that these mechanisms have contributed substantially to the broader decline of Chinook salmon. However, the ubiquity of the decline throughout Alaska (ADF&G 2013) in streams with different freshwater conditions suggests that more universal mechanisms are also involved. We therefore agree with Schindler et al. (2013) that the regional decline probably has multiple causes, all of which warrant further research. However, this paper strengthens the evidence that freshwater conditions are an influential piece of the broader puzzle.

Better understanding the accuracy, generality, and specific mechanisms behind the effects we detected will require expanded data collection and research on both population-level and individual-level processes. The generality of our results cannot be established immediately because the Chena and Salcha rivers have the only spawning-stream-specific run reconstructions in the Yukon drainage. Long-term monitoring of Chinook salmon recruitment is expanding to more spawning streams in the Yukon River drainage and others nearby (ADF&G 2013). It would be valuable to continue this expansion to other individual spawning streams and to record stream discharge data concurrent with all recruitment records. However, these long-term efforts take many years to generate informative data series. In the meantime, mechanistic studies relating competition, predation, and foraging behavior to individual fitness could improve confidence in our understanding of population trends.

In summary, poor Chinook salmon productivity in the Chena and Salcha rivers was strongly associated with high stream discharge during the summer they spent in freshwater as fry. Weaker evidence supported the observation that cold water during spawning and incubation also reduced productivity. The hypothesis that these factors combined have caused the recent decline in productivity is consistent with both the statistics evaluated here and recent work on ecological processes in the Chena River (Neuswanger et al. 2014; Benson et al. 2013; Gutierrez 2011). Although available data cannot conclusively establish a causal relationship in these rivers or elsewhere, our findings do bolster the plausibility of the hypothesis that freshwater habitat variables such as discharge have contributed substantially to the greater Yukon drainage or statewide declines of Chinook salmon.

#### **4.6 Acknowledgments**

This work was supported by the Arctic-Yukon-Kuskokwim Sustainable Salmon Initiative, the Institute of Arctic Biology, Alaska EPSCoR NSF award #OIA-1208927 and the Alaska Department of Fish and Game, and the Department of Biology and Wildlife and College of Natural Sciences and Mathematics at the University of Alaska Fairbanks. Milo Adkison, Mike Bradford, and David Neuswanger helpfully critiqued this manuscript. Any use of trade, product, or firm names in this publication is for descriptive purposes only and does not imply endorsement by the U.S. Government.

#### **4.7 References**

ADF&G Chinook Salmon Research Team. 2013. Chinook salmon stock assessment and research plan, 2013. Alaska Department of Fish and Game, Special Publication No. 13-01, Anchorage.



Baker, D. B., Richards, R. P., Loftus, T. T., and Kramer, J. W. 2004. A new flashiness index: Characteristics and applications to midwestern rivers and streams. *J Am Water Resour As* 40(2): 503-522.

Benson, E. R., Wipfli, M. S., Clapcott, J. E., and Hughes, N. F. 2013. Relationships between ecosystem metabolism, benthic macroinvertebrate densities, and environmental variables in a sub-arctic Alaskan river. *Hydrobiologia* 701(1): 189-207.  
doi:10.1007/s10750-012-1272-0.

Bradford, M. J. 1995. Comparative review of Pacific salmon survival rates. *Can. J. Fish. Aquat. Sci.* 52 (6): 1327-1338.

Bradford, M. J., Grout, J. A., and Moodle, S. 2001. Ecology of juvenile chinook salmon in a small non-natal stream of the Yukon River drainage and the role of ice conditions on their distribution and survival. *Can J Zool* 79 (11): 2043-2054.

Burnham, K. P. and Anderson, D. R. 2002. Model selection and multi-model inference : a practical information-theoretic approach (2nd edition). Springer, Secaucus, NJ, USA.

Daum, D. W., and Flannery, B. G. 2011. Canadian-origin Chinook salmon rearing in nonnatal U.S. tributary streams of the Yukon River, Alaska. *Trans. Am. Fish. Soc.* 140(2): 207-220. doi:10.1080/00028487.2011.545004.

DeVries, P. 1997. Riverine salmonid egg burial depths: review of published data and implications for scour studies. *Can. J. Fish. Aquat. Sci.* 54(8): 1685-1698.

DuBois, L., J. M. Berger, N. A. DeCovich, and W. D. Templin. 2009. Origins of Chinook salmon in the Yukon River fisheries, 2004. Alaska Department of Fish and Game, Fishery Data Series No. 09-13, Anchorage.

Durbin, J., and Watson, G. S. 1950. Testing for serial correlation in least squares regression: I. *Biometrika* 37(3/4): 409-428.

Eiler, J. H., T. R. Spencer, J. J. Pella, M. M. Masuda, and R. R. Holder. 2004. Distribution and movement patterns of Chinook salmon returning to the Yukon River Basin in 2000-2002. U. S. Department of Commerce, NOAA Technical Memorandum NMFS-AFSC-148.

Eiler, J. H., T. R. Spencer, J. J. Pella, and M. M. Masuda. 2006a. Stock composition, run timing, and movement patterns of Chinook salmon returning to the Yukon River Basin in 2003. U. S. Department of Commerce, NOAA Technical Memorandum NMFS-AFSC-163.

Eiler, J. H., T. R. Spencer, J. J. Pella, and M. M. Masuda. 2006b. Stock composition, run timing, and movement patterns of Chinook salmon returning to the Yukon River Basin in 2004. U. S. Department of Commerce, NOAA Technical Memorandum NMFS-AFSC-165.

Elliott, J. M. 1989a. The critical period concept and its relevance for population regulation in young sea trout. *J. Fish. Biol.* 35: 91-98.

Elliott, J. M., and Hurley, M. A. 1999. A new energetics model for brown trout, *Salmo trutta*. *Freshw Biol* 42: 235-246.

Elliott, J. M. 1989b. Mechanisms responsible for population regulation in young migratory brook trout, *Salmo trutta*. I. The critical time for survival. *J Anim Ecol* 58(3): 987-1001.

From, J., and Rasmussen, G. 1991. Growth of rainbow trout, *Oncorhynchus mykiss* (Walbaum, 1792) related to egg size and temperature. *Dana* 9: 31-38.

Gibbins, C., Vericat, D., and Batalla, R. J. 2007. When is stream invertebrate drift catastrophic? The role of hydraulics and sediment transport in initiating drift during flood events. *Freshw Biol* 52(12): 2369-2384.

Greene, C. M., Jensen, D. W., Pess, G. R., Steel, E. A., and Beamer, E. 2005. Effects of environmental conditions during stream, estuary, and ocean residency on Chinook salmon return rates in the Skagit River, Washington. *Trans. Am. Fish. Soc.* 134(6): 1562-1581. doi:10.1577/T05-037.1.

Grossman, G. D., Rincón, P. A., Farr, M. D., and Ratajczak, R. E. J. 2002. A new optimal foraging model predicts habitat use by drift-feeding stream minnows. *Ecol Freshw Fish* 11: 2-10.

Gutierrez, L. 2011. Terrestrial invertebrate prey for juvenile Chinook salmon: abundance and environmental controls in an interior Alaskan river. *Biology M.S.*: 63 pp.

Healey, M. C. 1991. Life history of Chinook salmon (*Oncorhynchus tshawytscha*). In *Pacific salmon life histories*, eds. Groot, C., and Margolis, L., pp. 313-393. Vancouver, BC: UBC Press.

Hilborn, R., and Walters, C. J. 1992. Quantitative fisheries stock assessment: Choice, dynamics & uncertainty. Chapman and Hall, New York.

Hughes, N. F., and Dill, L. M. 1990. Position choice by drift-feeding salmonids - model and test for arctic grayling (*Thymallus arcticus*) in sub-arctic mountain streams, interior Alaska. Can. J. Fish. Aquat. Sci. 47 (10): 2039-2048.

Jenkins, T. M., Jr 1969. Social structure, position choice, and micridistribution of two trout Species (*Salmo trutta* and *Salmo gairdneri*) resident in mountain streams. Anim Behav Monogr 2(2): 57-123.

Jennings, G. B., K. Sundet, and A. E. Bingham. 2010. Estimates of participation, catch, and harvest in Alaska sport fisheries during 2007. Alaska Department of Fish and Game, Fishery Data Series No. 10-02, Anchorage.

Keeley, E. R. 2001. Demographic responses to food and space competition by juvenile steelhead trout. Ecology 82(5): 1247-1259.

Kennedy, B. P., Nislow, K. H., and Folt, C. L. 2008. Habitat-mediated foraging limitations drive survival bottlenecks for juvenile salmon. Ecology 89(9): 2529-2541.

Milkowski, S. October 3, 2009. Scarcity of king salmon hurt Alaskan fishermen. The New York Times Business: B1.

Murphy, J., Howard, K., Eisner, L., Andrews, A., Templin, W., Guthrie, C., Cox, K., and Farley, E. 2013. Linking abundance, distribution, and size of juvenile Yukon River Chinook salmon to survival in the northern Bering Sea. North Pacific Anadromous Fish Commission (NPAFC) Third International Workshop on Migration and Survival Mechanisms of Juvenile Salmon and Steelhead on Ocean Ecosystems 2-13.

Myers, R. A. 1998. When do environment-recruitment correlations work? *Rev Fish Biol Fisher* 8(3): 285-305.

Neuswanger, J., Wipfli, M. S., Rosenberger, A. E., and Hughes, N. F. 2014. Mechanisms of drift-feeding behavior in juvenile Chinook salmon and the role of inedible debris in a clear-water Alaskan stream. *Environ. Biol. Fish.* 1-15.

O'Brien, W. J., and Showalter, J. J. 1993. Effects of current velocity and suspended debris on the drift feeding of Arctic grayling. *Trans. Am. Fish. Soc.* 122: 609-615.

Ottaway, E. M., and Clarke, A. 1981. A preliminary investigation into the vulnerability of young trout (*Salmo trutta* L.) and Atlantic salmon (*S. salar* L.) to downstream displacement by high water velocities. *J. Fish. Biol.* 19(2): 135-145.

Piccolo, J. J., Frank, B. M., and Hayes, J. W. 2014. Food and space revisited: The role of drift-feeding theory in predicting the distribution, growth, and abundance of stream salmonids. *Environ. Biol. Fish.* doi:10.1007/s10641-014-0222-2.

Piccolo, J. J., Hughes, N. F., and Bryant, M. D. 2008. Water velocity influences prey detection and capture by drift-feeding juvenile coho salmon (*Oncorhynchus kisutch*) and steelhead (*Oncorhynchus mykiss irideus*). *Can. J. Fish. Aquat. Sci.* 65 (2): 266-275.

Quinn, T. J., and Deriso, R. B. 1999. Quantitative fish dynamics. Oxford University Press, New York.

Ricker, W. E. 1954. Stock and recruitment. Journal of the Fisheries Board of Canada 11(5): 559-623.

Savereide, J. W. 2012. Salmon studies in the Chena, Salcha, Goodpaster, and Delta Clearwater rivers, 2010. Alaska Department of Fish and Game, Fishery Data Series No. 12-05, Anchorage.

Schindler, D., C. Krueger, P. Bisson, M. Bradford, B. Clark, J. Conitz, K. Howard, M. Jones, J. Murphy, K. Myers, M. Scheuerell, E. Volk, and J. Winton. 2013. Arctic-Yukon-Kuskokwim Chinook salmon research action plan: Evidence of decline of Chinook salmon populations and recommendations for future research. Prepared for the AYK Sustainable Salmon Initiative (Anchorage, AK). v + 70 pp.

Snyder, G. 1980. Effects of starvation on presmolt coho salmon. National Marine Fisheries Service, Northwest and Alaska Fisheries Center, Coastal Zone and Estuarine Studies Division,

Stewart, D. B., Mochnacz, N. J., Reist, J. D., Carmichael, T. J., and Sawatzky, C. D. 2007. Fish diets and food webs in the Northwest Territories: Arctic grayling (*Thymallus arcticus*). Can Manuscr Rep Fish Aquat Sci 2796: 21.

Stuby, L. and M. J. Evenson. 1998 salmon studies in interior Alaska, 1997. Alaska Department of Fish and Game, Fishery Data Series No. 98-11, Anchorage.

Sundstrom, L. F., Kaspersson, R., Naslund, J., and Johnsson, J. I. 2013. Density-dependent compensatory growth in brown trout (*Salmo trutta*) in nature. PLoS One 8(5): e63287. doi:10.1371/journal.pone.0063287.

van Vliet, M. T. H., Ludwig, F., Zwolsman, J. J. G., Weedon, G. P., and Kabat, P. 2011. Global river temperatures and sensitivity to atmospheric warming and changes in river flow. Water Resour Res 47(2): doi:10.1029/2010WR009198.

#### 4.8 Tables

Table 4.1. Chinook salmon run reconstructions for the Chena River (1986-2005) and Salcha River (1987-2005). Source: Alaska Department of Fish and Game.

Brood year	Chena spawners	Chena recruits	Salcha spawners	Salcha recruits
1986	9065	13584	-	-
1987	6404	11029	4771	13416
1988	3346	23751	4322	28185
1989	2730	31294	3294	34860
1990	5603	6854	10728	8260
1991	3172	18259	5608	28827
1992	5580	5068	7862	6474
1993	12241	19507	10007	18382
1994	11877	5532	18399	5840
1995	11394	8941	13643	13653
1996	7153	12044	7570	14027
1997	13390	11236	18514	14553
1998	4745	20837	5027	33432
1999	6485	7381	9198	10297
2000	4694	8510	4595	16492
2001	9696	8025	13328	20459
2002	6967	4474	9000	8130
2003	11100	9739	15500	15996
2004	9645	3581	15761	7275
2005	4075	7753	5988	24779

**Note:** The number of spawners each brood year equals escapement that year; and the number of recruits produced each brood year equals total in-river harvest plus escapement over the lifespan of the cohort.



Table 4.2. Variables evaluated in generalized Ricker models for Chena and Salcha River Chinook salmon. The “Chena” and “Salcha” columns list the total Akaike weights of all models containing each variable for each river in the full exploratory analysis.

Variable	Year	Period	Chena	Salcha	Description
-S	Brood	-	0.99999	0.99997	Number of spawners (parents) in a brood year.
DISCH	Brood+1	4/26 – 9/30	0.999754	0.976167	Indicator variable equal to 0 when discharge was high during the summer growing season and 1 when discharge was low. The threshold between high and low was a fitted parameter.
INCTMP	Brood	7/20 – 10/25	0.796958	0.315757	Temperature (degree-days) during the spawning and incubation period.
INCFLD	Brood	7/20 – 10/25	0.34717	0.10899	Maximum flood peak during the spawning and incubation period.
SUMFLD	Brood+1	4/26 – 9/30	0.327366	0.214724	Maximum flood peak during the summer growing season.
EMGFLSH	Brood+1	5/15 – 6/15	0.265704	0.183761	Flashiness during the critical emergence period.
FLDFRE	Brood+1	4/26 – 9/30	0.157909	0.189318	Number of floods exceeding seven times the long-term median summer discharge.
SUMFLSH	Brood+1	4/26 – 9/30	0.117426	0.094218	Flashiness during the summer growing season.
FLDDUR	Brood+1	4/26 – 9/30	0.111235	0.451539	Mean duration (days) of floods exceeding seven times the median summer discharge.
EMGTMP	Brood+1	5/15 – 6/15	0.102561	0.254221	Temperature (degree-days) during the critical emergence period.
EMGFLD	Brood+1	5/15 – 6/15	0.0865573	0.104117	Maximum flood peak during the critical emergence period.
SUMTMP	Brood+1	4/26 – 9/30	0.0774589	0.092464	Degree-days during the summer growing season.

Table 4.3. Model performance compared for all models in the confirmatory analysis of spawner density (S) and the threshold variable for median summer growing season discharge (DISCH).

Model	$R_a^2$	$\Delta AICc$	Weight	
Chena	-0.0001943 S - 0.98207 DISCH + 1.2669	0.789	0.00	0.837
	-0.00016754 S - 1.2423 DISCH + 0.00003478 S DISCH + 1.0664	0.779	3.28	0.162
	-0.00019515 S + 1.8624	0.497	13.83	0.001
	-0.98949 DISCH - 0.18862	0.222	24.18	0.000
Salcha	-0.00013715 S - 0.79799 DISCH + 1.3745	0.823	0.00	0.688
	-0.000091735 S - 1.4689 DISCH + 0.00006049 S DISCH + 0.82776	0.829	1.76	0.285
	-0.000168 S + 2.1759	0.696	6.52	0.026
	-1.3196 DISCH - 0.27667	0.378	21.82	0.000

Table 4.4. Top ten models (ranked by  $\Delta AICc$  relative to the best model) of log productivity of Chinook salmon in the Chena and Salcha rivers, from an exploratory analysis of all 4,095 possible models for each river combining the variables in Table 4.2.

Model	$R_a^2$	$\Delta AICc$	Weight	
Chena River	-0.00021648 S - 0.97806 DISCH + 0.0055618 INCTMP - 0.97251	0.853	0.00	0.116
	-0.00021125 S - 1.0368 DISCH + 0.005006 INCTMP + 0.00090902 SUMFLD - 1.0008	0.865	1.16	0.065
	-0.00021389 S - 1.0203 DISCH + 0.0053244 INCTMP - 2.5887 EMGFLSH - 0.44336	0.865	1.19	0.064
	-0.00020481 S - 1.1252 DISCH + 0.0040777 INCTMP - 0.0011996 INCFLD + 0.001091 SUMFLD - 0.57066	0.883	1.72	0.049
	-0.00021215 S - 1.0397 DISCH + 0.0049045 INCTMP - 0.00096502 INCFLD - 0.62198	0.861	1.81	0.047
	-0.00021858 S - 1.0633 DISCH + 0.0050252 INCTMP + 0.11997 FLDFRE - 0.85967	0.857	2.34	0.036
	-0.00018685 S - 1.173 DISCH - 0.0016164 INCFLD + 0.0013791 SUMFLD + 1.0284	0.851	3.10	0.025
	-0.00021852 S - 0.99185 DISCH + 0.0053411 INCTMP + 1.7741 SUMFLSH - 1.1845	0.851	3.17	0.024
	-0.00020941 S - 1.0693 DISCH + 0.0048452 INCTMP - 2.337 EMGFLSH + 0.00082151 SUMFLD - 0.52032	0.874	3.24	0.023
	-0.00020975 S - 1.079 DISCH + 0.0046935 INCTMP - 2.5243 EMGFLSH - 0.00093493 INCFLD - 0.11691	0.872	3.47	0.020
Salcha River	-0.00013271 S - 0.9698 DISCH + 0.17829 FLDDUR + 1.0919	0.853	0.00	0.070
	-0.00013532 S - 1.0288 DISCH + 0.0074707 EMGTMP + 0.22698 FLDDUR - 0.51836	0.872	0.40	0.057
	-0.00014625 S - 0.88624 DISCH + 0.0034999 INCTMP + 0.15812 FLDDUR - 0.22801	0.869	0.74	0.049
	-0.00012842 S - 0.99431 DISCH + 0.0010197 SUMFLD + 0.76212	0.846	0.87	0.045
	-0.00015233 S - 0.72331 DISCH + 0.004076 INCTMP - 0.19991	0.846	0.94	0.044
	-0.00013715 S - 0.79799 DISCH + 1.3745	0.823	1.12	0.040
	-0.0001218 S - 1.0829 DISCH - 3.2602 EMGFLSH + 0.20038 FLDDUR + 1.4501	0.863	1.69	0.030
	-0.0001309 S - 0.87899 DISCH + 0.2403 FLDFRE + 1.1619	0.837	2.03	0.025
	-0.00014249 S - 0.89977 DISCH + 0.0033891 INCTMP + 0.00085113 SUMFLD - 0.44577	0.860	2.09	0.025
	-0.00012493 S - 1.1332 DISCH - 3.0742 EMGFLSH + 0.007178 EMGTMP + 0.24591 FLDDUR - 0.11748	0.881	2.61	0.019

**Note:** Model coefficients are based on variables calculated from discharge values in m<sup>3</sup>/s and temperatures in °C.

## Figures

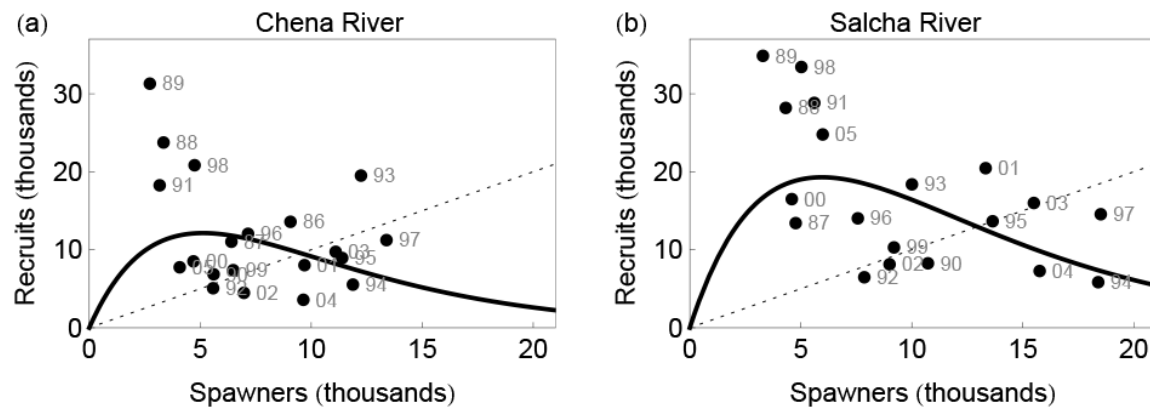


Fig. 4.1. Basic Ricker model fit for the (a) Chena River (1986-2005) and (b) Salcha River (1987-2005). The dotted line indicates replacement—one recruit per spawner.

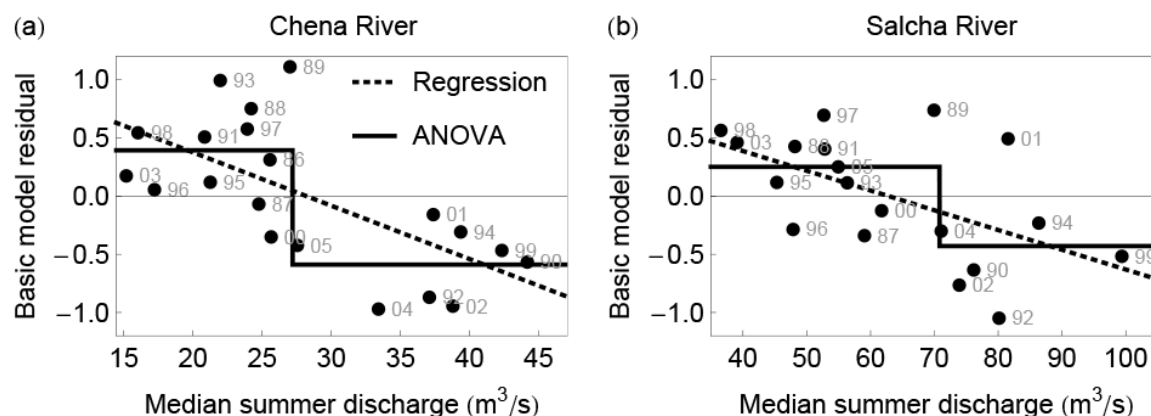


Fig. 4.2. Relationship between discharge during the summer growing season and Chinook salmon log-productivity relative to the predictions of the basic Ricker model for (a) the Chena River and (b) the Salcha River. The dotted line shows the fit from linear regression, and the solid line shows the fit from an ANOVA model treating discharge as a categorical variable classified as either above or below 27.2  $\text{m}^3/\text{s}$  (for the Chena River) or 70.8  $\text{m}^3/\text{s}$  (for the Salcha River).

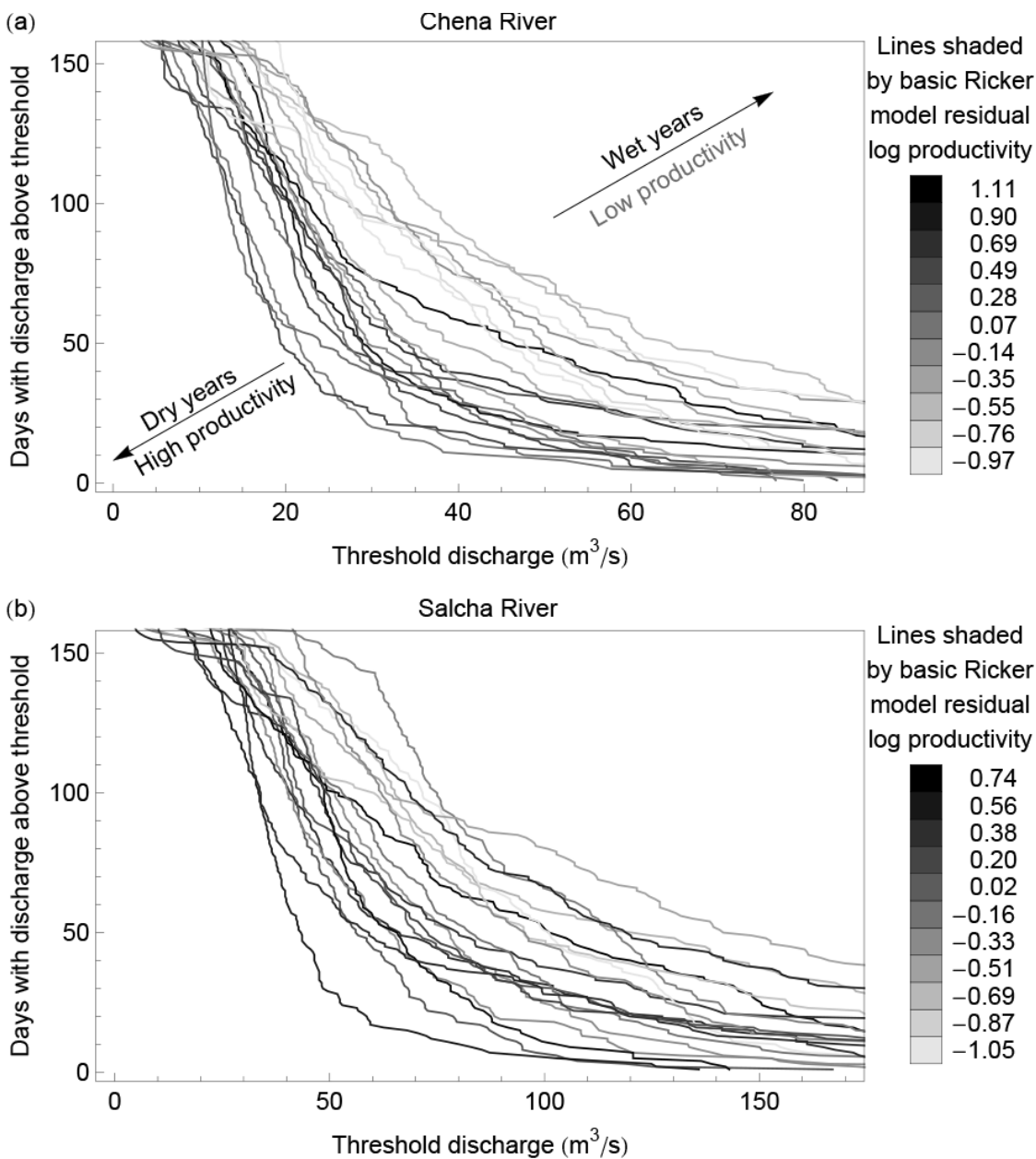


Fig. 4.3. Annual (a) Chena River and (b) Salcha River discharge summaries shaded by residuals from the basic Ricker model, i.e. the portion of log productivity that is not explained by linear density dependence. Each line represents one year. Lighter-shaded lines indicate years of low productivity relative to the predictions of the basic model, and darker lines indicate higher-than-expected productivity. For each threshold discharge on

the horizontal axis, the vertical position of a line indicates the number of days on which discharge exceeded the given threshold during the summer growing season. Therefore, lines toward the lower left corner of the graph represent low-discharge years.

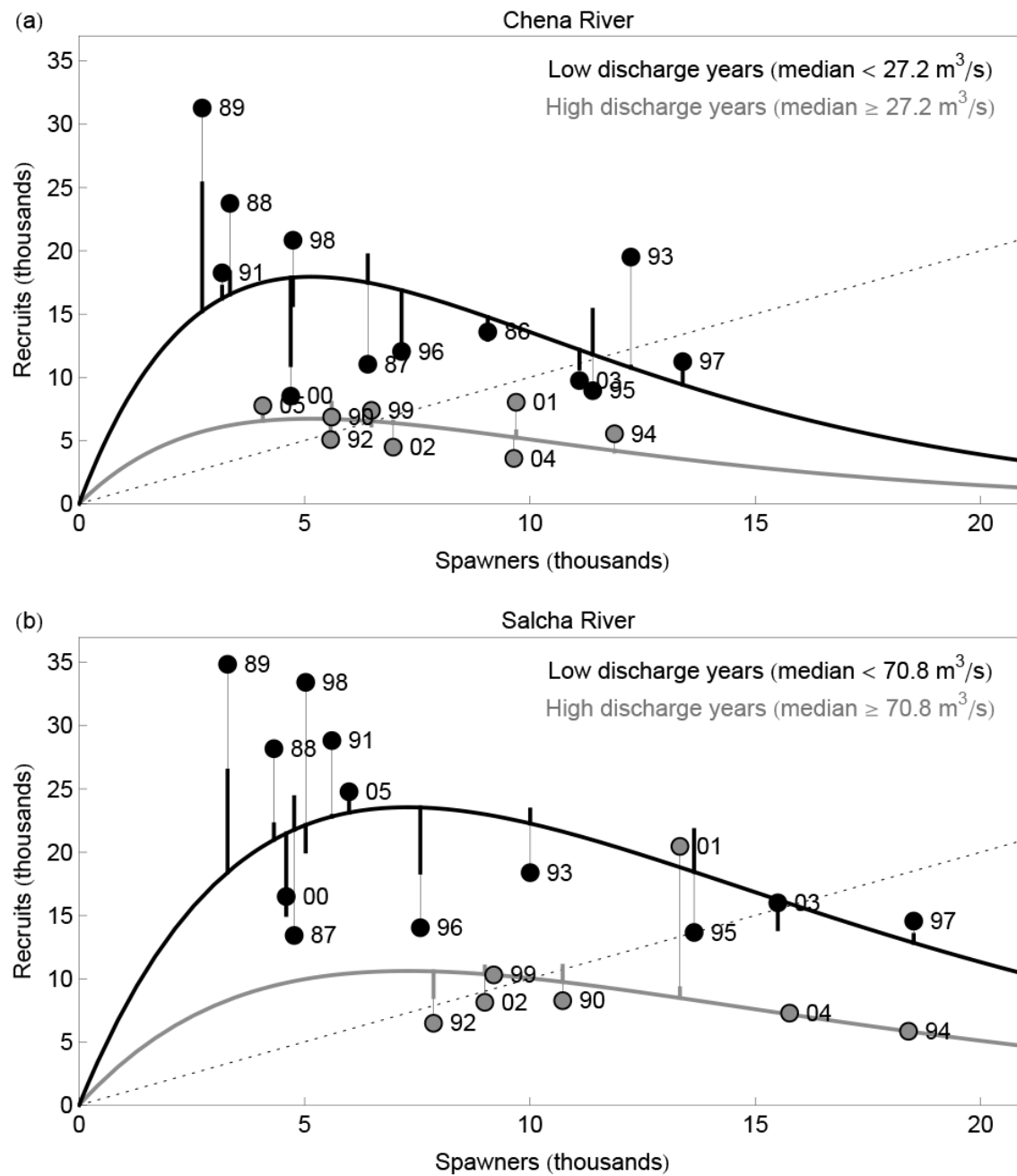


Fig. 4.4. Predictions of the discharge and full models for (a) the Chena River and (b) the Salcha River. The curves represent the predictions of the discharge model, and the thick vertical projections from each curve lead to the predictions of the full model, which incorporates temperature during spawning and incubation.



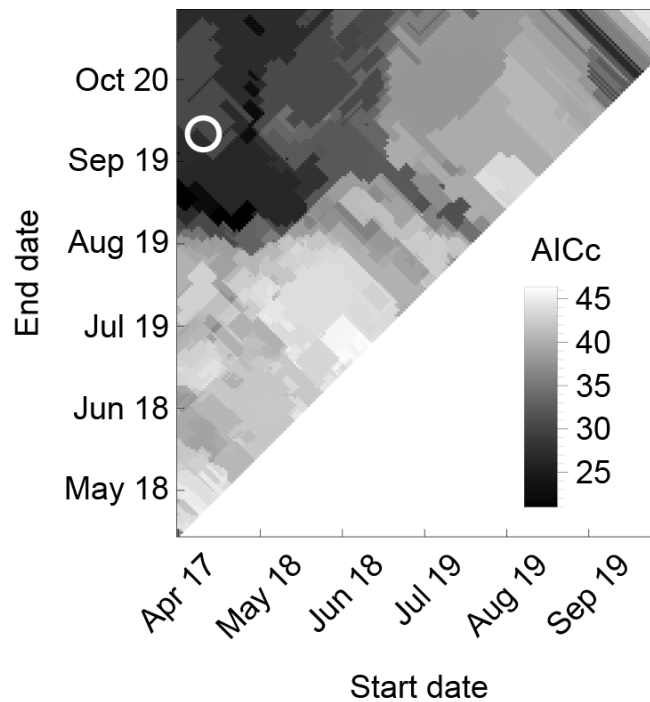


Fig. 4.5. AICc values for the discharge model for the Chena River using different start and end dates for calculating median discharge. Lower AICc values (dark shading) correspond to better performance of the discharge model using the start and end dates specified by the axes. The center of the white circle corresponds to the time period selected *a priori* for the discharge model as used elsewhere in the paper, April 23 to September 30, which had an AICc of 29.7.

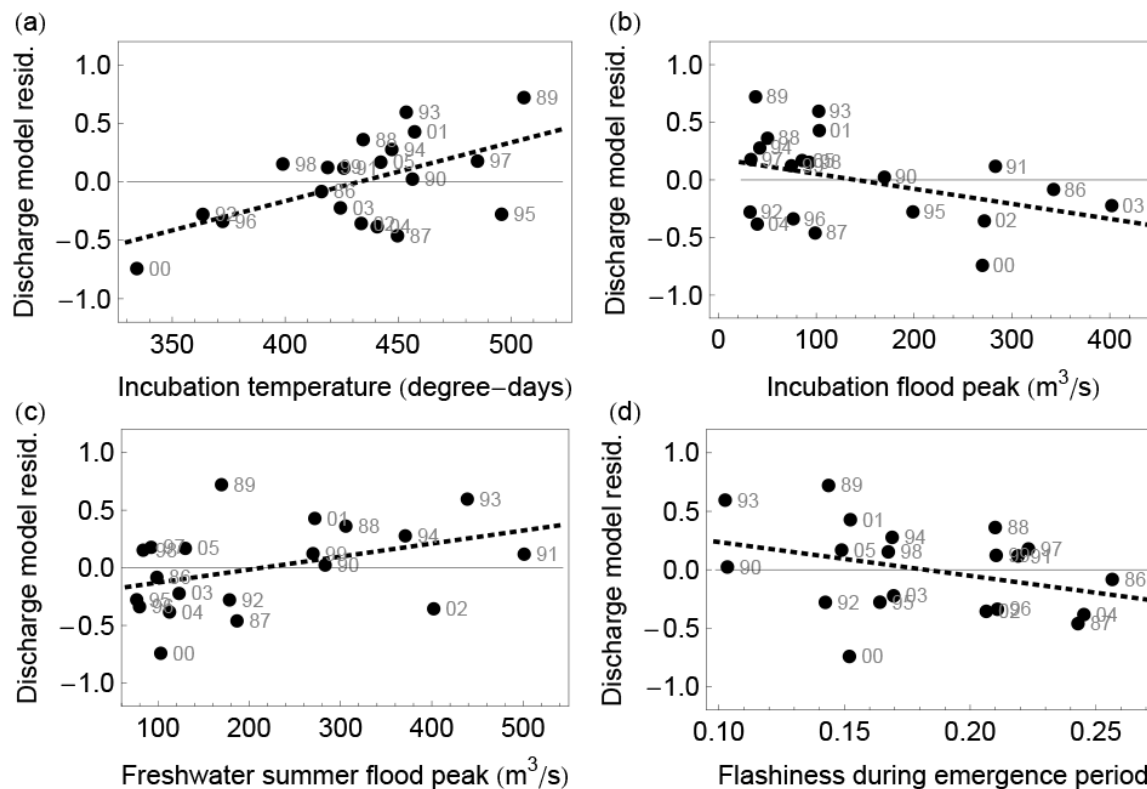


Fig. 4.6. Residuals from the discharge model plotted against the top four other environmental correlates identified in an exploratory analysis of the Chena River. During the pre-winter spawning and incubation period, (a) cold temperatures and (b) large floods were possibly associated with poor recruitment relative to the discharge model's predictions. The next strongest relationships, with (c) a positive effect of maximum flood peak during the summer growing season and (d) a negative effect of flashiness during the critical emergence period were weakly supported and probably spurious.

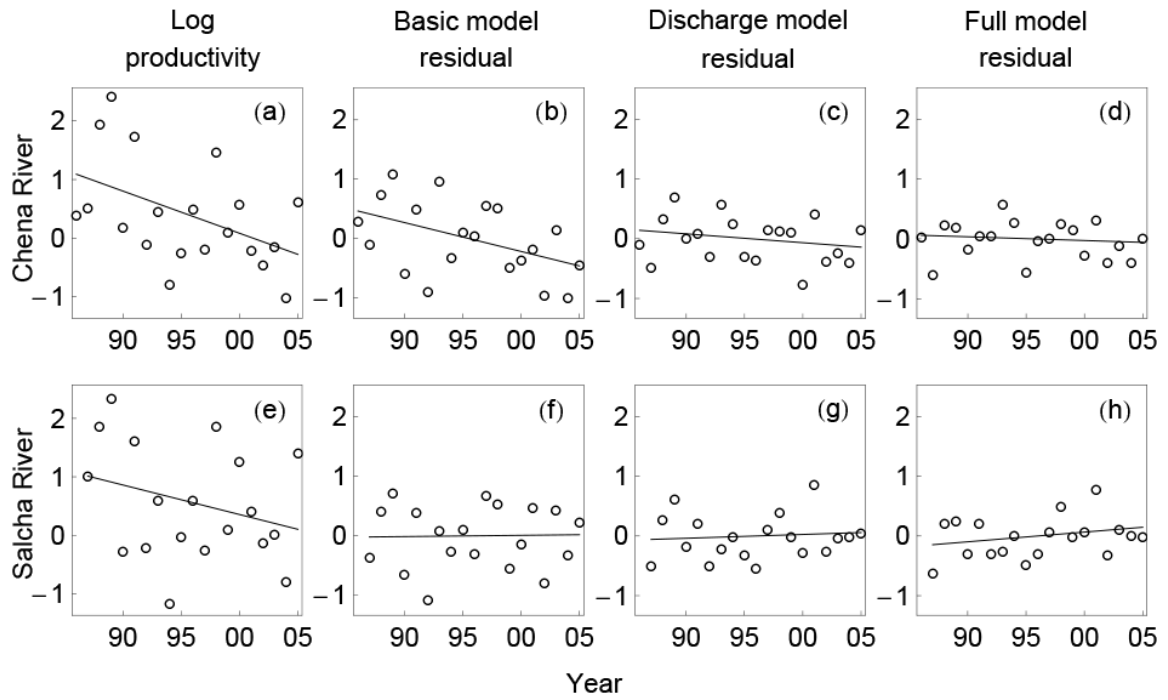


Fig. 4.7. Trends over time in log productivity (*a, e*) and residual log productivity left unexplained by the basic Ricker model (*b, f*), discharge model (*c, g*), and full model (*d, h*) for the Chena and Salcha rivers. The linear regression trendlines are intended to help visualize the direction of the data, not to imply that the real temporal trends are linear.



## General Conclusions

Chapter 4 of this dissertation strengthened the evidence that the Chena River Chinook salmon population exhibits density dependence, and that its productivity is negatively affected by high stream discharge during the summer juveniles spend drift feeding in freshwater. Chapter 3 showed that the apparent mechanism of density dependence in many other salmonids—competition between successful holders of exclusive territories and transient, non-territorial “floaters”—was present in Chinook salmon fry. This behavior was masked from easy observation by the 3-D schooling behavior of fry, but it was revealed by the 3-D video analysis methods developed in Chapter 1 and new methods for analyzing temporally dynamic 3-D space use described in Chapter 3.

Detailed analysis of population productivity in Chapter 4 suggested it is negatively influenced by the effects of sustained high discharge on foraging conditions, not by sudden mortality during floods. The negative effect of debris on foraging efficiency, identified in Chapter 2, could be one of many mechanisms driving the negative effect of sustained high discharge on productivity. This work complements the concurrent work of my lab mates who found that, during periods of high discharge, primary production in the Chena River decreased (Benson et al. 2013), and juvenile Chinook salmon had less food in their stomachs than during low-discharge periods (Gutierrez 2011).

Three chapters significantly contributed to a broader understanding of ecology beyond the study of Chinook salmon. The video analysis methods and corresponding VidSync software (<http://www.vidsync.org>) described in Chapter 1 have been used for remote length measurement, biodiversity surveys, and behavioral studies in New Zealand, Argentina, the Seychelles, Alaska (e.g., Perry 2012), and elsewhere in the United States. The effect of debris established in Chapter 2 is probably of universal importance to drift-feeding fishes, and it suggests that some disproven mechanisms central to existing drift-feeding models should be replaced with a cognitive model of prey

detection as a process of discriminating between the signal (prey) and the noise (debris). Chapter 3 revealed that schooling and feeding territoriality are not mutually exclusive behaviors, and territories can be distributed in three dimensions (with horizontally overlapping territories fully separated vertically). This chapter also presented a new representation of animal space use—the “instantaneous region of influence”—which could prove useful for any studies of temporally dynamic space use, especially for animals inhabiting 3-D environments such as forest canopies or reefs.

This dissertation added a few solid pieces to the foundation of mechanistic knowledge required to eventually model the full chain of connections between individual-level mechanisms and population-level responses. However, many gaps remain in our understanding of Chinook salmon and drift-feeding fish more generally. We need to know more about spatiotemporal heterogeneity in the distribution of drifting invertebrates, and the physical processes such as dispersion that can affect the distribution of drifting prey and influence habitat quality in systematic ways (Hayes et al. 2010). This would be part of a broader effort to increase the appreciation of variation in prey density as a critical environmental variable for drift-feeding fishes (Piccolo et al. 2014). To better understand competition within Chinook salmon schools, we also need to learn how each individual affects food availability for adjacent competitors and those downstream via shadow competition (Elliott 2002). This will require the development of a drift-feeding model that can accurately predict a fish’s probability of capturing prey items at various distances in a natural environment with visually diverse prey and debris in the drift. Understanding how prey slip past the fish at the upstream end of a school will be critical to modeling the foraging success of their downstream competitors. Finally, to relate Chinook salmon foraging behavior to population dynamics, we require an understanding of how Chinook salmon fry respond to a lack of foraging success and how those responses contribute to their chance of mortality. All of these are tractable research questions, and I hope this work helps to convince others they are worthy of investigation.

## References

Benson, E. R., Wipfli, M. S., Clapcott, J. E., and Hughes, N. F. 2013. Relationships between ecosystem metabolism, benthic macroinvertebrate densities, and environmental variables in a sub-arctic Alaskan river. *Hydrobiologia* 701(1): 189-207.

doi:10.1007/s10750-012-1272-0.

Elliott, J. M. 2002. Shadow competition in wild juvenile sea-trout. *J. Fish. Biol.* 61: 1268-1281.

Gutierrez, L. 2011. Terrestrial invertebrate prey for juvenile Chinook salmon: abundance and environmental controls in an interior Alaskan river. *Biology M.S.*: 63 pp.

Hayes, J. W., Olsen, D. A., and Hay, J. 2010. The influence of natural variation in discharge on juvenile brown trout population dynamics in a nursery tributary of the Motueka River, New Zealand. *N Z J Mar Freshw Res* 44(4): 247-269.

doi:10.1080/00288330.2010.509905.

Perry, M. T. 2012. Growth of juvenile Chinook salmon (*Oncorhynchus tshawytscha*) in an interior Alaska river: responses to supplemental feeding and temperature. *Biology M.S.*: 77 pp.

Piccolo, J. J., Frank, B. M., and Hayes, J. W. 2014. Food and space revisited: The role of drift-feeding theory in predicting the distribution, growth, and abundance of stream salmonids. *Environ. Biol. Fish.* doi:10.1007/s10641-014-0222-2.